Title

FRACTURE TOUGHNESS DEMANDS IN SEISMIC MOMENT FRAME CONNECTIONS OF BOX COLUMNS

Author

Yasumoto, Hiroshi

Publication Date

2023

Peer reviewed|Thesis/dissertation

Fracture Toughness Demands in Seismic Moment Frame Connections of Box Columns

By

HIROSHI YASUMOTO

THESIS

Submitted in partial satisfaction of the requirements for the degree of

MASTER OF SCIENCE

in

Civil and Environmental Engineering

in the

OFFICE OF GRADUATE STUDIES

of the

UNIVERSITY OF CALIFORNIA

DAVIS

Approved:

Amit Kanvinde, Chair

Sashi Kunnath

John E. Bolander Jr.

Committee in Charge

2023

ABSTRACT

Welded connections between beams and built-up box columns in steel moment frames require the attachment of a continuity plate to the inside of the box column using Complete Joint Penetration (CJP) welds. Electroslag Welding (ESW) is often used to weld one of the sides of this continuity plate to the inside box column. These welds are susceptible to fracture owing to decreased material toughness and the installation of containment plates that create a notch condition. Finite element based fracture mechanics simulations are presented to examine the effect of various design and detailing parameters on the fracture toughness demands in these connections for reversed cyclic loading (earthquake type loading). The results indicate that the use of improved bevel details in the containment plate, and the use of a Reduced Beam Section (RBS) connection strongly mitigate fracture toughness demands, whereas eccentricity in the weld (with respect to the continuity plate) and mismatch between the beam and column flange widths exacerbate fracture toughness demands. The beam and column size, as well as weld access hole details are determined to have only a modest effect on the fracture toughness demands. Simulations are also conducted to examine column wall thickness limits beyond which continuity plates may not be required. These suggest that using limits similar to wide-flanged columns may not provide adequate performance. Limitations of the study are presented, along with directions for future work.

KEYWORDS: Box columns; Fracture; Welded Connections

ACKNOWLEDGEMENTS

I and the collaborators acknowledge support from the National Science Foundation (Grant CMMI 2129445). I would like to thank to Professor Michael Engelhardt of the University of Texas, Austin for his constructive advice. I am extremely thankful to Professor Chia-Ming Uang at UC San Diego and Rupa Garai for collaborating with my work and giving me great advices. The views and findings presented in this article are entirely of the authors.

I would like to thank my graduate advisor, Professor Amit M. Kanvinde, for his support and guidance through the analytical and writing this thesis. Not only for his kindness, but also for helping me out with all sorts of brilliant ideas when I got stuck, which made the last two years I spent at UC Davis a fruitful one. I am grateful of Kajima Corporation for the enough scholarship to focus on my studies. I would like to thank all the Civil and Environmental Engineering Professors at the University of California, Davis who have helped me know a lot of advanced studies for Structural Engineering, in particular the members of my reading committee, Professor Sashi Kunnath and Professor John E. Bolander Jr.. I also thank a lot of research group members for helping to give me all kinds of advice on campus life and living abroad for the first time.

TABLE OF CONTENTS

LIST OF TABLES

LIST OF FIGURES

For my Loving and Caring Family.
Thank you Dearly for your Understanding and Support.

CHAPTER 1
INTRODUCTION

Built up box columns are used in seismically designed Steel Moment Frames (SMFs) to resist biaxial bending, and to provide economy in meeting seismic strength and drift requirements in an economical manner, in comparison to rolled wide flanged (i.e., W-) sections. While they are increasingly popular, especially for high-rise steel buildings in seismic regions, some factors limit their widespread use. These columns are usually constructed from plate steel with longitudinal CJP welds to form the box. A key issue, which is the focus of this paper, pertains to the beam-to-column connections in these columns. Figure 1.1a shows a typical beam-to-column connection used in such columns. Referring to Figure 1.1a, a continuity or diaphragm plate (similar to that provided in conventional beam-to-W-section column connections) is usually provided to effectively transfer the forces introduced by beam flanges into the column flange plate. The continuity plate presents a fabrication challenge, because it must be attached to all four sides of the box from the inside, using Complete Joint Penetration (CJP) welds. Conventional welding techniques cannot be used, because access to the inside of the box column is not available once the box is closed. Electro-Slag Welding (ESW) has been proposed as a solution to this problem. Figures 1.1b and c schematically illustrate the process for installation of the continuity plate within the box column, using the ESW technique.

Referring to these figures, first three sides of the box are welded together; this is usually accomplished by introducing longitudinal CJP welds along the length of these plates using

Submerged Arc Welding (SAW). Then, the continuity plate is CJP welded on three sides of the box using Flux-Cored Arc Welding (FCAW), before the fourth plate is welded to close the box. This leaves the fourth side of the continuity plate unattached to the box plate. To attach this plate to the box wall, the ESW welding technique is employed, as shown in Figure 1.1c. See Padilla-Llano et al. 2021, Gilmer et al. 2005 for a historical overview of the development and use of the ESW welding process. This technique involves inserting an electrode through a hole in an adjacent flange plate, and then depositing weld filler material between the continuity plate and the box plate. The electrode is gradually raised as the filler material is deposited (in a single weld pass), until the entire length of the continuity plate is CJP welded to the box plate. The electrode is continuously fed into the rising weld pool in the joint. Although the ESW process overcomes the fabrication challenges outlined above, it raises other issues from the standpoint of structural performance of the beam-column connections. These issues are related to two factors:

- The extremely high weld deposition rates (on the order of ~45lbs/h, relative to 3~9lbs/h commonly seen in conventional FCAW welds) result in heat input that is on the order of 10 times greater than FCAW welds, along with low cooling rates that result in wide Heat Affected Zones (HAZs) with coarse grained microstructures. This ultimately leads to decreased material toughness in these welds.
- The ESW welds entail attachment of containment plates on the inside of the box (see Figure 1.1d) to contain the weld pool as the filler metal is deposited. These typically lead to stress concentrations or notch conditions due to lack-of-fusion regions or re-entrant corners. Various details have been proposed to mitigate these discontinuities.

The combination of the decreased material toughness, and the discontinuities in weld regions raises concerns regarding the seismic performance of these connections, such that there are significant

restrictions in design standards regarding their use. Specifically, AISC 358-22 (AISC, 2022) which includes prequalified moment connections, disallows the use of ESW welded box column details in columns that have either a depth or width greater than 24 inches (588 mm), and RBS beams that are larger than W36 X 300. Additionally, AISC 358-22 indicates that "where moment frame beams do not connect to all four sides of the box column, it is recommended that the ESW side of the column be located where there is no moment frame." Moreover, seismic design codes, including AISC 358 as well as the Seismic Provisions, i.e., AISC 341-22 (AISC, 2022) do not provide guidance regarding when the continuity plate need not be specified. This is in contrast to beam-to-W-section column connections for which clear guidance exists. Designers must either adapt such guidance to box columns or conservatively specify a continuity plate, resulting in the aforementioned problems with the ESW joint. Collectively, these considerations constrain the effective use of box sections to economically design SMFs. As a result, development of technologies and details that mitigate these problems has been of interest to researchers and professional communities internationally (Verma et al. 2005, Lin et al. 2012, Tsai et. al. 2020). Nonetheless, the research in this area is somewhat limited, relative to other similar structural details. Specifically, in the United States, only one test program (Lee et al., 2016) has been conducted in which only one out of three experiments showed acceptable response, i.e., met prequalification standards (AISC 341-22). Previous testing in Taiwan (Lin et al. (2010)) included 22 experiments, of which 12 showed premature failure. These results, in part, have contributed to the current guidelines outlined above. Developing robust provisions to support the use of beam to box column connections requires research and synthesis on the following fronts: (1) understanding fracture toughness demands in these connections, and the effect of various detailing and geometric parameters on these demands, (2) the development of welding technologies that provide adequate

toughness to meet these demands, and (3) large-scale qualification testing to demonstrate connection performance. This paper addresses the first of these, by using Continuum Finite Element (CFE) based fracture mechanics simulations to examine the effect of detailing considerations and parameters on internal stress distributions and fracture toughness demands in box column beam-column connections. These include different types of containment plate configurations, beam and column dimensions (section sizes, wall thicknesses, access hole geometry, and the use of RBS details) as well as continuity plates sizes, with the objective to develop insights that may be used to support effective details for such connections. Additionally, the sensitivity to fracture toughness is also assessed. The paper begins by providing background regarding relevant research in the area that has a direct bearing on the CFE simulations conducted in this study. This is followed by a description of the CFE simulation methodology, including the underlying fracture mechanics approaches used. The effect of each parameter is then examined in the context of prospective connection detailing strategies. The paper concludes by outlining limitations of the study, while providing direction for future work.

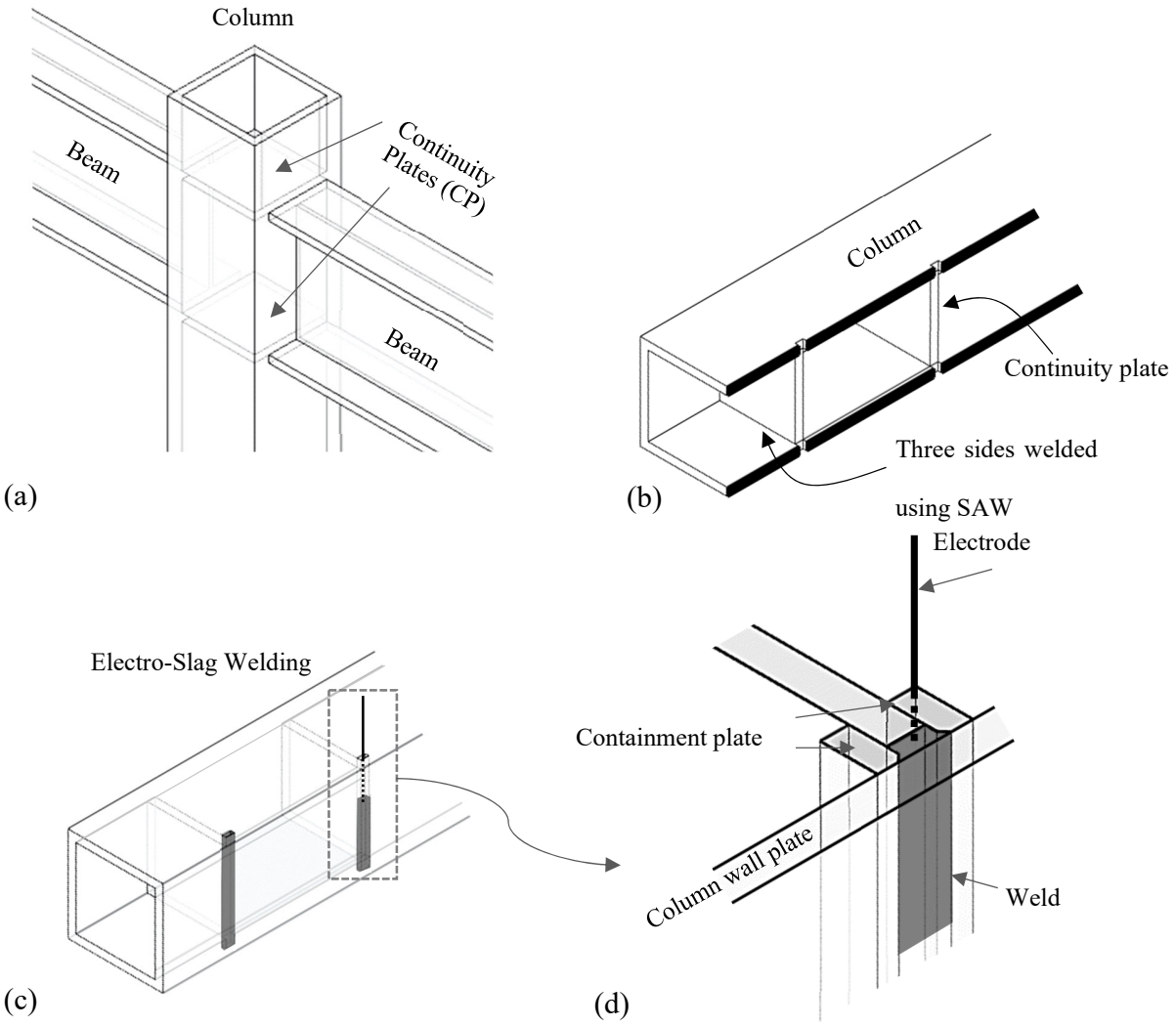

Figure 1. 1 – Fabrication of beam-box-column connection: (a) overview, (b) welding on three sides of box using SAW, (c) ESW welding on fourth side after closing box (d) detail of ESW weld process

CHAPTER 2
BACKGROUND AND PREVIOUS WORK

Research on ESW welds, and their application to box column continuity plate welds, has been a focus of research internationally. In the United States, qualification testing on box column connections has been conducted in support of a 24-story building in San Diego, California (Lee et al., 2016). This testing featured three Reduced Beam Sections (RBS) moment connections attached to 24"x36" (610x914mm) built up steel box columns. Figures 2.1a and b schematically illustrate the ESW details used in these connections to connect the continuity plate to the box column. Referring to these figures, two types of containment plate details were used, these are: (1) a conventional detail – Figure 2.1a, and (2) an improved detail, mitigating the notch condition of conventional detail– Figure 2.1b. The detail shown in Figure 2.1b also includes shim plates between the containment plate and the continuity plate, intended to cool the weld more effectively. Two of these specimens (termed Specimen #1 and #2 by Lee et al., 2016) with the conventional bevel detail (such as shown in Figure 2.1a) suffered brittle fracture at unacceptably low story drift ratios (i.e., less than 4.0% drift) under an applied ATC-SAC protocol (AISC 341-22), whereas Specimen #3 with the improved bevel detail (similar to Figure 2.1b) survived the applied protocol through cycles corresponding to 4% drift without significant strength deterioration, meeting the standard for prequalification. Figure 2.1c shows another type of beveled detail developed by Lin et al. (2012) in Taiwan, mitigating the notch condition of conventional detail. Such beveling moves the notch tip out of the path of direct stresses under the flange, reducing fracture toughness demands. Figures 2.2a-c show post-test photographs of the ESW joint region, indicating the weld, containment plate, as well as the cracking/fracture observed in Specimens #1, #2, and #3, of the

Lee et al., (2016) tests, hereafter referred to as the UCSD tests. Each of the figures indicates the notch condition introduced by the containment plates, at which cracks initiated under the applied load, as well as some other features of interest. Referring to Figures 2.2a and b, the cracking that initiated at the notch resulted in these connections being completely severed. On the other hand, the specimen with the improved detail (shown in Figure 2.2c) showed the initiation of cracking at the notch but without brittle propagation.

Significant research on ESW connections has also been conducted in Japan and Taiwan. Notable within this is work by Tsai et al., (2015) who reported a statistical evaluation of 22 box column moment frame connections, and determined that 12 of these specimens did not achieve the 0.04 rad story drift angle requirement for SMFs. Similar research conducted in Japan led to the publication of a guidebook (JSSC, 2016). Additionally, work by Chen (2009), and more recently Tsai et al., (2020) and Chen et al., (2020) used CFE simulations to assess the effects of parameters (specifically, the ESW the weld bulb radius, and the eccentricity between the continuity plate and the beam flange) on local strain and fracture toughness demands. Cumulatively, this research indicates that box-column moment connections with ESW diaphragm welds require serious innovation, research, and guideline development for more widespread use in construction, in the United States as well as overseas. The details examined in this study are derived from these previously tested details.

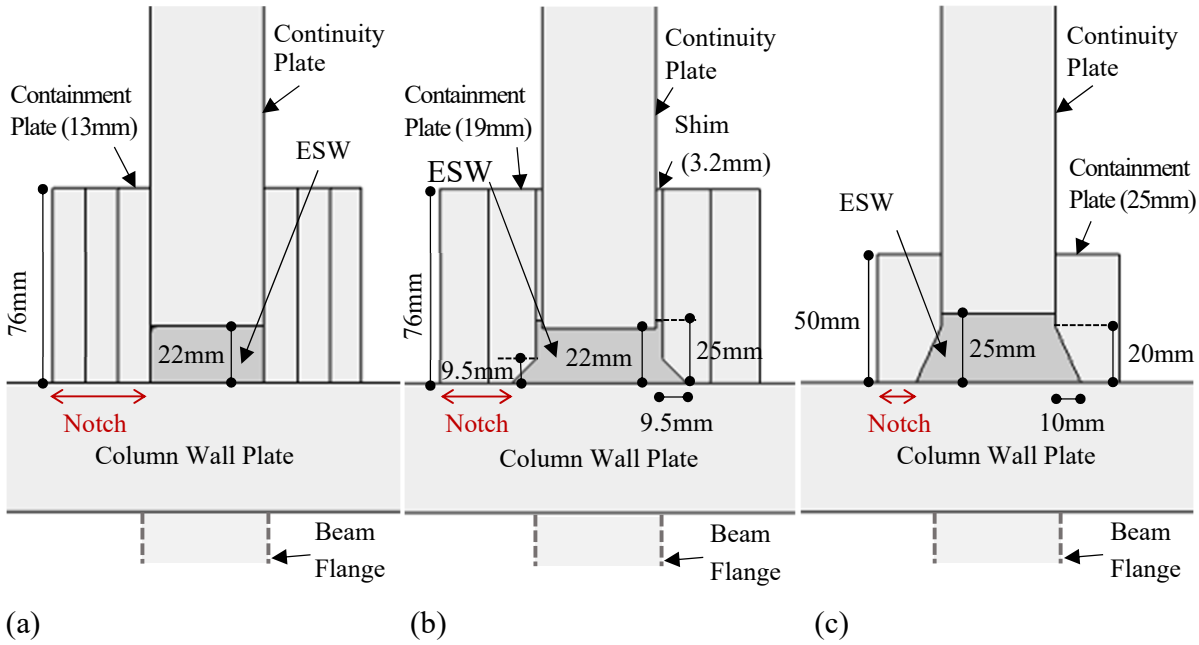

(a) (b) (c)

Figure 2. 1 – Electroslag Weld joint detail (a) Standard – S, (b) Beveled detail – B1, (c) Beveled detail – B2

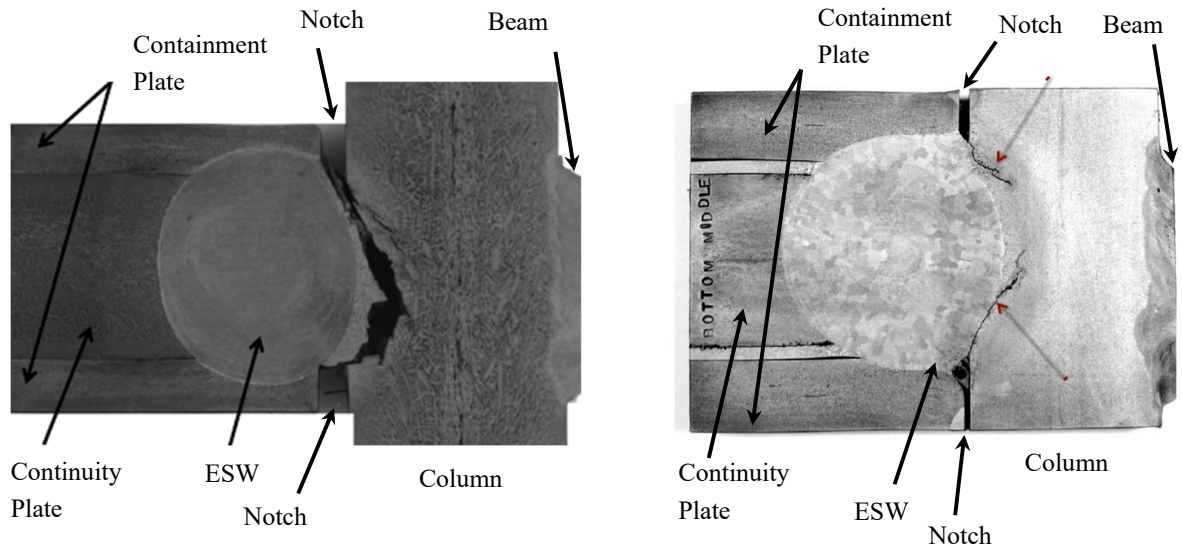

(a) (b)

Figure 2. 2 – Electroslag Weld Joint after testing: (a) Test #2, (b) Test #3 from the UCSD test series

CHAPTER 3
OVERALL METHODOLOGY AND SIMULATION MATRIX

The primary objective of this study is to examine fracture toughness demands in variations of box column moment connections through CFE simulations. Consequently, the overall methodology includes three parts, as schematically illustrated in Figure 3.1. Referring to the figure, the main research component is the Continuum Finite Element (CFE) simulations that are used to relate externally applied loading to fracture toughness demands at critical locations within the structural component. The CFE models in turn rely on inputs that pertain to detail configuration and geometry as well as material properties, and fracture criteria for interpretation of the results. This section addresses the various input parameters and effects examined through the CFE simulations that are described in detail in the next section. Tables 3.1 and 3.2 summarize the simulations conducted. Specifically, Table 3.1 presents the simulation matrix for box column connections with the internal continuity plate and ESW welds, whereas Table 3.2 illustrates simulations designed to examine the necessity of the continuity plate itself, depending on the column wall plate thickness and other factors. In these, no ESW weld is present, and the fracture critical location is on the outside of the column between the beam bottom flange and the column. Since these simulations (and their purpose) is functionally different from the ESW simulations, a separate simulation matrix is generated for them. Referring to the Table 3.1, a total of 15 simulations were conducted for the ESW joint, interrogating the following parameters:

1. *Containment plate detail:* Three details were considered; these include a standard containment plate detail without any bevel as shown in Figure 2.1a previously (this is denoted S), and two beveled details (denoted B1 and B2). Of these, detail B1 (shown previously in Figure 2.1b)

refers to a detail developed in the United States which includes a bevel within the containment plate to minimize the notch effect, in addition to the introduction of a shim plate whose purpose is to cool the ESW efficiently. The detail B2 reflects one developed by Lin et al. (2012) in Taiwan, which includes the bevel but not the shim plate. The thicknesses of the containment and shim plates are 3/4" (18mm) and 1/8" (3.2mm) respectively. The introduction of the shim plate affects the heat transfer during the welding process, ultimately altering the local material properties in a favorable way. While the simulations in this study simulate the geometric effect of the shim plate and the containment plate, the effect on material properties is not simulated.

2. *Effect of beam and column size:* Referring to Table 3.1, two beam sizes (W36x302 and W27x368), along with four column sizes were used.
3. *Effect of using a Reduced Beam Section (RBS) in the beam*: Two levels of beam flange reduction were used (in addition to an un-reduced flange, i.e., a Welded Unreinforced Flange-Welded Web, i.e., WUF-W connection) following the geometric requirements of AISC 358-22, Section 5.8; these include flange reductions of 2.625" (67mm) and 4.125" (105mm) flange reductions – see Figure 3.2a. These RBS configurations (denoted RBS1 and RBS2 respectively) represent a reduction in the effective plastic modulus to 76% and 62% with respect to the WUF-W connection. The purpose of the RBS is to mitigate stress demands in the connection at the column face and at the ESW joint. This was one of the strategies pursued by Lee et al., (2016) to successfully achieve ductile performance in their experimental program.
4. *Weld Access Hole (WAH) geometry:* Two geometries for the WAH were used; these include the geometric requirements of AISC 360 Fig. C-J1.2 (AISC 360-2022) and a larger web access hole geometry, based on AWS D1.8 (Ricles, et al., 2002). Figure 3.2b shows the two weld access hole geometries; these are termed Standard and Improved respectively.

5. *Eccentricity of ESW weld bulb:* The electrode moves laterally within the containment plates as it is being retracted during the welding process, sometimes resulting in an unintended eccentricity that exacerbates the notch effect. This was observed in one of the UCSD specimens (Test #2). Moreover, the eccentricity of the weld bulb was identified to be an important issue during previous CFE simulations by Chen et al., (2020) and Tsai et al., (2020). Figure 3.2c illustrates the definition of the eccentricity parameter defined as e. Two values of e, i.e., $e = 0$ and $e = 10$mm were examined in this study, based on the measured eccentricity in Test #2. The eccentricity is assumed to be constant through the entire length of the ESW weld. It is important to note here that in both these cases, the continuity plate and the beam flange are perfectly aligned; the issue of misalignment between these is a distinct matter, and has been examined previously by Chen et al., (2020).

Referring to Table 3.1, the simulation matrix is fractional-factorial, such that while the effect of each parameter outlined above is examined, all the cross-dependencies are not examined. However, subsets of the simulations may be used to isolate the effects of individual parameters. Referring to Table 3.2, additional simulations were conducted to examine the necessity of the continuity plate itself, considering that: (1) provisions governing the use of such plates for box columns do not yet exist, and (2) removing the continuity plate will eliminate the entire problem associated with the ESW joint. However, the absence of the continuity plate influences the fracture potential in the CJP groove weld outside the column. This is because the continuity plate constrains out of plane bending of the column wall plate when loaded by the beam flange, and mitigates stress concentrations in the beam-flange groove weld. Thus, these simulations examine a different issue as compared to those in Table 3.1. The relevant parameters expected to influence the continuity plate are the beam flange thickness and the column thickness. The Seismic Provisions (AISC 341,

2022) indicate continuity plates are required unless the column flange thickness is greater than the following:

$$t_{cf-WF}^{\text{AISC}} = \max\left(0.4\sqrt{1.8 b_{bf} t_{bf} \frac{F_{yb}}{F_{yc}}}, \frac{b_{bf}}{6}\right) \quad (1)$$

In the above equation, b_{bf} and t_{bf} are the beam flange width and thickness, and F_{yb} and F_{yc} are the expected yield strengths of the beam and column respectively. Although the above equation is not prescribed for box columns, the thickness implied above is used here as a reference value to interpret simulation results. Table 3.2 shows the ratio between the column flange thickness and the threshold thickness shown above. The thickness of the continuity plate (normalized by the beam flange thickness) is also shown in the table. Note that for a single sided connection (as analyzed in this study), the minimum required continuity plate thickness is $0.5t_{bf}$.

Table 3. 1 Simulation Matrix for Column Connections with the Internal Continuity Plate and ESW

#	Column	Beam Section	Access Hole	Z_{RBS}/Z_X	Conta-inment Plate	Ecce-ntri-city	b_{bf}/b_{cf}	Drift when D>1 (%)		
								Web	BE	CC
1	610x914	W36x302	AWSD1.8	1.0 [1]	S	e=0	0.70	0.75	-	-
2	610x914	W36x302	AWSD1.8	1.0 [1]	B1	e=0	0.70	3.00	1.00	-
3	610x914	W36x302	AWSD1.8	1.0 [1]	S	e=10	0.70	0.50	-	-
4	610x914	W36x302	AWSD1.8	1.0 [1]	B1	e=10	0.70	0.75	-	-
5	610x914	W36x302	AWSD1.8	0.76	B1	e=0	0.70	4.00	-	-
6	610x914	W36x302	AWSD1.8	0.62	B1	e=0	0.70	5.00	1.50	-
7	610x914	W36x302	AISC360	1.0 [1]	B1	e=0	0.70	2.00	-	-
8	610x914	W27x368	AWSD1.8	1.0 [1]	B1	e=0	0.74	2.00	1.00	-
9	610x914	W27x368	AWSD1.8	1.0 [1]	S	e=0	0.74	0.75	-	-
10	610x914	W27x368	AISC360	1.0 [1]	B1	e=0	0.74	2.00	-	-
11	610x914	W36x302	AWSD1.8	1.0 [1]	B2	e=0	0.70	2.00	-	-
12	610x914	W36x302	AISC360	0.76	S	e=0	0.70	-	-	-
13	610x610	W36x302	AWSD1.8	0.62	B1	e=0	0.70	6.00	2.00	-
14	432x914	W36x302	AWSD1.8	0.62	B1	e=0	1.0	D<1	D<1	-
15	762x914	W36x302	AWSD1.8	0.62	B1	e=0	0.56	4.00	2.00	5.00

Unit: mm, t_{cf}=50.8, [1]: WUF-W

Table 3. 2 Simulation Matrix for Examining the Necessity of the Continuity Plate, Depending on the Column Wall Thickness and Other Factors

#	t_{cf}	Beam Section	b_{bf}	t_p/t_{bf}	Contain-ment Plate	$\frac{t_{cf}}{t_{cf-WF}^{\text{AISC}}}$	$D_{4\%}$
16	50.8	W36x302	427	1.0	B1	0.71	0.76
17	50.8	W36x302	427	0.52	B1	0.71	1.92
18	50.8	W36x302	427	-	w/o	0.71	54
19	76.2	W36x302	427	1.0	B1	1.06	0.68
20	76.2	W36x302	427	0.52	B1	1.06	0.93
21	76.2	W36x302	427	-	w/o	1.06	2.25
22	127	W36x302	427	1.0	B1	1.76	0.45
23	127	W36x302	427	0.52	B1	1.76	0.49
24	127	W36x302	427	-	w/o	1.76	0.59
25	50.8	W27x368	630	1.0	B1	0.62	0.67
26	50.8	W27x368	630	0.50	B1	0.62	1.33
27	50.8	W27x368	630	-	w/o	0.62	5.8
28	76.2	W27x368	630	1.0	B1	0.93	0.48
29	76.2	W27x368	630	0.50	B1	0.93	0.64
30	76.2	W27x368	630	-	w/o	0.93	2.13
31	127	W27x368	630	1.0	B1	1.55	0.37
32	127	W27x368	630	0.50	B1	1.55	0.40
33	127	W27x368	630	-	w/o	1.55	0.54
34	102	W36x302	427	1.0	B1	1.41	0.53
35	102	W36x302	427	0.52	B1	1.41	0.60
36	102	W36x302	427	-	w/o	1.41	0.97
37	152	W36x302	427	1.0	B1	2.12	0.39
38	152	W36x302	427	0.52	B1	2.12	0.40
39	152	W36x302	427	-	w/o	2.12	0.43

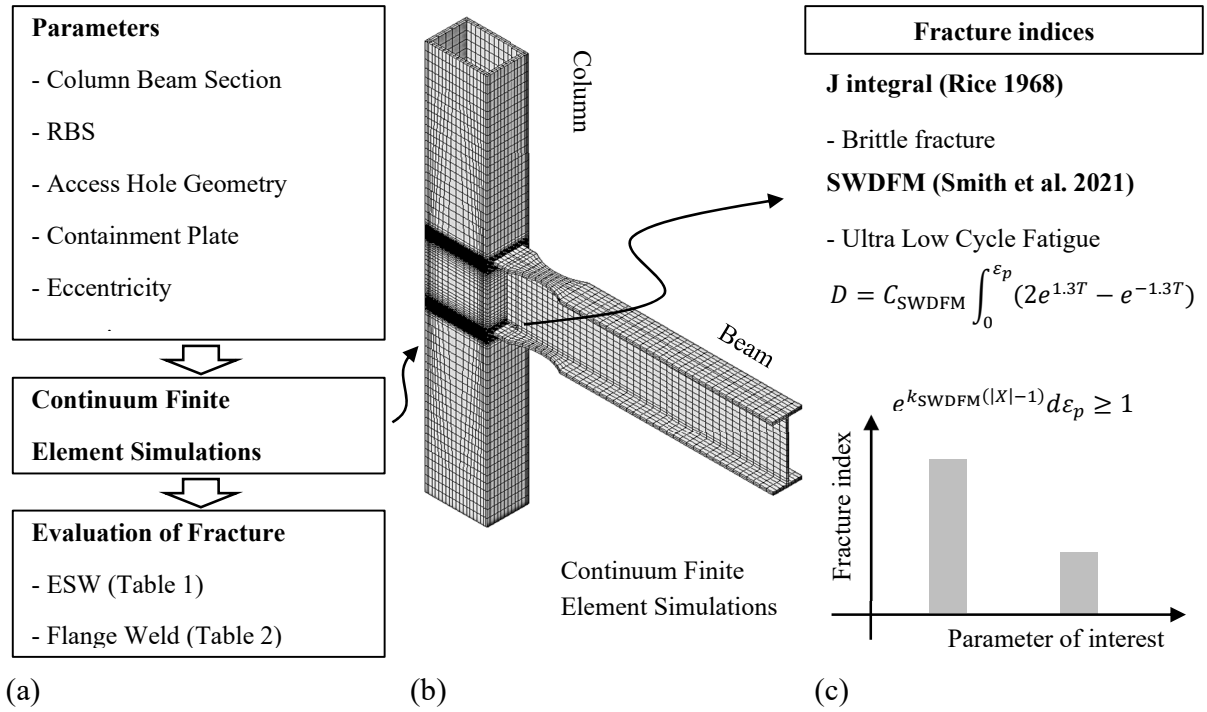

Figure 3. 1 – Schematic illustration of methodology

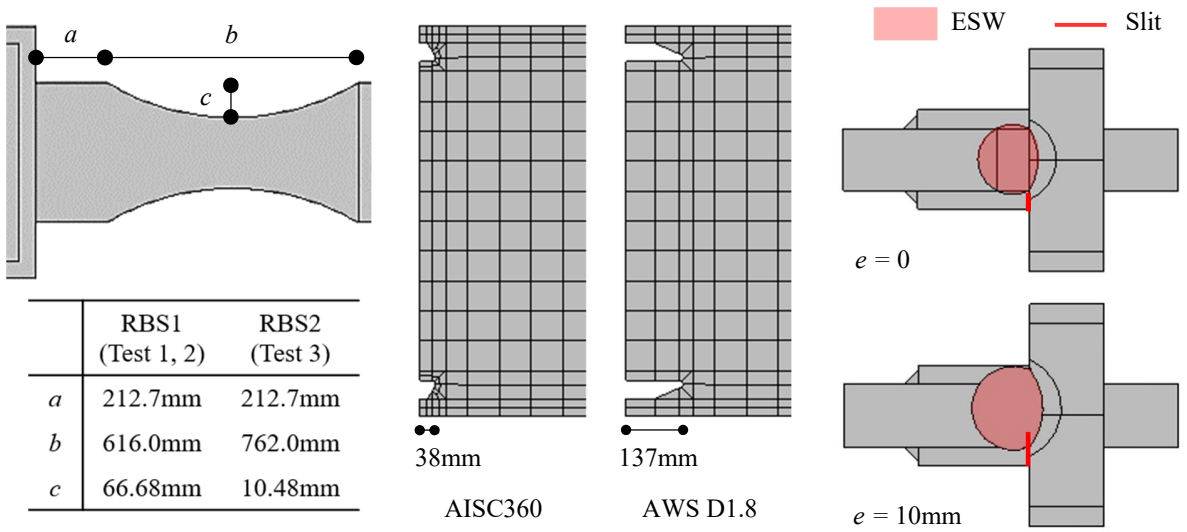

Figure 3. 2 – Continuum Finite Element Models (a) Global model, and (b) Local model

CHAPTER 4
CONTINUUM FINITE ELEMENT MODELS

Each of the parameter sets defined in Tables 3.1 and 3.2 above was examined through Continuum Finite Element (CFE) simulations to assess the fracture toughness demands at critical locations in the box column connections. The simulations were conducted on the platform ABAQUS (Ref ABAQUS 2020, Dassault Systems) and share some features in terms of overall methodology, constitutive material models as well as fracture indices used, but are different in other aspects – specifically pertaining to their geometric construction and meshing. The following subsections summarize each set of simulations, before describing the features common to both.

Simulations to examine fracture toughness demands at the ESW joint

The parameter sets indicated in Table 3.1 may be arranged in a hierarchy wherein some share identical global characteristics (e.g., beam size and RBS ratio, column size and continuity plate thickness) but differ at a local detailing level (i.e., containment plate configuration or ESW eccentricity). To simulate these various conditions with computational efficiency, a global model-submodel scheme was used, which is illustrated in Figure 4.1. This scheme includes two steps: (1) three dimensional CFE models of the complete connection configuration including the beam, column, and continuity plate are constructed for each of the "global" parameter sets and subjected to loadings and boundary conditions to reflect component level actions (e.g., story drifts) – this is shown in Figure 4.1 for one of the simulations, i.e., Sim #6, which is complementary to Test #3 from the UCSD test program, and (2) submodels are then created to reflect the local detailing. The submodels are driven by the displacement demands determined from the global models, and feature fine meshes and notch or crack tip geometries to compute stresses and strains at resolutions

required to characterize fracture toughness demands. These are shown in Figure 4.1b. This is a well-established procedure such that ABAQUS provides on-board capabilities for submodeling. This approach results in significant computational efficiency because: (1) it allows for extremely fine meshing of critical regions of interest while the global model may be meshed coarsely without the associated problems of mesh transition, and (2) it allows for a limited number of global model runs, for which numerous submodel runs may be conducted to interrogate local effects, e.g., by altering submodel details or by inserting the submodels at different locations within the overall component configuration.

The global model was constructed to reflect all aspects of the overall geometry of the beam-column subassemblage, including 9.14m of the beam and 4.88m of the column – which is consistent with a typical story height and bay width. A single sided connection was used in this study. Pinned boundary conditions (applied in the form of knife-edge displacements) were applied at the top and bottom of the column segment – these are indicated in Figure 4.1. Two types of loading were applied to each model: (1) an upwards monotonic displacement up to an equivalent drift of 6% - this produced tension in the lower flange, and (2) cyclic displacement history at the beam tip as per the AISC 341-22 protocol, expressed in terms of story drift. The story drift was determined as the tip displacement of the beam divided by the length of the beam as measured from the beam tip to the centerline of the column – this is consistent with AISC 341-22, as well as how the drift was determined in the UCSD test program (Lee et al. 2016). The beam and column were modeled with the properties of A992 Grade 50 (345MPa) steel, whereas the ESW weld bulb was modeled to occupy the entire region bounded by the continuity plate, containment plates, and the column wall. The calibration of material properties for each of these are discussed in a subsequent section. The

model included large-strains and geometric nonlinearity, and appropriately scaled imperfections (see Elkady and Lignos 2018) to induce local buckling. The global model utilized 37,000 hexahedral (i.e., C3D8R, C3D20R and C3D20) elements to simulate the beam, column as well as all attached plates, i.e., the continuity plates and containment plates. This results in element sizes ranging from ~1mm (in the vicinity of the notch) to ~100mm over the length of the beam or column.

Figure 4.2c shows load-deformation curves from the CFE simulation for both the monotonic and cyclic loadings for one of the simulations (i.e., Simulation #12) superimposed on the counterpart experimental data from the UCSD Test #1 and #2 (with a 610x914x51mm column, W36x302 beam, Standard WAH, Z_{RBS}/Z_X, = 0.76, and containment plate type S), whereas Figure 4.2d shows the deformed shape including the formation of local buckles at an instant in the loading (indicated on Figure 4.2c). Figures 4.2a and b are similar to Figures 4.2c and d, except that they correspond to Sim #6 and Test #3. Referring to Figures 4.2a and c, the overall match between the experimental and simulated load-deformation curves is reasonably good, while Figures 4.2b and d indicate that the simulations are also able to capture the modes of local buckling. A closer inspection indicates that the simulated curves show slightly higher loads as compared to the experimental ones; this may be attributed to two factors: (1) the experimental specimens undergo significant crack propagation during cyclic loading, which is not modeled in the simulations – see Figure 2.2 shown previously, and (2) The material properties of the weld-bulb in the direction perpendicular to the axis of the bulb are not known independently – see subsequent section about material models. Nonetheless, from the standpoint of providing a sense of the fracture toughness demands at the un-fractured ESW joint (which is the intent of this study), the simulations may be considered conservative, since they possibly overestimate the stresses in this region. Figure 4.1b shown previously illustrates the detail of a local model, shown for Simulation #6. Referring to this figure,

the local features in ESW joint are modeled with significantly greater detail as compared to the global model – this includes the containment plates bevels, as well as the gaps within them. The notch tip is simulated with a diameter of 0.025mm – which also reflects the width of the gap between the containment plate and the column wall (see Figure 4.1). This value is roughly 10% of the estimated critical Crack Tip Opening Displacement (CTOD) for the material. Studies by McMeeking and Parks (1979), suggest that simulating the notch in this manner produces results comparable to those with perfectly sharp cracks. Previous studies (Stillmaker et al., 2015; Kanvinde et al., 2008) suggest that modeling weld root flaws as perfectly sharp cracks is appropriate. Referring to Figure 4.1, the representation of the notch in this manner necessitates the use of a fine mesh, in which elements are on the order of 0.005mm in size.

As discussed previously, the local model may be inserted at any location within the width of the connection (e.g., at the centerline of the beam, in line with the web) or towards the tips of the beam flanges, to interrogate the fracture toughness demands at those locations. This insertion implies that the deformation fields (as obtained from the global model at the location of interest) is used to drive the simulation of the local model. In this study, the local models are inserted at 3 locations within the global model (i.e., at the centerline– denoted "web," at a location in line with the edge of the beam flange – denoted "EB," and at the edge of the column plate – denoted "EC") to interrogate the fracture toughness demands at these locations – see Figure 4.1. The fracture toughness measures used are summarized in a subsequent section.

Simulations to examine fracture toughness demands in beam-flange groove weld

Figure 4.3 shows a CFE model corresponding to simulations in Table 3.2, which examine the necessity of specifying the continuity plate. The purpose of the continuity plate is to transfer the forces from the beam flanges into the column without excessive bending or stress concentration in the column flange wall plate, which may lead to fracture in the groove weld between the beam flange and the column. Referring to Table 3.2, a total of 3 parameters are assessed for this situation, featuring combinations of the continuity plate thickness (including absence of the continuity plate) and the column-wall thickness – variables that are anticipated to most strongly influence the stress/strain field in the groove weld. Consequently, the need for the continuity plate is assessed based on the fracture toughness demand in the groove weld outside the column, i.e., between the column and the beam flange. These simulations are similar in terms of overall construction to the ones for the ESW joint discussed above, but with some differences. A range of column wall plate thicknesses is chosen relative to the current limit t_{cf-WF}^{AISC} for wide-flanged columns (see Equation 1). It is important to note that only some of these simulations contain the continuity plate. Two continuity plate thicknesses are chosen – one represents the minimum required for a single-sided connection with a wide-flanged column as per AISC 341-2022, i.e., $0.5t_{bf}$, and another is t_{bf} to examine if the stress distribution in box columns connections may imply different limits compared to a wide-flanged column. In these simulations, the purpose of the continuity plate is to generate a benchmark estimate of fracture toughness demands in the groove weld, relative to which the demands from the simulations without the plate may be evaluated. In the simulations with the continuity plate, the internal joint between the continuity plate and the column wall plate is modeled simply as a tie constraint, without the complexity of the ESW detail or the containment plates, because the detail in this region does not influence the stress or strain state the groove weld between the beam and the column. In all simulations (i.e., with and without the continuity plate),

the groove weld on the outside is modeled as shown in Figure 4.3, based on typical dimensions used in similar CFE studies previously (e.g., Skiadopoulous and Lignos 2022). Second, it is noted that the details reflect a post-Northridge detail such that there are no backing bars or other discontinuities in the flange groove weld area. Consequently, the fine mesh (and the associated transitions) are not needed for these models, as they are for the ESW joints. Figure 4.3 shows the detail of the mesh in this region; the elements are all C3D8R and on the order of 0.5mm. A mesh convergence study indicates that this degree of mesh refinement is sufficient to capture the strain/stress gradients in the region. Since the fine meshing around the notch tip is not needed, only global models are constructed for this set of simulations.

Simulation of material constitutive response

For all materials (i.e., beam, column plate, and weld bulb or groove weld), a von Mises plasticity model with combined isotropic kinematic hardening (specifically, the Frederick and Armstrong – 1966) model was used. Based on previous studies (e.g., see Elkady and Lignos 2018, and Skiadopoulous and Lignos 2022, and Tsai et al., 2020), these models are able to represent the constitutive response of these materials with sufficient accuracy. Table 4.1 summarizes the parameters used for the model. The footnotes of Table 4.1 briefly summarize the role of each parameter; the full description of the constitutive model may be found in (Smith et al., 2014). The parameter selection for these was conducted based on the following:

1. Column wall plate base material and containment plate material: Values adopted directly from Lee et al., (2016)
2. Beam base material: Values adopted directly from Lee et al., (2016)
3. Electroslag weld as well as groove weld: Values calibrated to the stress strain curves obtained by Myers (2009) for all-weld E70 weld assemblies.

It is acknowledged here that direct measurements of the stress-strain response of the weld materials (especially the ESW welds) are not available. As a result, the parameters used in this study are best estimates. Moreover, anisotropy in material properties, which arise due to directionality of the welding, is also not considered. Finally, the constitutive properties of the Heat Affected Zones (HAZ) are not directly modeled. This appears to be an acceptable approach based on previous simulation studies by Kanvinde et al., (2008), as well as Myers et al., (2009).

Fracture toughness measures used to interpret results of the CFE models

Two types of fracture toughness demands were monitored in the models – one was the contour J-integral, which provides a measure of the crack driving force or fracture toughness demand under monotonic loading, whereas the other was a continuum damage mechanics based model – specifically, the Stress-Weighted Damage Fracture Model – SWDFM, Smith et al., (2021) which is able to characterize the damage under cyclic loading and Ultra Low Cycle Fatigue (ULCF – Kanvinde and Deierlein, 2007) which occurs during earthquake type loading. Both these measures were used for the details with the ESW, which has a relatively sharp notch as shown previously. Only the SWDFM was used for the simulation models without the ESW (i.e., those summarized in Table 3.2) because these do not contain a sharp notch, and are subject to large scale yielding over the groove weld region. The calibration and implementation of these fracture measures is now described:

1. The contour J-integral (Rice, 1968) was determined for each of the notch tips produced by the containment plates. The J-integral (denoted J_I – where the subscript denotes Mode-I crack opening) is an indicator of the crack driving force or fracture toughness demands produced by

the notch under monotonic loading. Consequently these calculations are performed only for the monotonic cases. Specifically, the J-integral contours are determined along multiple locations along the front of the notch, which extends along the length of the ESW weld. At each of these locations, standard procedures (implemented within ABAQUS 2020) were used to determine J_I; a total of 7 contours were used to achieve a stable value of J_I, following best practices outlined by Jhunjhunwala and Kanvinde (2023). The J-integral determined in this manner may be converted to an equivalent stress-intensity factor K_I, as per the relationship below:

$$K_I = \sqrt{\frac{EJ_I}{(1-\nu^2)}} \tag{2}$$

Where the term ν represents the Poisson's ratio (taken as 0.3 for steel), and E is the elastic modulus. For the simulations conducted in this study (i.e., considering all the parameter sets), the value of K_I at any location along the crack front was in the range of 45-100 $MPa\sqrt{m}$ at an applied equivalent interstory drift of 4%. This is lower than typical K_{IC} values for steel base as well as weld materials (including ESW welds) that are in the range of 80-180 $MPa\sqrt{m}$. These, in turn are based on CVN material testing from the UCSD specimens (converted to equivalent K_{IC} values using the Barsom, 1999 correlation – as per a process outlined by Jhunjhunwala and Kanvinde, 2023). This preliminary comparison suggests that from a pure fracture mechanics standpoint, the toughness demands produced by the notch are somewhat unlikely to directly produce fracture under monotonic loading. This was examined more rigorously using a weakest link approach that determines the probability of failure of the weld considering that properties may vary along the length of the weld, with the weakest-link controlling. The approach is based on work by Beremin (1983), and Wallin 1985, synthesized by Jhunjhunwala

and Kanvinde (2023). As per this approach, the probability of fracture at any location along the crack front may be expressed as:

$$P_f = 1 - \exp\left\{-\int_0^{L_{ESW}} \left(\frac{K_I(x) - K_{\min}}{K_0 - K_{\min}}\right)^4 dx\right\} \quad (3)$$

In the above equation $K_I(x)$ denotes toughness demand at any location x along the length of the ESW, which is denoted L_{ESW}. The term K_0 is a parameter in the Weibull distribution and connotes fracture toughness with 63.2% fracture probability of exceedance, the term $K_{\min}$ refers to a lower threshold for fracture toughness. The values for these parameters were taken as $K_{\min}$ = 20 $MPa\sqrt{m}$, K_0 = 178 $MPa\sqrt{m}$. These are representative values based on work by Jhunjhunwala and Kanvinde (2023). When processed in this manner, the probabilities of failure (considered across all the simulations) at an interstory drift of 4% was in the range of 0.08-10.8%. This further suggests that fracture of the detail under monotonic loading, without pre-accumulated damage is unlikely. In fact, experimental data from both the United States (Lee et al., 2016) and Taiwan (Tsai et al., 2020) appears to corroborate this, wherein fracture was observed only after significant cyclic loading, even if the net stress (or load) demands do not increase from cycle to cycle.

2. While the J-integral is an indicator of the crack driving force (or energy release rate) ahead of sharp crack under monotonic loads, it is not a valid index to assess fracture under cyclic loads that cause Ultra Low Cycle Fatigue (ULCF - Kanvinde and Deierlein, 2007), which occurs under seismic loading (and the cyclic loading histories applied to the models). Continuum damage mechanics models have been shown to predict ULCF fracture (Kanvinde 2017, Berdin and Besson et al. 2004) with good accuracy. In this study, one such model, i.e., the Stress Weighted Damage Fracture Model (SWDFM – Smith et al. 2021) is used to assess fracture.

The SWDFM is based on the micromechanics of ULCF, and has been extensively validated against both coupon (Smith et al., 2021) and full-scale (Zhu et al., 2021) test data and unlike the J-integral, the SWDFM is determined at each continuum location in the vicinity of the notch tip, as well as over the entire joint, and is able to track the progression of damage during cyclic loading. Specifically, the SWDFM predicts ULCF fracture to initiate if:

$$D = C_{\mathrm{SWDFM}} \int_0^{\varepsilon_p} (2\exp(1.3T) - \exp(-1.3T)) \exp[k_{\mathrm{SWDFM}}(|X| - 1)]\, d\varepsilon_p \geq 1 \quad (4)$$

In the above equation D represents the damage which must exceed unity over a material length scale defined by the parameter l^*, usually taken as 0.1mm, based on numerous studies (Kanvinde and Deierlein, 2008, Ziccarelli et al., 2023). The damage is determined by numerically integrating the function on the right hand side of Equation (4) above that weighs two stress invariants – the stress triaxiality $T = \sigma_m/\sigma_{eff}$ (the ratio of the mean stress σ_m to the von Mises stress σ_{eff}) and the Lode parameter X over the entire loading history. The Lode parameter is related to J_3 - the third invariant of the stress tensor and J_2 (the second invariant), such that $X = 3\sqrt{3} \cdot J_3 / (2 \cdot J_2^{3/2})$, distinguishing shear stress states from axisymmetric ($X = \pm 1$) to plane strain ($X = 0$). The terms C_{SWDFM} and k_{SWDFM} are material parameters that must be calibrated to test data using coupon tests. Since such coupon data is not available for this study, best estimates of the C_{SWDFM} and k_{SWDFM} parameters are developed based on previous studies. For ESW welds, Tsai et al., (2020) report parameter calibration for a continuum damage mechanics model (the Cyclic Void Growth Model - CVGM) developed previously by Kanvinde and Deierlein (2007). The SWDFM is a major improvement over the CVGM capturing the effect of the Lode parameter which the CVGM does not (see a comparative analysis between the two models by Smith et al., 2021). However, an equivalence between

parameters may be established by equating the damage functions for both models over the stress histories used in the calibration tests. Such an exercise yields a value of $C_{\text{SWDFM}} = 0.907$; this is conducted for the Heat Affected Zone (HAZ) which is determined to be the least tough material as per testing by Tsai et al. (2020). This is also the region where ULCF fracture initiates and propagates in the tests considered in this study – e.g., see Figure 2.2. Similar calibration studies were conducted by Myers et al., 2009 for the HAZ in toughness rated FCAW groove welds that reflect post-Northridge construction (e.g., see AISC 341-22). Based on these calibration studies the C_{SWDFM} value is estimated as 0.399. The parameter k_{SWDFM}, which controls the Lode dependence, cannot be independently calibrated from these studies, since they all feature axisymmetric specimens for which $X = 1$ (i.e., there is only one value of X). Consequently, a characteristic value of X based on literature (Smith et al., 2021) is used in this study for both the FCAW and the ESW materials. The subjectivity in estimating these parameters is acknowledged. Nonetheless, this is deemed acceptable in the context of this study because: (1) the overarching aim of the study is to examine the fracture susceptibility of different details in relative, rather than an absolute sense, and (2) a range of fracture parameters (in the vicinity of the best estimates) is used to conduct a sensitivity study which is used to support the interpretation of results. Note that the SWDFM is monitored only for the cyclic simulation runs, because the damage from SWDFM is extremely low if the connection is loaded monotonically.

Table 4. 1 Material constitutive parameters

Input Material Properties (Abaqus)	Beam	Column	Continuity Plates	ESW	HAZ
Yield Stress, F_y (MPa)	410	412	427	464	489
Q_∞ (MPa)[1]	89.6	130	130	103	103
b[2]	12.0	7.69	7.69	5.00	5.00
C (MPa)[3]	3376	3318	3318	1450	2140
γ[4]	20.0	16.9	16.9	8.00	11.5

[1] Maximum possible increase in yield surface size under isotropic hardening

[2] Parameter controlling the rate of increase of the yield surface under isotropic hardening with respect to equivalent plastic strain

[3] Parameter controlling linear kinematic hardening

[4] Recall term controlling the saturation value of kinematic hardening

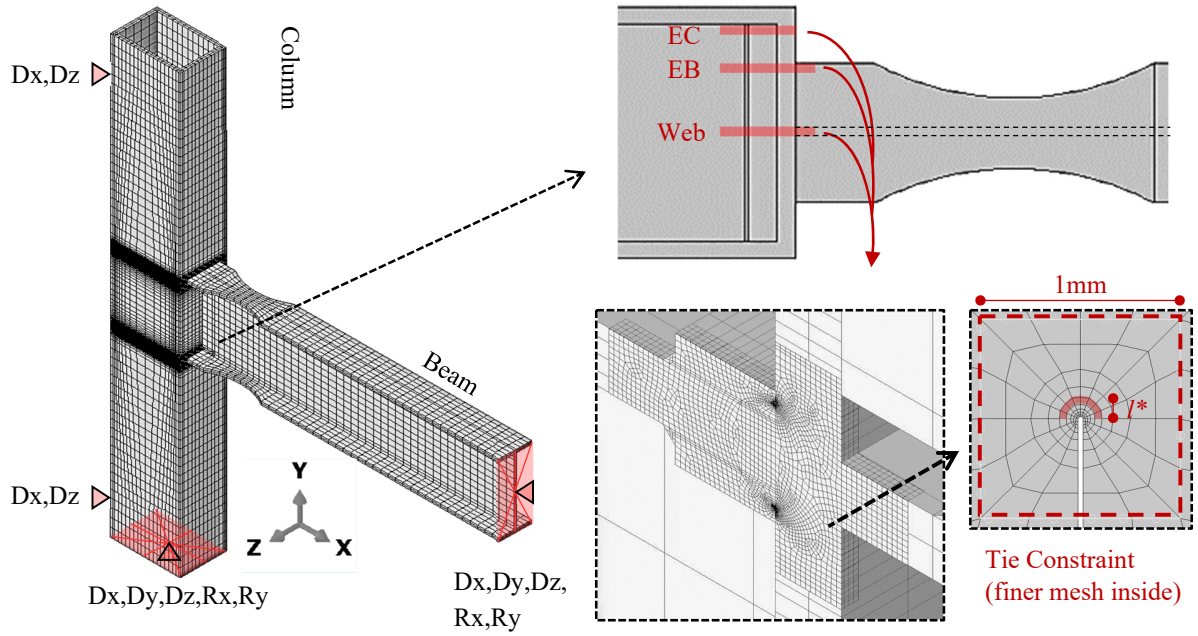

(a) (b)

Figure 4. 1 – Continuum Finite Element Models (a) Global model showing boundary conditions, and (b) Local model

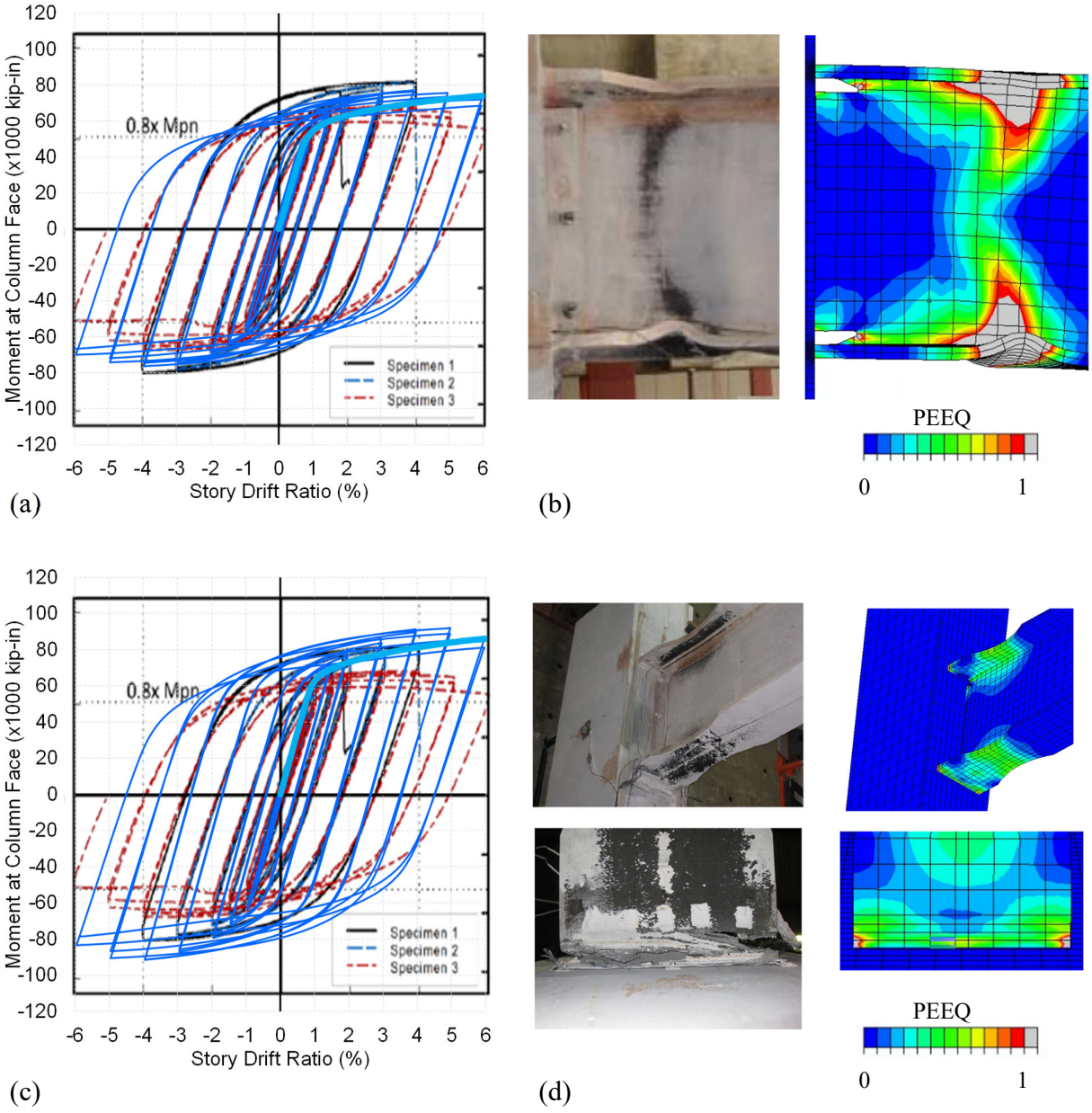

Figure 4. 2 – Comparison between simulation and experimental data (a) Load deformation response of UCSD Test #3, (b) deformations and plastic strains at instant shown by circle marker (c) Load deformation response of UCSD Test #1, (c) deformations and plastic strains at instant shown by circle marker

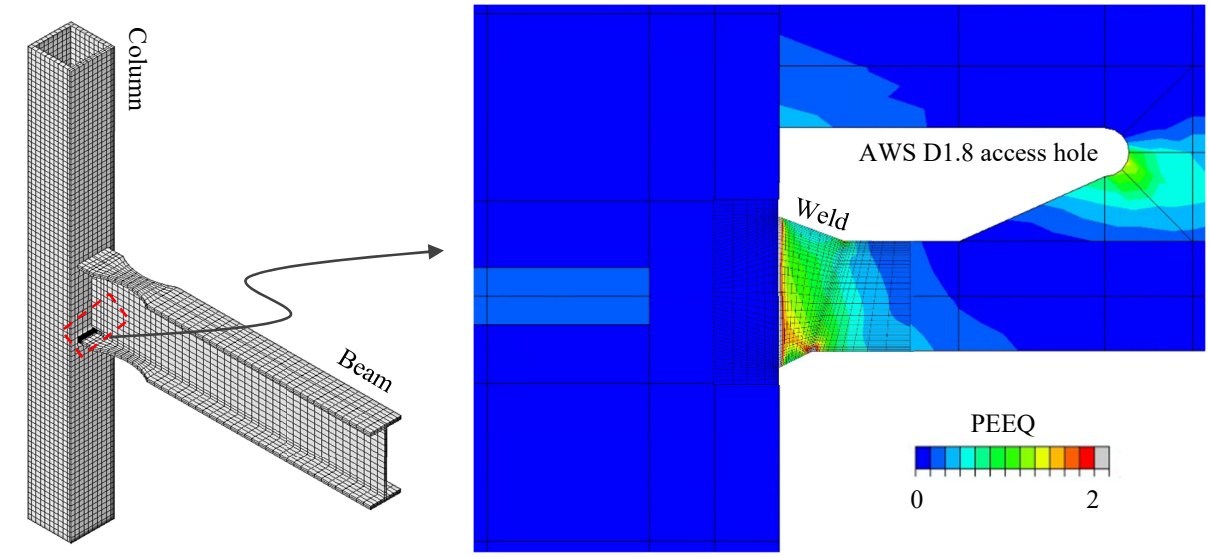

(a) (b)

Figure 4. 3 – Continuum Finite Element model of simulations to examine fracture toughness demands in beam flange to column groove weld outside the box column

CHAPTER 5
RESULTS AND DISCUSSION

Figure 5.1 plots the evolution of damage one of the simulations (from Table 3.1), using the parameters above. Each curve represents a location through the width of the ESW weld. Within each curve, the plotted damage represents the damage D as determined from Equation (4) at distance of l^* from the notch tip in the angular direction where it is the maximum. This respects the SWDFM criterion including the characteristic length. While shown in Figure 5.1 for the details with the ESW weld (i.e., from Table 3.1), similar damage evolution plots are also generated for the simulations where the outside groove weld is investigated (i.e., from Table 3.2). For the ESW simulations, the damage is monitored at three locations along the ESW weld (these are termed Web, EB, and EC – see Figure 4.1) for the cases where the beam flange is less wide as compared to the column flange; these are distinguished by the square, triangle, and circle marker respectively in Figure 5.1d. When the beam flange is as wide as the column flange, damage at only two locations (i.e., Web and EB) are monitored. Referring to Figure 5.1c and d, the damage at EB locations tends to be higher than that at Web and EC. This is due to a stress concentration that occurs due to the out-of-plane bending of the column wall, and the discontinuity introduced by the edge of the beam flange. Figure 5.1c also indicates the damage corresponding to the end of the 4% drift loading cycles in the loading protocol. This instant in the loading history is particularly relevant, because the 4% drift is associated with acceptance criteria for moment connections as per AISC 341-22 (80% moment strength must be maintained at this value). The damage values at this instant are retained and denoted $D_{4\%}^{web}$ for the damage at the center (i.e., in line with the web) and $D_{4\%}^{EB}$ for damage at edge of the beam, and $D_{4\%}^{EC}$ for damage at edge of the column. Similar damage

evolution curves are generated for the simulations shown in Table 3.2 as well. In these, the damage is monitored at every location along the groove weld, and the highest value at any instant is recorded. Similar to the ESW simulations, damage values $D_{4\%}$ are recorded for these simulations as well. For these simulations, the damage tends to be higher at edge of the groove weld (i.e., near the tip of the flange).

A comparison of the $D_{4\%}$ values across the various configurations provides a direct way to assess the fracture vulnerability of various details both in an absolute sense, and also relative to each other in the context of acceptance criteria for such connections. To this end, Figures 5.2a-g plot the damage terms $D_{4\%}^{Web}$, $D_{4\%}^{EB}$ (and $D_{4\%}^{EC}$ where applicable) against each parameter of interest shown in Table 3.1 (i.e., for the ESW welds). A similar figure is plotted later for the simulations in Table 3.2. Each subfigure evaluates the effect of a single parameter. For example, Figure 5.2a plots the damage values $D_{4\%}$ against the different types of bevel detail. The bars of similar color indicate configurations that are otherwise identical, except for the primary variable plotted on the horizontal axis; consequently, a comparison between bars of the same color isolates the effect of the primary variable. The points on each bar represent the damage at different locations (Web, EB and EC) for each of the simulation. Referring to Figures 5.2a-g, some parameters clearly have a much larger effect on the fracture toughness demands. Table 3.1 also includes information regarding the drift at which the damage first exceeds 1.0 at each location, indicating the drift at which fracture would initiate. Based on Table 3.1 and Figures 5.2a-g, the following observations may be made:

- Referring to Figure 5.2a, the type of containment plate bevel detail has a major effect on the fracture toughness demand. Specifically, the conventional containment plate, without the

bevels results in damage at all locations along the flange, that is 2-5 times larger than both B1 and B2 (i.e., the US and Taiwan bevels). Note however, that the simulations only capture the geometric differences between the bevels, and not material effects that may be generated due to different cooling rates (e.g., between bevel B1 with the shims, and B2 without). Further, the absolute values of the damage indicate that only the B1 and B2 conditions are even viable, i.e., the damage is in the neighborhood of 1. This is consistent with experimental data in the US (see Figure 2.2b shown earlier) which indicates the initiation of fracture in every specimen that has been tested in the United States, with these details.

- An examination of the last three columns of Table 3.1 indicates that in most specimens, fracture initiates (i.e., the damage exceeds 1.0) for drifts in the range of 0.5% to 6% (with a median value of 2%). This suggests early initiation of fracture in most of the simulations. In fact, the only simulation where the fracture initiation drift is greater than 4.0% at all locations is Simulation #14 (in which the damage remains below 1.0 for the entirety of loading). In this simulation, the beam flange width and the column width are exactly the same. In general, this is difficult to achieve in practice. However, from a behavioral standpoint, this appears to be extremely beneficial because it prevents the out of plane bending of the column wall and greatly mitigates the stress concentration shown previously in Figure 5.1d. In fact, as noted in Figure 5.1b, this results in a uniform damage throughout the length of the ESW, which is by far the lowest among all the simulations. This suggests that stiffening the column flange from the outside, either having a wide beam flange or other details should be explored as a means to improve connection performance.
- Referring to Figure 5.2b, the eccentricity of the weld bulb has a major effect on the toughness demands as well – i.e., an eccentric bulb (with e = 10mm) produces demand that are nearly 3-

6 times the centered bulb. This does not consider the eccentricity of the continuity plate with respect to the beam flange, which (as shown by Tsai et al. 2020) has an even larger influence on toughness demands – indicating that alignment tolerances for both the continuity plate and the weld itself are critical for a successful connection detail.

- The use of the RBS detail to reduce stress demands at the ESW also appears to be a highly effective strategy, such that the reduction in the Z_{RBS}/Z from a value of 1.0 (i.e., a WUF-W connection) to 0.62 results in a decrease of damage values by 40-50%.
- Three parameters have only a modest influence on fracture toughness demands. These include: (1) the weld access hole detail with the AWS D1.8 detail resulting in slightly lower toughness demand as compared to the AISC360 detail, (2) the beam depth – see Table 3.1, and (3) the column size – see Table 3.1. Of these, the insensitivity to column size is particularly important because currently, column depths in box column connections are limited to 24 inches (610 mm), mainly because test data for larger columns does not yet exist. The simulations indicate that increasing the column size does not result in a significant change in fracture toughness demands. This provides support for larger column sizes that may reduce material costs by reducing plate thickness.

In summary, the simulation results suggest that the most favorable conditions for fracture may be achieved through a combination of: (1) using improved bevel details, i.e., either the B1 or B2 type, (2) reduction of demands using RBS details, (3) maintaining strict tolerances for alignment between the plates and weld bulb eccentricity with respect to the plates, and (4) using beams with flanges that are as wide as the columns. Additionally, the use of improved weld access hole details is somewhat useful. It is useful to study the most favorable combination of parameters for which test data exists – this combination corresponds to Simulation #6 (from Table 3.1, which

corresponds to UCSD Test #3). For this condition, $D_{4\%}^{web}$ is 0.79 and $D_{4\%}^{EB}$ is 1.8. In the context of these observations, it is noted that:

- Despite favorable parameters from a geometric standpoint, the presence of the notch effect (in combination with the local material toughness properties) is likely to initiate ductile (or ULCF) type fracture at some point in the ESW, even if it does not propagate. This is consistent with experimental response in which all tests showed some extent of ductile initiation and propagation. It is noted that the transition of these ductile cracks to brittle cleavage is a random process (Beremin 1983), whose probability grows as the ductile crack propagates. In two out of the three tests conducted at UCSD, such propagation occurred.
- It is important to note that the values of damage listed in Table 3.1, and shown in Figures 5.2a-) use a single set of values for the SWDFM material parameters (i.e., C_{SWDFM} = 0.907, k_{SWDFM} = 0.5) based on best estimates. To assess the sensitivity to these, Figures 5.3a and b plot the value of damage at 4% (for Simulation #6 – the trends for other simulations are similar), i.e., $D_{4\%}$ against the C_{SWDFM} for three different values of k_{SWDFM}. Figure 5.3a plots the damage at the centerline location, whereas Figure 5.3b plots the damage at EB location. The range of C_{SWDFM} shown in these figures as well as the values of k_{SWDFM} represent the typical values noted in literature for similar steel materials (ref Zhu et al., 2021). Also indicated in these figures are the values used to determine the damage values shown in Figures 5.1, 5.2 and 5.4. Referring to these figures, it is evident that the damage is fairly sensitive to the selection of material parameters. This has two implications. First, is it important to characterize local material properties with accuracy for effective simulation and prediction of fracture performance. Second, and perhaps more important is that (in addition to improvement of geometric parameters) the enhancement of local material toughness (e.g., through filler metal

selection) or weld-process modification has the potential to significantly limit the potential for fracture.

The results of the simulations to examine the necessity of the continuity plate are shown in Table 3.2 (last column) and Figure 5.4. Table 3.2 shows the value of the damage $D_{4\%}$ determined for each of the simulations; this is the maximum value at any location along the length of the groove weld, i.e., the width of the beam flange. In general, the maximum damage for both the simulations with and without the continuity plate occurs at the edge of the beam flange. From the last column of Table 3.2, it is immediately apparent that the damage in configurations with the continuity plate is generally lower than the damage without the continuity plate. Further, it is apparent that the damage values for the configurations with continuity plate are lower than 1.0 (i.e., the groove weld is generally not susceptible to fracture) except for #17. Figure 5.4 plots the ratio of these two damage values (i.e., without and with continuity plate) for each of the configurations that are otherwise identical. These ratios are plotted against the ratio $t_{cf}/t_{cf-WF}^{\text{AISC}}$ which indicates how thick the column flange is, relative to the AISC limit (for wide-flanged beams – AISC 341-22) at which the continuity plate is not required. This data is plotted for the two values of the continuity plate thickness (i.e., $t_{bf}/2$ and t_{bf}). Note that the former is the requirement for single sided connections as per AISC 341-22, but the latter (i.e., thicker continuity plate) is provided as an additional parametric variable, recognizing that the stress flow in box columns may be more adverse because the column web is not present behind the beam web. Referring to the figure, a clear trend is noted between the ratio $D_{4\%}^{no-plate}$ and $D_{4\%}^{plate}$ for all the configurations, i.e., combinations of beam size and continuity plate thickness (suggesting that the trend itself is independent of the configuration). Specifically, as the t_{cf} increases, the ratio $D_{4\%}^{no-plate}/D_{4\%}^{plate}$ approaches 1.0, indicating that the continuity plate has a decreased effect on lowering the strains

(a value close to 1.0 indicates that the continuity plate is not needed). Interestingly the at the $t_{cf}/t_{cf-WF}^{\text{AISC}}$ value of 1.0, the $D_{4\%}^{no-plate}/D_{4\%}^{plate}$ is in the range of 2.4 to 4.4. This suggests that criteria for the use of continuity plates in wide flanged sections may not be applicable to box column connections. This is not unexpected, because unlike beam-column connections with wide-flanged columns, the box columns do not include a web directly in line with the beam web, resulting in a more adverse stress flow from the beam to the column flange. An examination of Figure 5.4 indicates that for both continuity plates with thickness $t_{bf}/2$ (the minimum required for wide-flanged column connections) as well as t_{bf}, the ratio $D_{4\%}^{no-plate}/D_{4\%}^{plate}$ approaches 1.0, only as $t_{cf}/t_{cf-WF}^{\text{AISC}}$ approaches 2.0. This suggests that for box column connections, the continuity plate requirement may need to be significantly more stringent as compared to wide-flanged column connections.

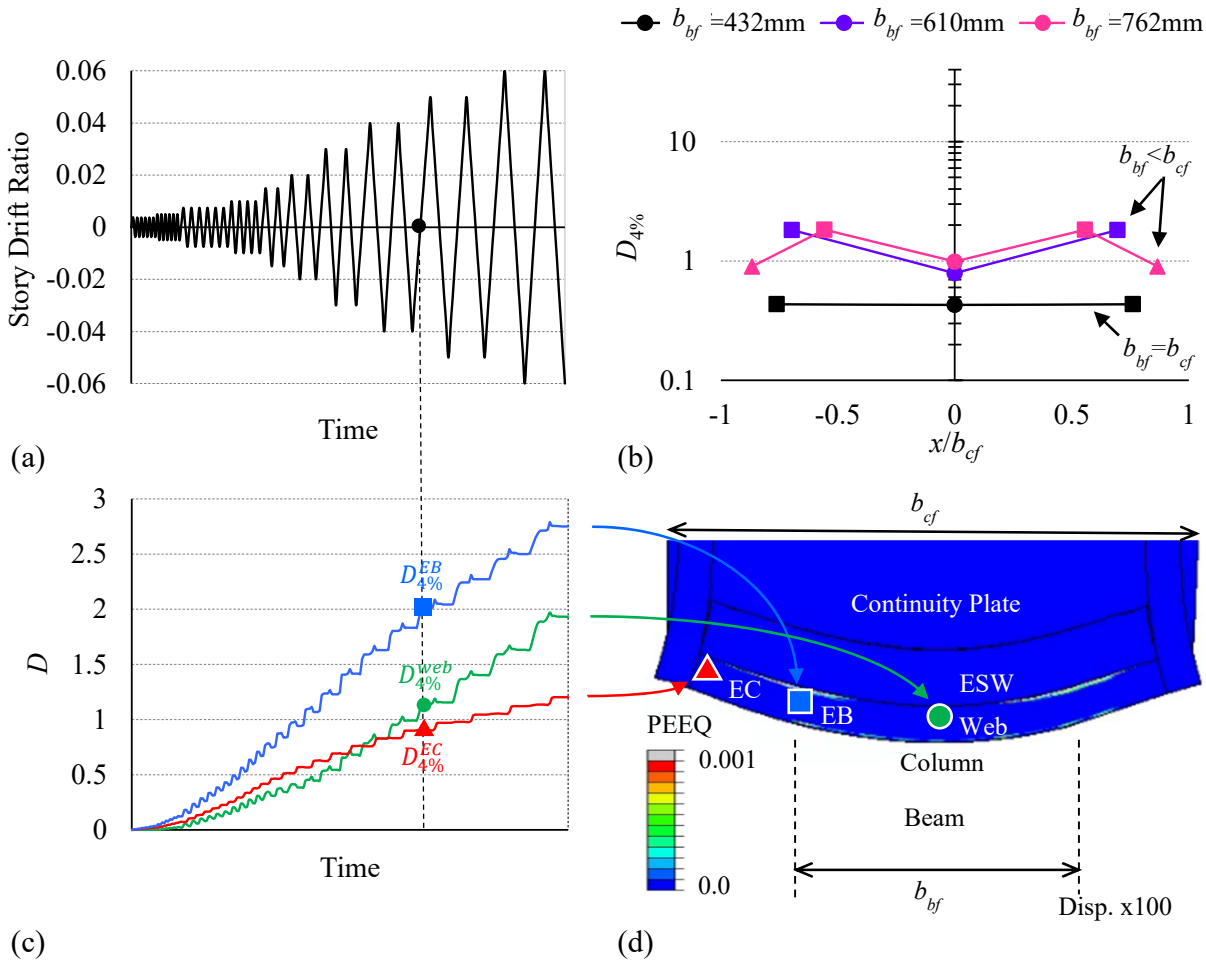

Figure 5. 1 – Damage evolution in ESW weld (a) loading protocol, (b) damage profile through the weld length at 4% drift, (c) temporal evolution of damage (d) locations at which damage is recorded

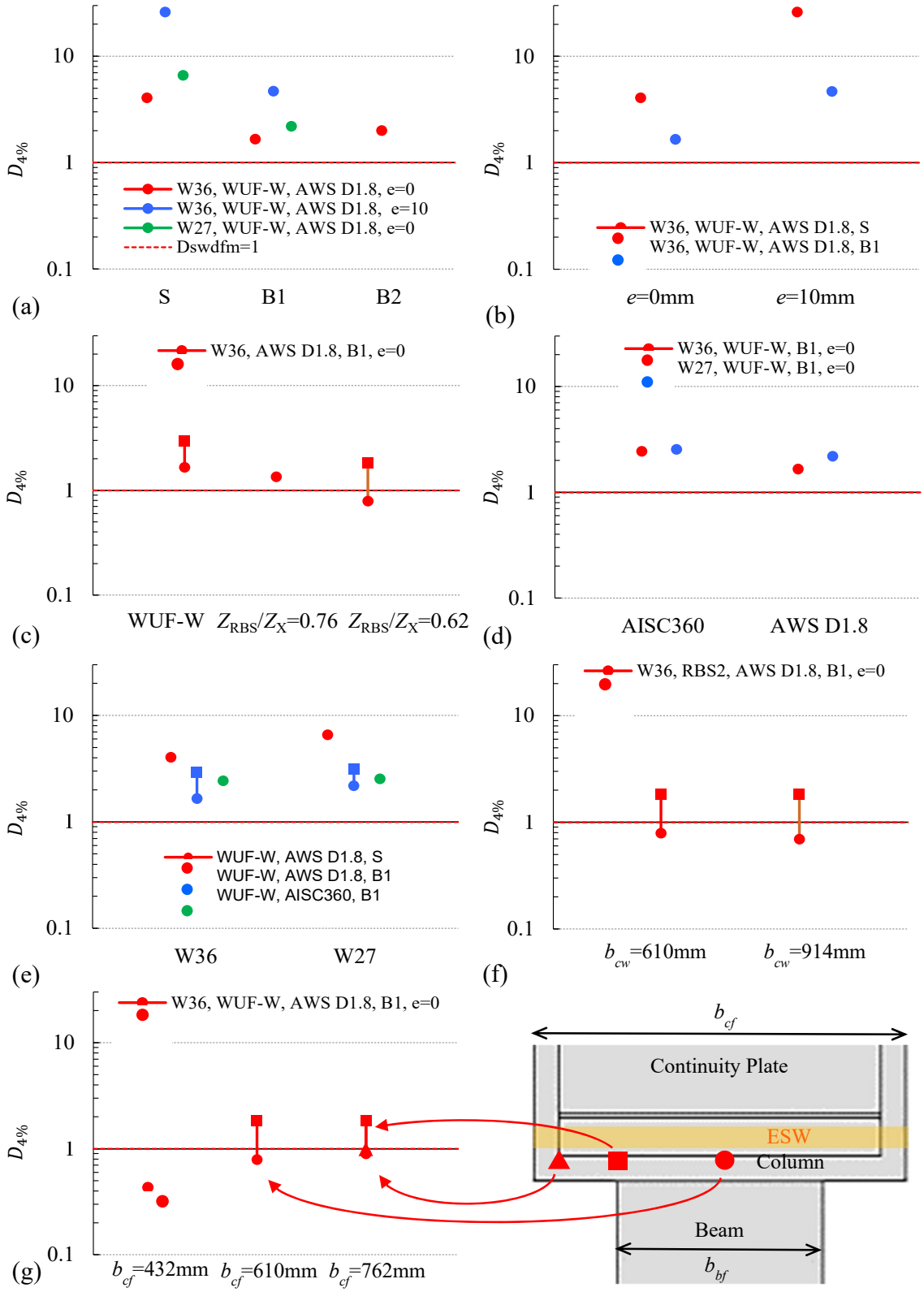

Figure 5. 2 – The damage at 4% drift plotted against parameters of interest (a) bevel detail (b) weld bulb eccentricity (c) section reduction (d) WAH detail (e) beam size (f) column depth (g) column width

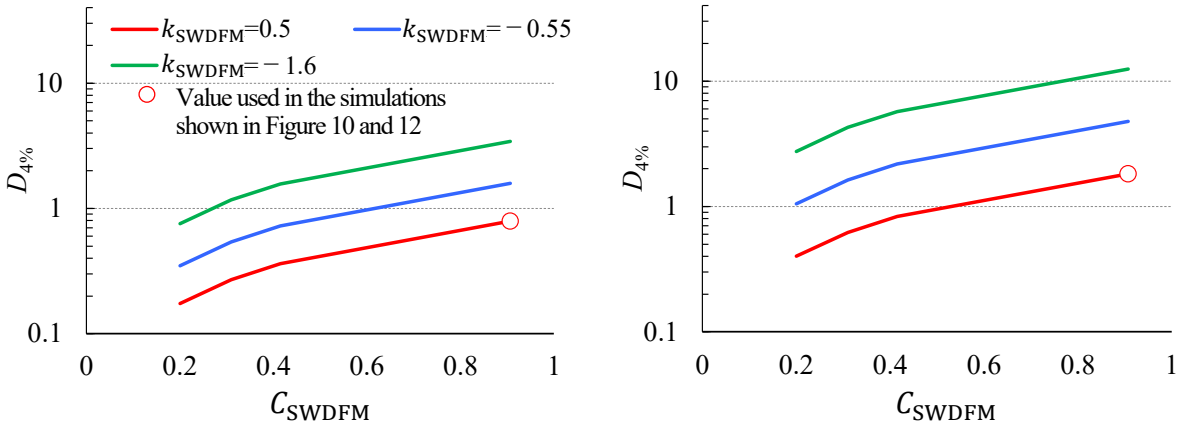

Figure 5. 3 – Sensitivity of estimated damage to material parameters of the SWDFM at two locations: (a) Location Web (b) Location EB

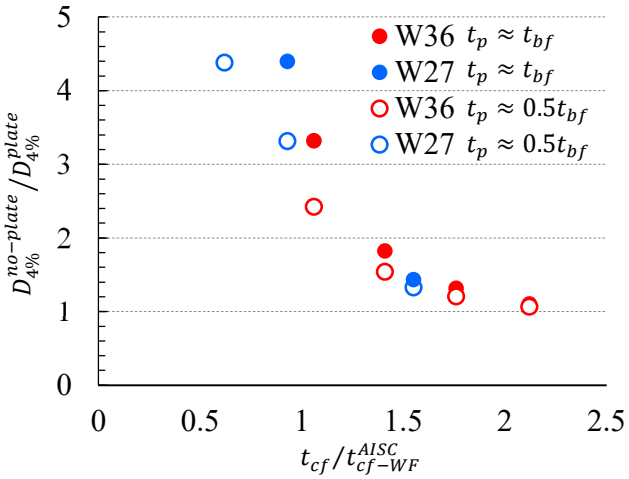

Figure 5. 4 – Effect of column flange (wall) thickness on fracture toughness demand relative to condition with the continuity plate

CHAPTER 6
SUMMARY, CONCLUSIONS AND LIMITATIONS

Beam to box column connections in seismically designed SMF buildings present special challenges that are not encountered in wide flanged column connections. These arise from the need to weld the continuity plate to all four sides of the box column from the inside. Electroslag welding is commonly used to weld the fourth side of the continuity plate after the column box is closed. The ESW process requires containment plates that create stress concentrations, and also results in lower toughness material due to high heat input. A combination of these factors raises concerns about the seismic performance of these connections, and places significant limitations on their use. However, due to the design economies provided by box columns, there is professional motivation to engineer box column to beam details that provide satisfactory seismic performance. Thus far, the experimental performance of these connections has been mixed, such that guidance for designing and fabricating prequalified or prescriptive connection details does not yet exist. Developing such guidance requires the synthesis of experimental as well computational research, professional insights, and development of weld procedure and fabrication techniques.

Within this overall context, the main objective of this study is to present results of a finite-element based parametric study that examines the relationship between configuration or geometric parameters that can be controlled in design, and fracture toughness demands. Two sets of simulations are conducted – one set investigates the effect of various parameters on toughness demands in the ESW detail, whereas the second set examines under what conditions it may be feasible to avoid the continuity plate (and the associated problems) altogether. A continuum damage mechanics based fracture index (i.e., the Stress Weighted Damage Fracture Model –

SWDFM) is used an indicator of ULCF-induced damage, and the potential for fracture. The main insights from the simulations with the ESW welds include the following:

- In terms of design variables, using an improved bevel detail, and utilizing a Reduced Beam Section (RBS) detail significantly reduces the fracture toughness demands. Additionally, specifying a column width equal to the beam flange width has the greatest potential for reducing demands because this minimizes out of plane bending of the column wall plate. However, this may not be feasible in a practical setting.
- The eccentricity of the weld bulb has a major, adverse effect on the fracture toughness demands; this is because the notch size increase as the weld bulb moves to one side. A similar dependency on the eccentricity between the continuity plate and the beam flange was noted previously by Tsai et al., (2020). The implication is that weld tolerances are especially important in ESW welds in seismic box-column connections.
- Some variables (the weld access hole configuration, as well as beam and column size) were found to have only a minimal effect on fracture toughness demands. Of these, the insensitivity to column size has important design implications because current guidelines limit both the beam and column size.
- The damage is also highly sensitive to the assumed fracture toughness capacity, indicating that improvement of welding processes and materials will have a significant impact on connection performance.

The key finding from the simulations without the continuity plate is that current guidelines for the use of continuity plates (based on the flange thickness of wide-flanged columns) may be inapplicable to box columns; this is attributed to the absence of the column web in line with the beam web which results in an adverse stress flow from beam to column. The simulations suggest

that using a column thickness limit two times as large as the current limit for wide-flanged sections may result in acceptable performance, i.e., damage comparable to connections with a continuity plate.

It is important to interpret the results of this study in the context of its limitations, which are numerous. First, this is a finite element based parametric study, and this results in significant idealizations about geometric tolerances and imperfections – for example, the representation of the containment plate notch as a sharp crack. The material properties (particularly the fracture toughness properties) are only estimates based on published literature, rather than direct measurements of these properties – although this is addressed to an extent through a sensitivity study. In this regard, some effects are not modeled – e.g., the effect of shim plates (as in bevel B2) is modeled only in terms or geometry, but not its effect on material properties. However, variations in material microstructure over small scales and even slight variation in the locations of these microstructures with respect to local stress concentrators such as the notches may result in significantly difficult results. Additionally, the continuum damage mechanics based model to represent ULCF itself is prone to a degree of error, both in calibration, as well as in application, owing to effects such as mesh sensitivity of near-tip crack fields. In light of these limitations, possibly the most useful interpretation of the results is in a relative sense, wherein the fracture susceptibility of different configurations may be assessed relative to one another, rather than in an absolute sense (e.g., the estimated drift or deformation at fracture). The expectation is that such relative assessments, and the qualitative insights provided by this study will support further development of experimental specimen configurations, as well as weld processes and materials that ultimately result in greater confidence in these connections.

NOMENCLATURE

a, b, c	-	Dimensions of RBS
b	-	Parameter controlling the rate of increase of the yield surface under isotropic hardening with respect to equivalent plastic strain
b_{bf}	-	Beam flange width
b_{cf}	-	Column flange width
b_{cw}	-	Column web width
C	-	Parameter controlling linear kinematic hardening
C_{SWDFM}	-	Material parameter calibrated using coupon tests for SWDFM
D	-	Damage
$D_{4\%}$	-	Damage corresponding to the end of the 4% drift loading cycles
$D_{4\%}^{web}$	-	$D_{4\%}$ at the center (i.e., in line with the web)
$D_{4\%}^{EB}$	-	$D_{4\%}$ at edge of the beam
$D_{4\%}^{EC}$	-	$D_{4\%}$ at edge of the column
$D_{4\%}^{plate}$	-	$D_{4\%}$ when there are continuity plates
$D_{4\%}^{no-plate}$	-	$D_{4\%}$ when there is no continuity plate
e	-	Eccentricity of ESW
E	-	Elastic modulus
F_y	-	Yield stress
F_{yb}	-	Expected yield strengths of the beam
F_{yc}	-	Expected yield strengths of the column
J_I	-	J-integral (Rice, 1968)

Nomenclature

J_2	-	Second invariant of the stress tensor
J_3	-	Third invariant of the stress tensor
k_{SWDFM}	-	Material parameter calibrated using coupon tests for SWDFM
K_I	-	Stress-intensity factor
$K_I(x)$	-	Toughness demand at any location x along the length of the ESW
K_0	-	Parameter in the Weibull distribution and connotes fracture toughness with 63.2% fracture probability of exceedance
$K_{\min}$	-	Lower threshold for fracture toughness
l^*	-	Characteristic length
L_{ESW}	-	Length of the ESW
P_f	-	Probability of fracture at any location along the crack front
Q_∞	-	Maximum possible increase in yield surface size under isotropic hardening
t_{bf}	-	Beam flange thickness
t_{cf}	-	Column thickness
t_p	-	Continuity plate thickness
$t_{cf-WF}^{\mathrm{AISC}}$	-	Requirement for W-section column that AISC 341-22 indicate continuity plates are required unless the column flange thickness is greater than the t_{cf}^{AISC}
T	-	Stress triaxiality= σ_m/σ_{eff}
X	-	Lode parameter
Z_{RBS}	-	Plastic section modulus of RBS
Z_X	-	Plastic section modulus of WUF-W
γ	-	Recall term controlling the saturation value of kinematic hardening

Nomenclature

ε_p	-	Equivalent plastic strain, PEEQ
ν	-	Poisson's ratio
σ_m	-	Mean stress
σ_{eff}	-	Von Mises stress

REFERENCES

Barsom, J. M., and S. T. Rolfe. 1999. Fracture and fatigue control in structures: Applications of fracture mechanics. West Conshohocken, PA: ASTM.

Berdin C, Besson J. Local Approach to Fracture. Les Presses de Ecole des Mines. Paris (France); 2004.

Beremin, F., A. Pineau, F. Mudry, J.-C. Devaux, Y. D'Escatha, and P. Ledermann. 1983. "A local criterion for cleavage fracture of a nuclear pressure vessel steel." Metall. Trans. A 14 (11): 2277–2287. https://doi

.org/10.1007/BF02663302.

Chen CC, Lai CL, Lin KC. Finite Element Analysis of Electro-Slag Welding for Diaphragms in Steel Box Column. Proceedings, The Eleventh Taiwan-Korea-Japan Joint Seminar on Earthquake Engineering for Building Structures SEEBUS 2009, Kyoto, Japan, 2009.

Chen CH, Lin KC, Jhuang SJ, Chang HY. Seismic performance evaluation of steel box-column connections with ESW stiffeners. Int J Steel Struct. 2020;766–776. https://doi.org/10.1007/s13296-020-00321-9

Eleventh Taiwan-Korea-Japan Joint Seminar on Earthquake Engineering for Building Structures SEEBUS 2009, Kyoto, Japan, 2009.

Frederick, C. O., and Armstrong, P. J. (1966). A mathematical representation of the multiaxial bauschinger effect, Berkeley Nuclear Laboratories, Research and Development Dept., Berkeley, U.K.

References

David A. Padilla-Llano, Justin Ocel, Qualification of Electroslag Welds made from HPS 485W (70W) and 345W (50W) Steels, Journal of Constructional Steel Research, Volume 183,2021

Elkady, A., and D. G. Lignos. 2018. "Improved seismic design and nonlinear modeling recommendations for wide-flange steel columns." J. Struct. Eng. 144 (9): 04018162. https://doi.org/10.1061/(ASCE)ST .1943-541X.0002166.

Gilmer, Implementation of Narrow-Gap Improved Electroslag Welding for Bridge Fabrication, World Steel Bridge Symposium Conference Proceedings 2005

Japanese Society of Steel Construction, Guide Book to Prevent Brittle Fracture at an Electroslag Weld on the Inner Diaphragm, 2016

Jhunjhunwala, A., and Kanvinde, A.M., (2023 – in press). "Fracture Mechanics based fragility assessment of pre-Northridge welded column splices," Journal of Structural Engineering, American Society of Civil Engineers.

Kanvinde, A. M., and Deierlein, G. G. (2007). "A cyclic void growth model to assess ductile fracture in structural steels due to ultra low cycle fatigue." J. Eng. Mech., 10.1061/(ASCE)0733-9399(2007)133:6(701), 701–712.

Kanvinde, A. M., Fell, B. V., Gomez, I. R., and Roberts, M. (2008). "Predicting fracture in structural fillet welds using traditional andmicromechanics-based models." Eng. Struct., 30(11), 3325–3335.

References

Kanvinde, A. M., Marshall, K., Grilli, D., Bomba, G. (2014). Forensic Analysis of Link Fractures in Eccentrically Braced Frames during the February 2011 Christchurch Earthquake – Testing and Simulation. Journal of Structural Engineering, 141(5),

Kanvinde, A.M., (2017). "Predicting fracture in civil engineering steel structures: State of the Art," Journal of Structural Engineering, ASCE. 10.1061/(ASCE)ST.1943-541X.0001704.

Krishna K. Verma, Narrow-Gap Improved Electroslag Welding for Bridges, 2005

Lee, P., Garai, R., Tsui, A. and Hua, Y., Special Moment Frame Qualifications: RBS to Box Column, SEAOC 2016 Convention Proceedings.

Lin, K. C., & Jhuang, S. J. (2010). Seismic behaviors and design method on steel beam-to-box column connections with cover plate. Structural Engineering, 25(2), 75–92. (in Chinese).

McMeeking, R. M., and Parks, D. M. (1979). "On criteria for J-dominance of crack-tip fields in large scale yielding." Elastic Plastic Fracture, ASTM STP 668, West Conshohocken, PA, 175–194.

Myers, A.T., Deierlein, G., Kanvinde, A., Testing and Probabilistic Simulation of Ductile Fracture Initiation in Structural Steel Components and Weldments, Technical Report 170 John A. Blume Earthquake Engineering Center, Stanford University, CA, 2009 94305.

Rice, J. R., and G. F. Rosengren. 1968. "Plane strain deformation near a crack tip in a power-law hardening material." J. Mech. Phys. Solids 16 (1): 1–12. https://doi.org/10.1016/0022-5096(68)90013-6.

References

Ricles, J.M., Fisher, J.W., Lu, L.W. and Kaufmann, E.J. (2002), "Development of Improved Welded Moment Connections for Earthquake-Resistant Design," Journal of Constructional Steel Research. Vol. 58, pp. 565–604.

R.-S. Lin, H.-Y. Chung, M.-H. Lin, Analysis and Improvement for the Inherent Backing-Bar Crack Problem of Electrogas and Electroslag Welding in Box-Columns, Journal of the Chinese Institute of Civil and Hydraulic Engineering, Volume 24(2), 2012, Pages 169-183

Rice JR, Tracey DM. On the ductile enlargement of voids in triaxial stress fields. J Mech Phys Solids 1969;17(3):201–17.

Skiadopoulos, Andronikos & Lignos, Dimitrios. (2022). Proposed Backing Bar Detail in Welded Beam-to-Column Connections for Seismic Applications. Journal of Structural Engineering. 148. 10.1061/(ASCE)ST.1943-541X.0003374.

Smith, C.M., Deierlein, G., Kanvinde, A., A Stress-Weighted Damage Model for Ductile Fracture Initiation in Structural Steel under Cyclic Loading and Generalized Stress States, Technical Report 187 Stanford University, John A. Blume Earthquake Engineering Center, California, 2014.

Smith, C., Ziccarelli, A., Terashima, M., Kanvinde, A., Deierlein, G., A stress-weighted ductile fracture model for steel subjected to Ultra Low Cycle Fatigue, Engineering Structures, Volume 245, 2021, 112964, ISSN 0141-0296, https://doi.org/10.1016/j.engstruct.2021.112964.

References

Stillmaker, Kimberly & Kanvinde, Amit & Galasso, Carmine. (2015). Fracture Mechanics-Based Design of Column Splices with Partial Joint Penetration Welds. Journal of Structural Engineering. 142. 04015115. 10.1061/(ASCE)ST.1943-541X.0001380.

Tsai, C.-Y., K.-C. Tsai, C.-H. Li, C.-C. Wu, K.-C. Lin, and S.-J. Jhuang.2020. "Seismic fracture evaluation of diaphragm joints in welded beam-to-box column moment connections."Earthquake Eng. Struct. Dyn.49 (Jan): 1344–1362.https://doi.org/10.1002/eqe.3293.

Tsai KC, Lin KC, Jhuang SJ, Li CH, Lin CH. Research and practice on seismic design of welded steel beam-to-box column moment connections in Taiwan. Proceedings, the Third Announcement of Symposium on Future of Development of Seismic Design, Hong Kong, February 13, 2015.

Wallin, K. 1984. "The scatter in KIC-results." Eng. Fract. Mech. 19 (6): 1085–1093. https://doi.org/10.1016/0013-7944(84)90153-X.

Wallin, K. 1985. "The size effect in KIC results." Eng. Fract. Mech. 22 (1): 149–163. https://doi.org/10.1016/0013-7944(85)90167-5.

Wallin, K. 1993. "Irradiation damage effects on the fracture toughness transition curve shape for reactor pressure vessel steels." Int. J. Press. Vessels Pip. 55 (1): 61–79. https://doi.org/10.1016/0308-0161(93)90047-W.

Zhu, Y., Fell, B., Kanvinde, A., Continuum damage mechanics based ductile fatigue-fracture prediction in buckling steel braces, Journal of Constructional Steel Research, Volume 184, 2021, 106812, ISSN 0143-974X, https://doi.org/10.1016/j.jcsr.2021.106812.

References

Ziccarelli, Andy & Kanvinde, Amit & Deierlein, Gregory. (2023). Cyclic adaptive cohesive zone model to simulate ductile crack propagation in steel structures due to ultra‐low cycle fatigue. Fatigue & Fracture of Engineering Materials & Structures. 10.1111/ffe.13964.

APPENDIX
DETAIL OF ANALYSES

Loading sequence

- In addition to the loading sequence according to AISC341-16, two cycles of 0.05 rad and 0.06 rad were loaded.
- The time increment values were 0.001s at the beginning, 6.8E-7s at the minimum, and 0.1s at the maximum.

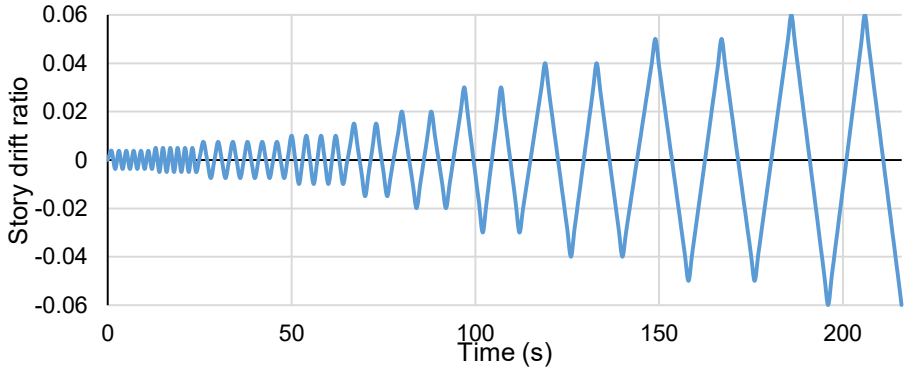

Fig A. 1 Loading Sequence

Overview of specimen (column length and beam length) Boundary conditions

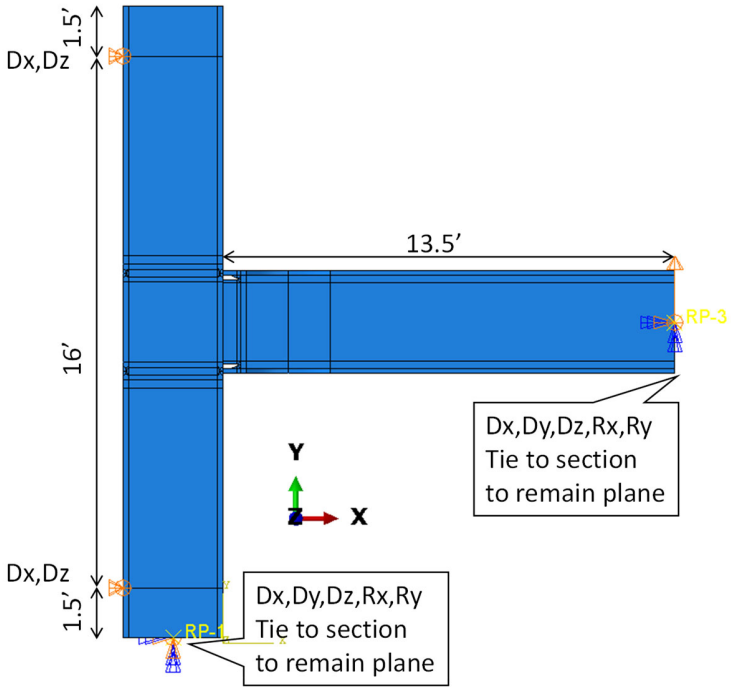

Fig A. 2 Column and Beam length and Boundary conditions

Appendix: Detail of Analyses

Element type

- The model consists only of solid elements. Twenty-node quadratic brick elements (C3D20*) were used near the connection (middle of column, ESW, beam end to RBS) with large deformation, and eight-node linear brick reduced-integration elements (C3D8R*) were used at other locations with small deformation.

* The name used in Abaqus 2020

Global model and submodel

- There are Global model and submodel (The analyses of Issue 3 don't have submodel)
- The boundary condition of submodel is global model's results.
- For the stability of analysis, The edge of slit is finer and have tie constraint to outer side.

Nonlinear material properties

Table A. 1 Nonlinear material properties

Input Material Properties (Abaqus)	Beam	Column	Continuity Plates	ESW	HAZ
Yield Stress, F_y (MPa)	410	412	427	464	489
Q_∞ (MPa)	89.6	130	130	103	103
b	12.0	7.69	7.69	5.00	5.00
C (MPa)	3376	3318	3318	1450	2140
γ	20.0	16.9	16.9	8.00	11.5
Q_∞	Maximum possible increase in yield surface size under isotropic hardening				
b	Parameter controlling the rate of increase of the yield surface under isotropic hardening with respect to equivalent plastic strain				
C	Parameter controlling linear kinematic hardening				
γ	Recall term controlling the saturation value of kinematic hardening				

Model:

$$\dot{\alpha} = \frac{C}{\sigma^o}(\sigma - \alpha)\dot{\varepsilon}^{pl} - \gamma\alpha\dot{\varepsilon}^{pl}$$

$$\sigma^o = \sigma_o|_0 + Q_\infty\left(1 - e^{-b\varepsilon^{pl}}\right)$$

Software

- Abaqus 2020

Appendix: Detail of Analyses

List of simulations

- The global model of Simulation 15 is used for simulation of specimen 1(2)
- The global model of Simulation 6(9) is used for simulation of specimen 3

Table A. 2 Simulation Matrix for Column Connections with the Internal Continuity Plate and ESW

#	Column	Beam Section	Access Hole	Z_{RBS}/Z_X	Conta-inment Plate	Ecce-ntri-city	b_{bf}/b_{cf}	Drift when D>1 (%)		
								Web	BE	CC
1	610x914	W36x302	AWS D1.8	1.0 [1]	S	e=0	0.70	0.75	-	-
2	610x914	W36x302	AWS D1.8	1.0 [1]	B1	e=0	0.70	3.00	1.00	-
3	610x914	W36x302	AWS D1.8	1.0 [1]	S	e=10	0.70	0.50	-	-
4	610x914	W36x302	AWS D1.8	1.0 [1]	B1	e=10	0.70	0.75	-	-
5	610x914	W36x302	AWS D1.8	0.76	B1	e=0	0.70	4.00	-	-
6	610x914	W36x302	AWS D1.8	0.62	B1	e=0	0.70	5.00	1.50	-
7	610x914	W36x302	AISC360	1.0 [1]	B1	e=0	0.70	2.00	-	-
8	610x914	W27x368	AWS D1.8	1.0 [1]	B1	e=0	0.74	2.00	1.00	-
9	610x914	W27x368	AWS D1.8	1.0 [1]	S	e=0	0.74	0.75	-	-
10	610x914	W27x368	AISC360	1.0 [1]	B1	e=0	0.74	2.00	-	-
11	610x914	W36x302	AWS D1.8	1.0 [1]	B2	e=0	0.70	2.00	-	-
12	610x914	W36x302	AISC360	0.76	S	e=0	0.70	-	-	-

Unit: mm, t_{cf}=50.8, [1]: WUF-W

- Since the fractures near the ESW were observed in specimens, the simulations without tie constraint between column and continuity plate were added.

Table A. 3 Study for the simulation of specimens

#	Column	Beam Section	Access Hole	Z_{RBS}/Z_X	Bevel	Eccent-ricity	Loca-tion	CPTie Constraint
6-2	610x914	W36x302	AWS D1.8	0.62	B1	*1	*1	No
12-2	610x914	W36x302	AISC360	0.76	S	*1	*1	No

*1) Only for simulation for specimen 1(2) and 3 so they don't have submodel

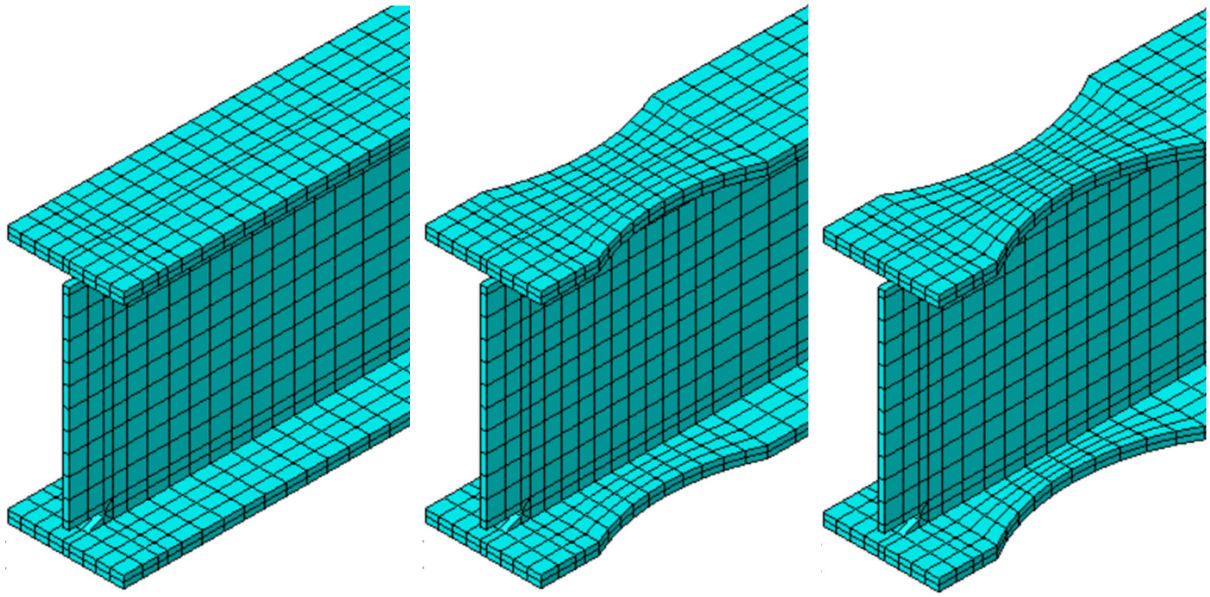

WUF-W RBS1 (Z_{RBS}/Z_X=0.76) RBS2 (Z_{RBS}/Z_X=0.62)

Fig A. 3 WUF-F and RBS

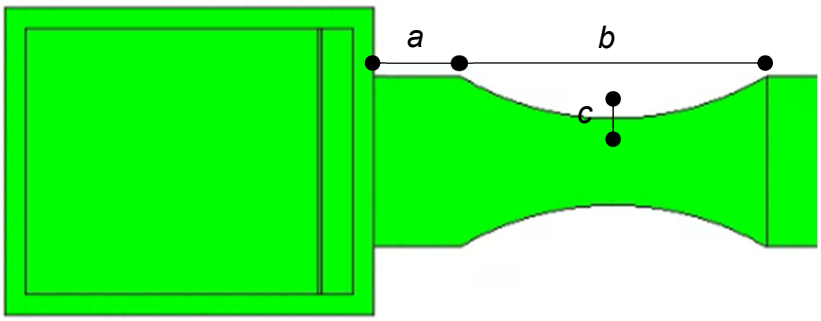

Fig A. 4 Definition of length *a*, *b* and *c* of RBS

Table A. 4 Dimensions of RBS

	a (in.)	*b* (in.)	*c* (in.)	c/b_f	Z_{RBS}/Z_X
RBS1 (Specimen 1(2))	8.375	24.25	2.625	0.157	0.76
RBS2 (Specimen 3)	8.735	30.00	4.125	0.247	0.62

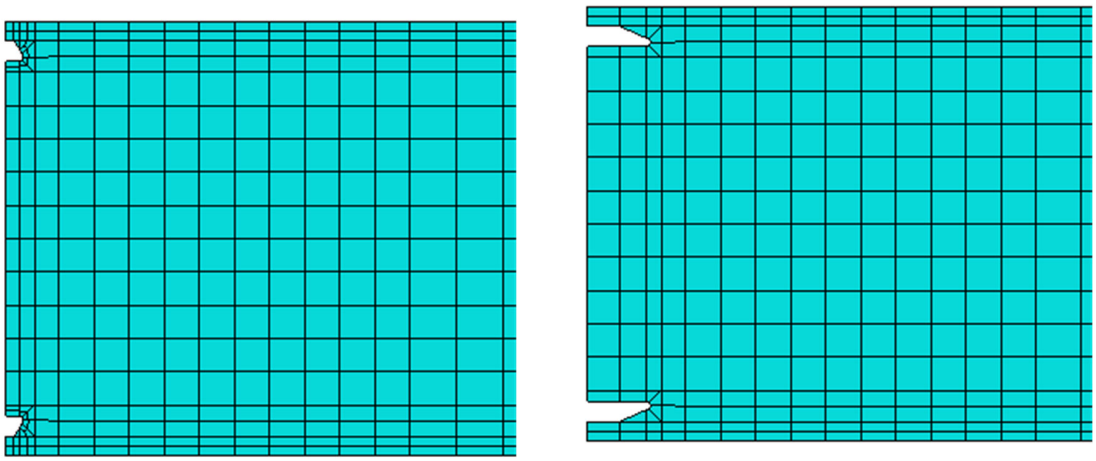

Length = 1.5” (AISC360) Length = 5.0” (AWS D1.8)

Fig A. 5 Access Hole

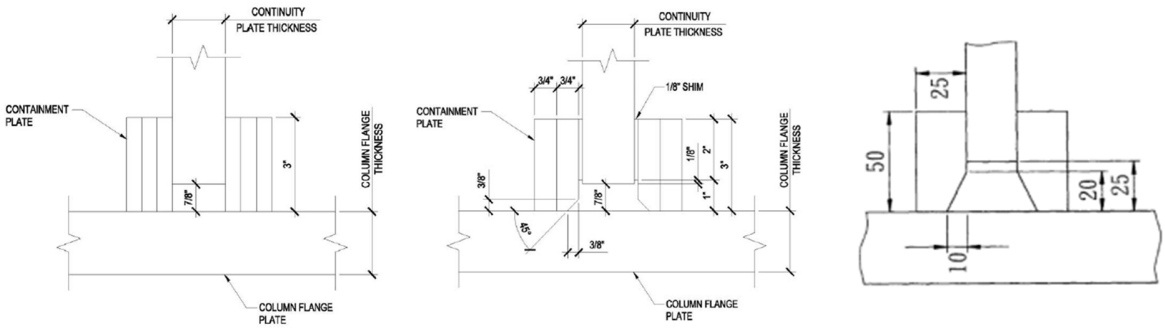

S (unit: inch) B1 (unit: inch) B2 (unit: mm)

Fig A. 6 Bevel

1. Choose 4 edge points

2. Make circle which intersects 4 points and make purple circle that go through 2 red points and its center is edge of former circle.

3. HAZ is assumed 0.5” at center 0.4” at edge. Make orange circle which go through 3 points

4. Area inside green is ESW
Area inside orange is HAZ

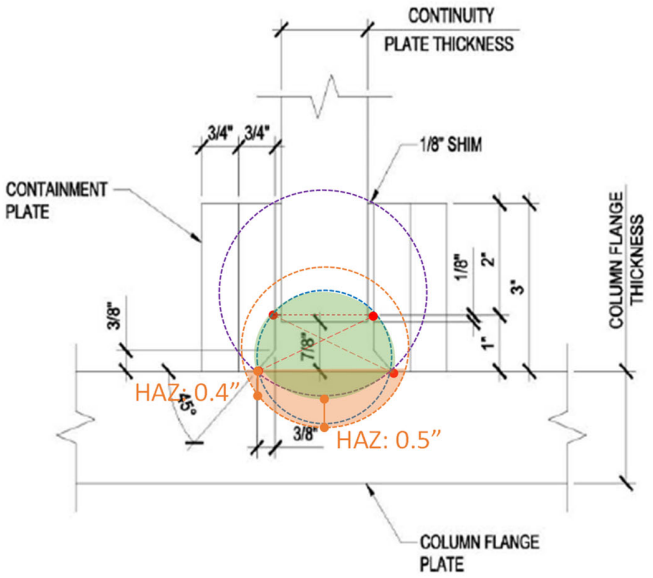

Fig A. 7 How to determine the areas of ESW and HAZ

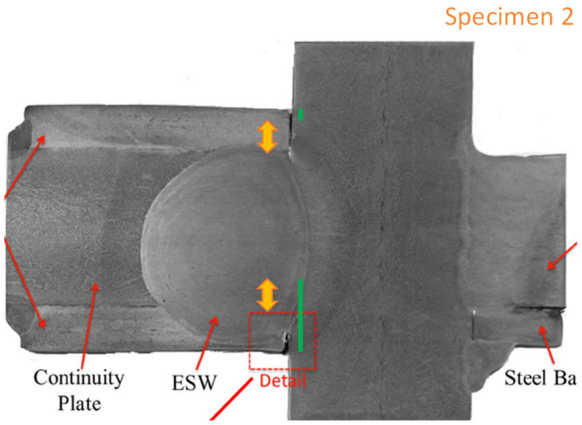

Eccentricity = 0.4” as observed in specimen 2

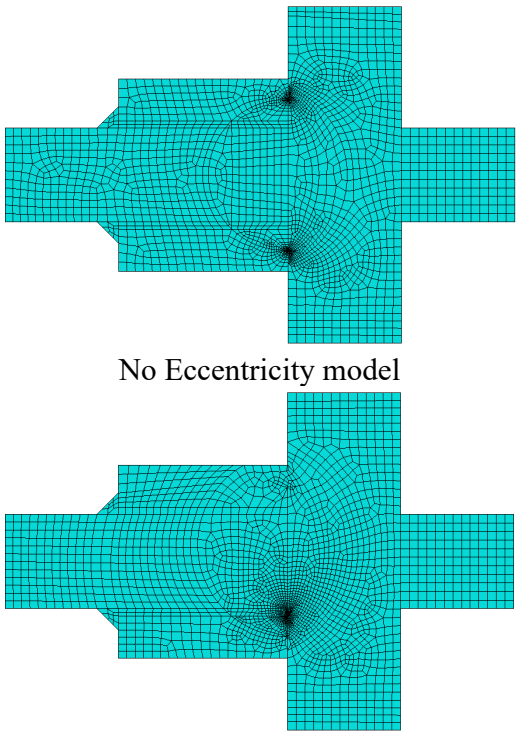

No Eccentricity model

Off center (Eccentricity = 0.4”) model

Fig A. 8 Eccentricity. When eccentricity is considered in analysis, longer slit is modeled.

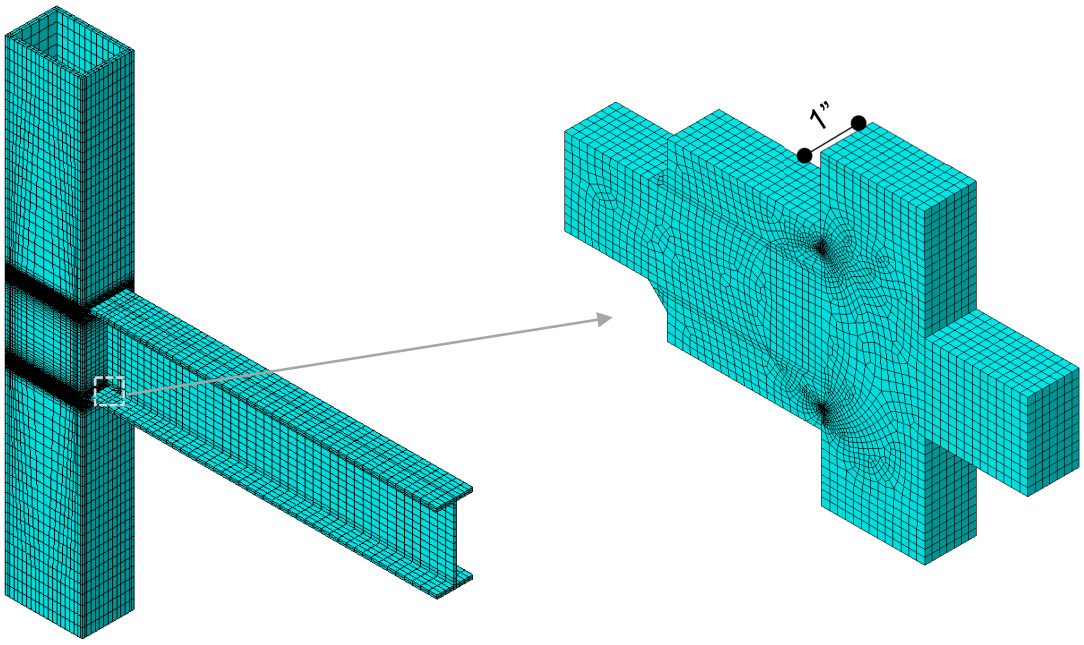

Global model Submodel

Fig A. 9 Global model and submodel

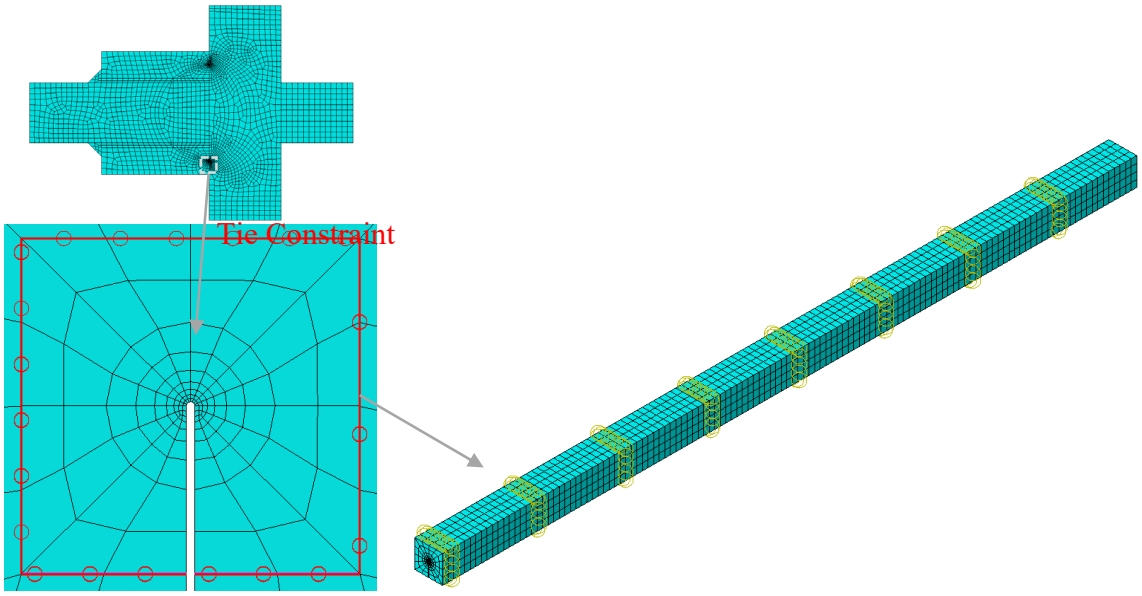

tip of slit Inside the tie constraint (Finer mesh)

Fig A. 10 Detail of submodel

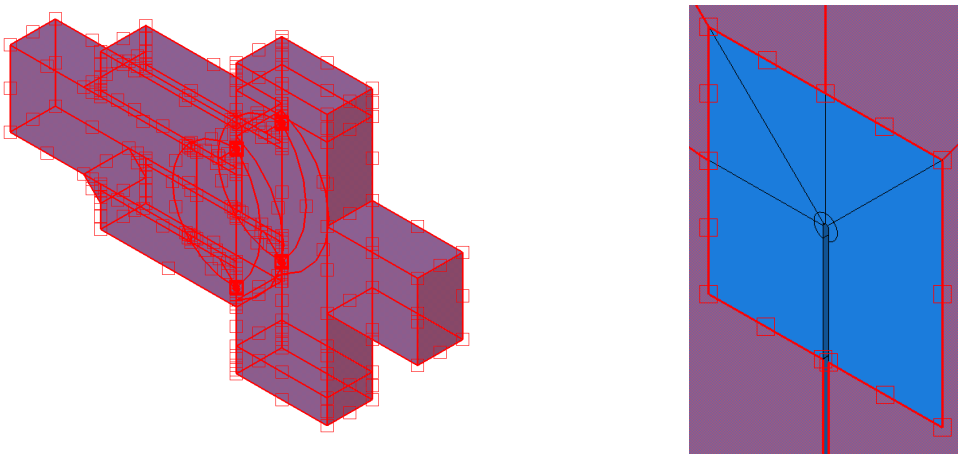

Overview tip of slit

Fig A. 11 Boundary conditions of submodel (Global model's displacement)

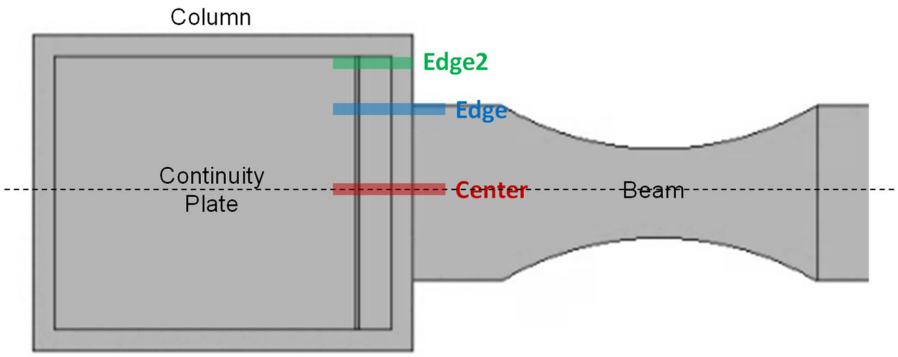

Fig A. 12 Location of submodel

Appendix: Detail of Analyses

Issue 1: Column depth study

Table A. 5 Column depth study

#	Column	Beam Section	Access Hole	Z_{RBS}/Z_X	Conta-inment Plate	Ecce-ntri-city	b_{bf}/b_{cf}	Drift when D>1 (%)		
								Web	BE	CC
13	610x610	W36x302	AWSD1.8	0.62	B1	e=0	0.70	6.00	2.00	-
14	432x914	W36x302	AWSD1.8	0.62	B1	e=0	1.0	D<1	D<1	-
15	762x914	W36x302	AWSD1.8	0.62	B1	e=0	0.56	4.00	2.00	5.00

Unit: mm, t_{cf}=50.8, [1]: WUF-W

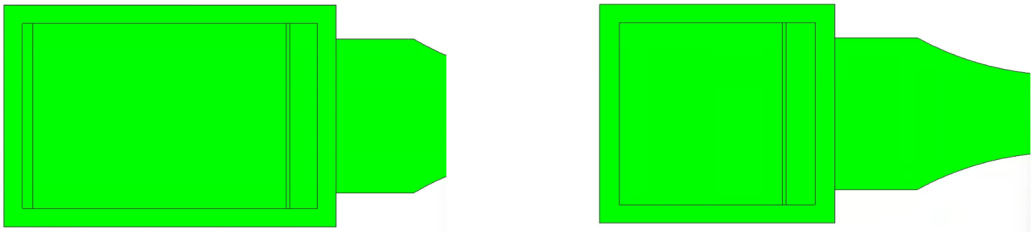

Depth = 3” (Part A, Simulation #6) Depth = 2” (Issue1-1 and 1-2)

Fig A. 13 The difference between Part A and Issue 1

Issue 2: Column width study

Table A. 6 Column width study

#	Column	Beam Section	Access Hole	Z_{RBS}/Z_X	Conta-inment Plate	Ecce-ntri-city	b_{bf}/b_{cf}	Drift when D>1 (%)		
								Web	BE	CC
15	762x914	W36x302	AWSD1.8	0.62	B1	e=0	0.56	4.00	2.00	5.00

Unit: mm, t_{cf}=50.8, [1]: WUF-W

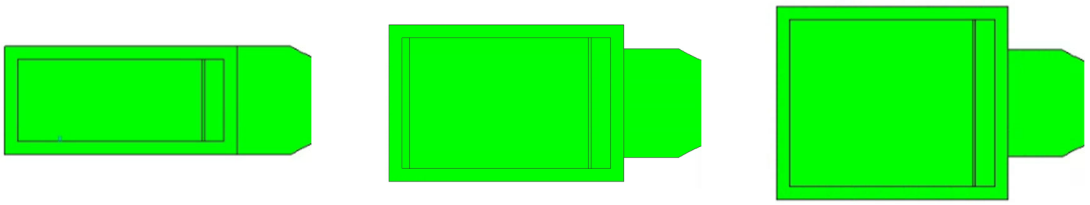

Width=17.6” (Issue 2-1 and 2-2)

Width=2’ (24”) (Issue 1-1 and 1-2)

Width=30” (Issue 2-3, 2-4 and 2-5)

Fig A. 14 The plan of Issue 2

Issue 3: Column thickness and without continuity plate study

Table A. 7 Simulation Matrix for Examining the Necessity of the Continuity Plate, Depending on the Column Wall Thickness and Other Factors

#	t_{cf}	Beam Section	b_{bf}	t_p/t_{bf}	Contain-ment Plate	$\frac{t_{cf}}{t_{cf-WF}^{\text{AISC}}}$	$D_{4\%}$
16	50.8	W36x302	427	1.0	B1	0.71	0.76
17	50.8	W36x302	427	0.52	B1	0.71	1.92
18	50.8	W36x302	427	-	w/o	0.71	54
19	76.2	W36x302	427	1.0	B1	1.06	0.68
20	76.2	W36x302	427	0.52	B1	1.06	0.93
21	76.2	W36x302	427	-	w/o	1.06	2.25
22	127	W36x302	427	1.0	B1	1.76	0.45
23	127	W36x302	427	0.52	B1	1.76	0.49
24	127	W36x302	427	-	w/o	1.76	0.59
25	50.8	W27x368	630	1.0	B1	0.62	0.67
26	50.8	W27x368	630	0.50	B1	0.62	1.33
27	50.8	W27x368	630	-	w/o	0.62	5.8
28	76.2	W27x368	630	1.0	B1	0.93	0.48
29	76.2	W27x368	630	0.50	B1	0.93	0.64
30	76.2	W27x368	630	-	w/o	0.93	2.13
31	127	W27x368	630	1.0	B1	1.55	0.37
32	127	W27x368	630	0.50	B1	1.55	0.40
33	127	W27x368	630	-	w/o	1.55	0.54
34	102	W36x302	427	1.0	B1	1.41	0.53
35	102	W36x302	427	0.52	B1	1.41	0.60
36	102	W36x302	427	-	w/o	1.41	0.97
37	152	W36x302	427	1.0	B1	2.12	0.39
38	152	W36x302	427	0.52	B1	2.12	0.40
39	152	W36x302	427	-	w/o	2.12	0.43

Unit: mm, Column:610x610,Access hole: AWS D1.8, RBS: Z_{RBS}/Z_X =0.62, Eccentricity e=0

$$t_{cf}^{\text{AISC}} = \max\left(0.4\sqrt{1.8 b_{bf} t_{bf} \frac{F_{yb}}{F_{yc}}}, \frac{b_{bf}}{6}\right)$$

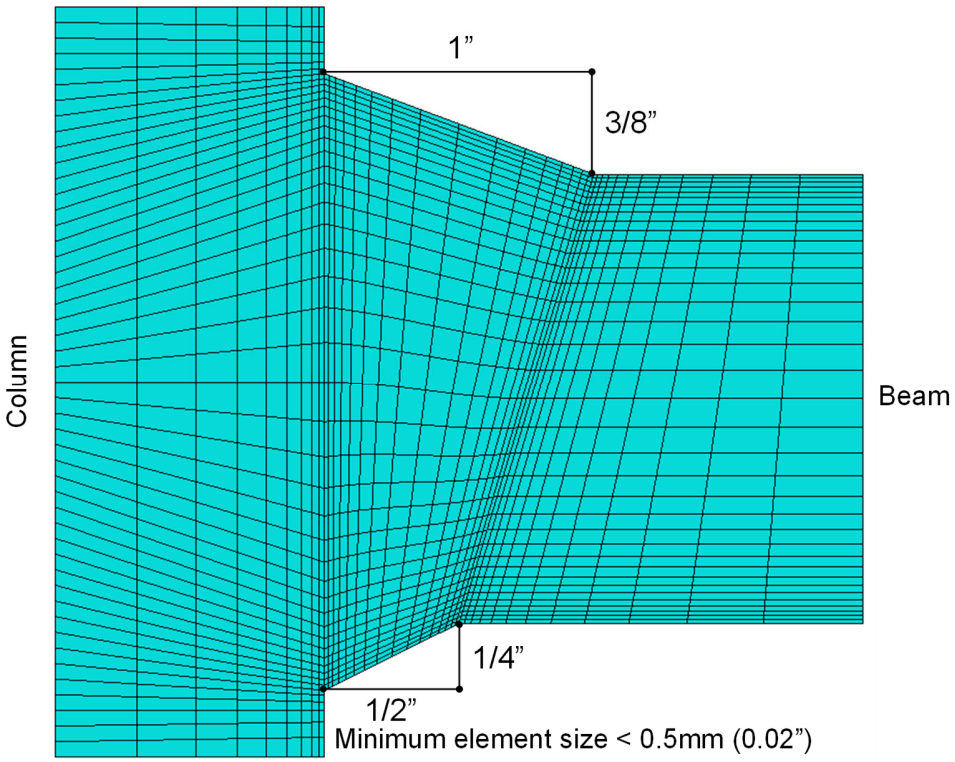

Fig A. 15 Weld of lower beam flange geometry and mesh (Issue 3)

			W36x302	W27x368
	Zx	inch3	1280	1240
beam web thickness	tbw	inch	0.945	1.38
beam flange thickness	tbf	inch	1.68	2.48
column flange thickness	tcf	inch	2	2
beam flange width	bbf	inch	16.7	14.7
column flange width	bc	inch	24	24
RyFy (column)		ksi	59.8	59.8
RyFy (beam)		ksi	59.5	59.5
$t_{cf} \geq 0.4\sqrt{1.8 b_{bf} t_{bf} \frac{R_{yb}F_{yb}}{R_{yc}F_{yc}}}$			2.84	3.23
[demand] / tcf			1.42	1.62
$t_{cf} \geq \frac{b_{bf}}{6}$			2.78	2.45
[demand] / tcf			1.39	1.23
tcf / tbw			2.12	1.45
bbf/bc			0.70	0.61

Column thickness = 2”

			W36x302	W27x368
	Zx	inch3	1280	1240
beam web thickness	tbw	inch	0.945	1.38
beam flange thickness	tbf	inch	1.68	2.48
column flange thickness	tcf	inch	3	3
beam flange width	bbf	inch	16.7	14.7
column flange width	bc	inch	24	24
RyFy (column)		ksi	59.8	59.8
RyFy (beam)		ksi	59.5	59.5
$t_{cf} \geq 0.4\sqrt{1.8 b_{bf} t_{bf} \frac{R_{yb}F_{yb}}{R_{yc}F_{yc}}}$			2.84	3.23
[demand] / tcf			0.95	1.08
$t_{cf} \geq \frac{b_{bf}}{6}$			2.78	2.45
[demand] / tcf			0.93	0.82
tcf / tbw			3.17	2.17
bbf/bc			0.70	0.61

Column thickness = 3”

			W36x302	W27x368
	Zx	inch3	1280	1240
beam web thickness	tbw	inch	0.945	1.38
beam flange thickness	tbf	inch	1.68	2.48
column flange thickness	tcf	inch	4	4
beam flange width	bbf	inch	16.7	14.7
column flange width	bc	inch	24	24
RyFy (column)		ksi	59.8	59.8
RyFy (beam)		ksi	59.5	59.5
$t_{cf} \geq 0.4\sqrt{1.8 b_{bf} t_{bf} \frac{R_{yb}F_{yb}}{R_{yc}F_{yc}}}$			2.84	3.23
[demand] / tcf			0.71	0.81
$t_{cf} \geq \frac{b_{bf}}{6}$			2.78	2.45
[demand] / tcf			0.70	0.61
tcf / tbw			4.23	2.90
bbf/bc			0.70	0.61

Column thickness = 4”

			W36x302	W27x368
	Zx	inch3	1280	1240
beam web thickness	tbw	inch	0.945	1.38
beam flange thickness	tbf	inch	1.68	2.48
column flange thickness	tcf	inch	5	5
beam flange width	bbf	inch	16.7	14.7
column flange width	bc	inch	24	24
RyFy (column)		ksi	59.8	59.8
RyFy (beam)		ksi	59.5	59.5
$t_{cf} \geq 0.4\sqrt{1.8 b_{bf} t_{bf} \frac{R_{yb}F_{yb}}{R_{yc}F_{yc}}}$			2.84	3.23
[demand] / tcf			0.57	0.65
$t_{cf} \geq \frac{b_{bf}}{6}$			2.78	2.45
[demand] / tcf			0.56	0.49
tcf / tbw			5.29	3.62
bbf/bc			0.70	0.61

Column thickness = 5”

Fig A. 16 Criteria check for w/o CP of Issue 3 (ANSI/AISC 358)

Abaqus .inp file on GitHub
https://github.com/HiroshiYasumoto/ESW_Fracture_FEM

Simulation 1

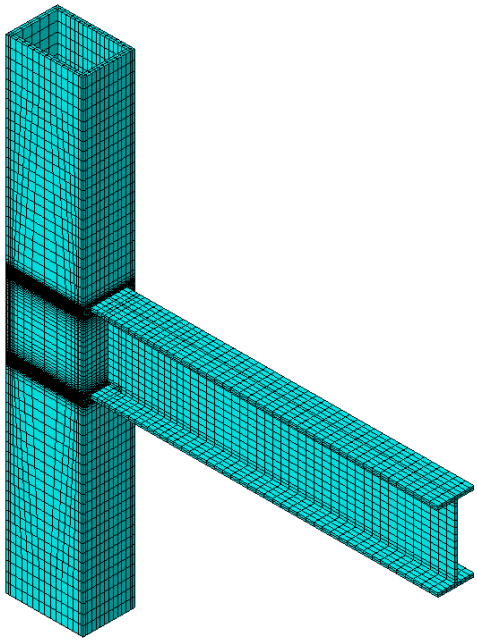

Global model

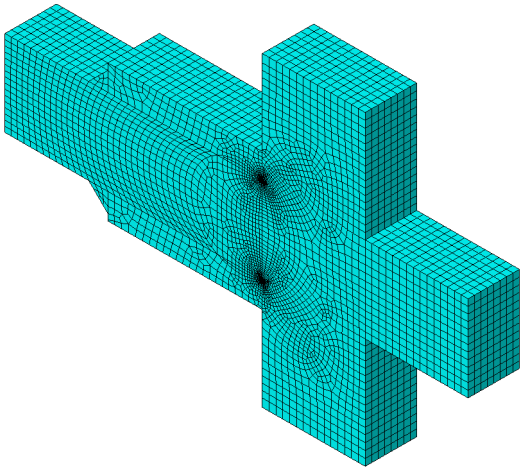

Submodel

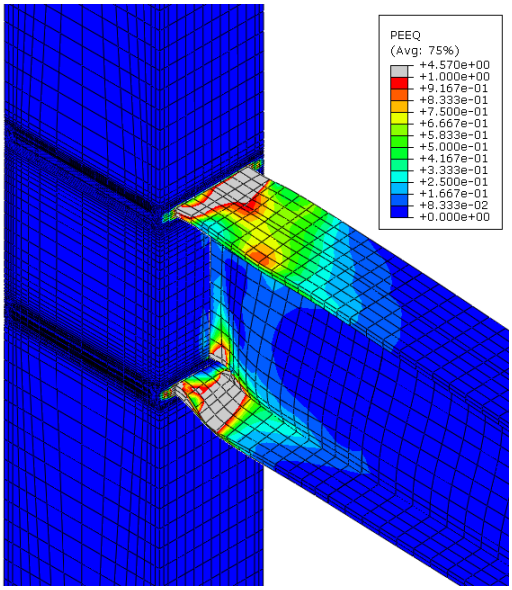

Final state of global model (PEEQ)

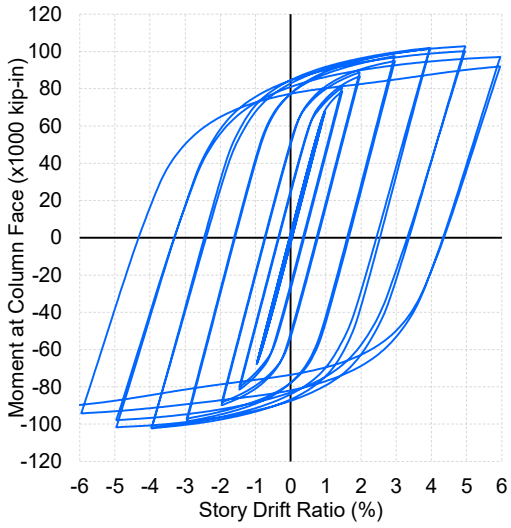

Load-displacement

Simulation 1 cont.

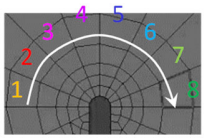

Element 5 and max (1~8)

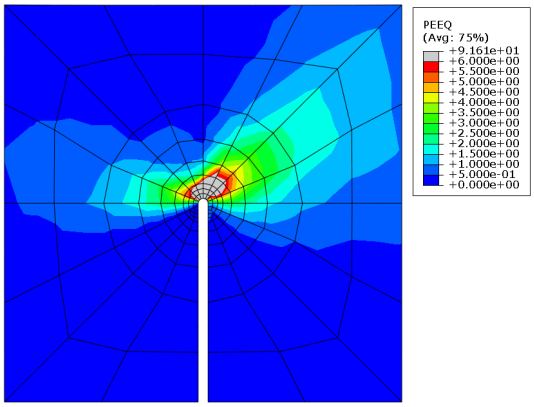

Final state of submodel (PEEQ)

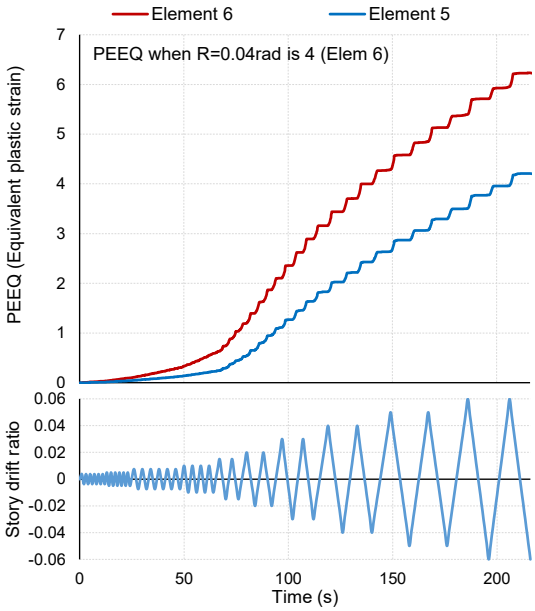

PEEQ

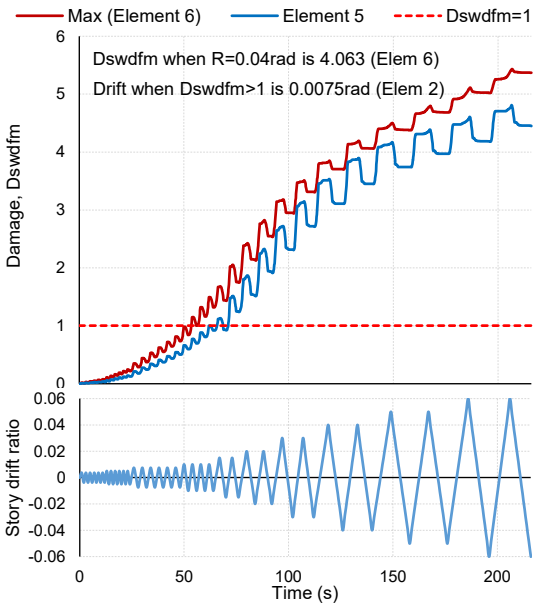

Damage

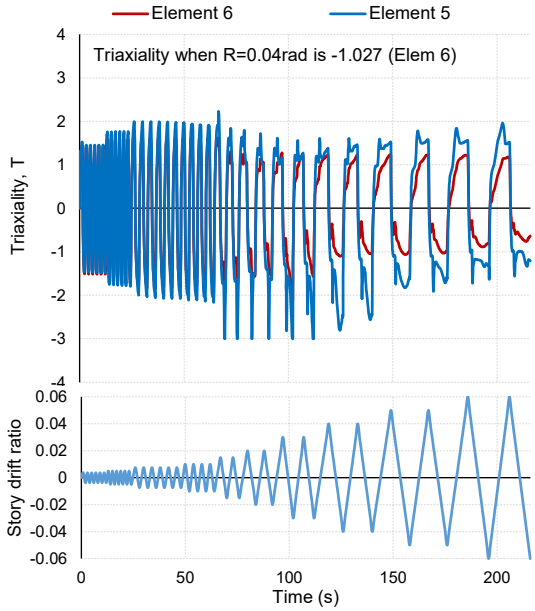

Triaxiality

Simulation 2

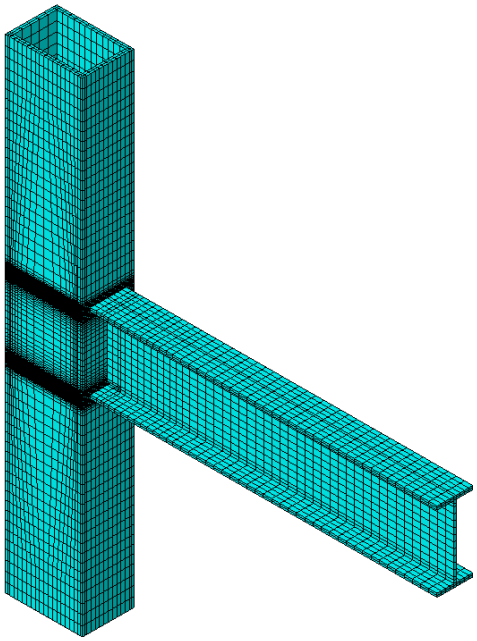

Global model

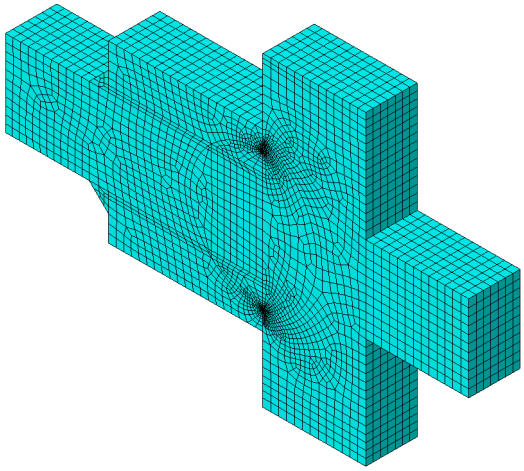

Submodel

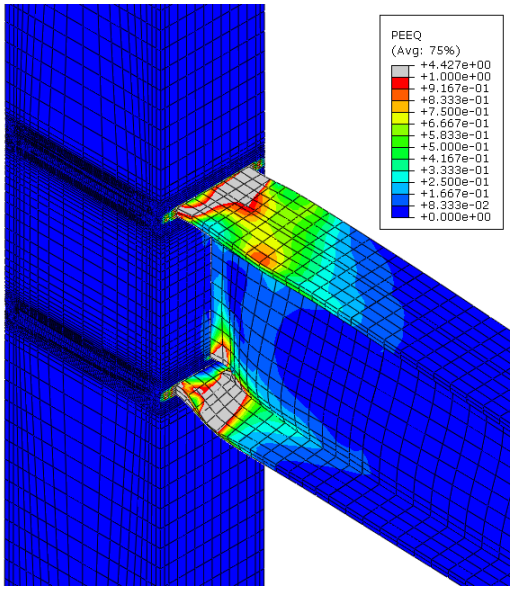

Final state of global model (PEEQ)

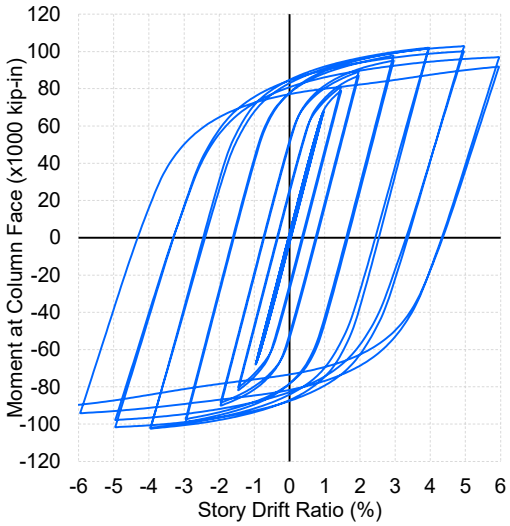

Load-displacement

Simulation 2 cont. (Center)

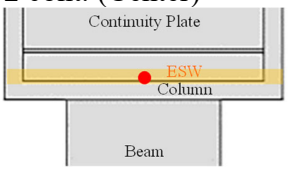

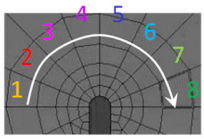

Element 5 and max (1~8)

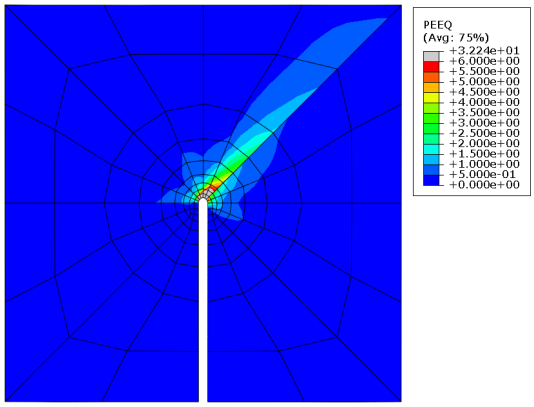

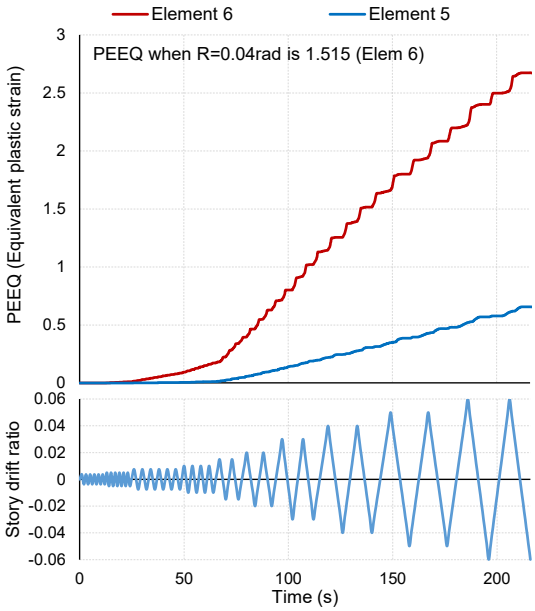

PEEQ

Final state of submodel (PEEQ)

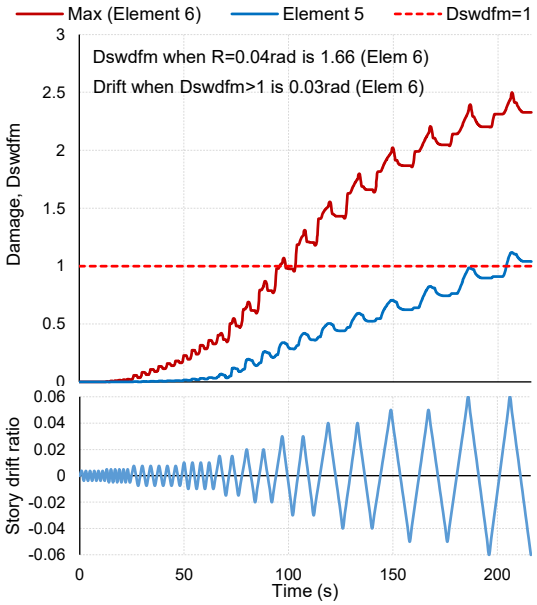

Damage

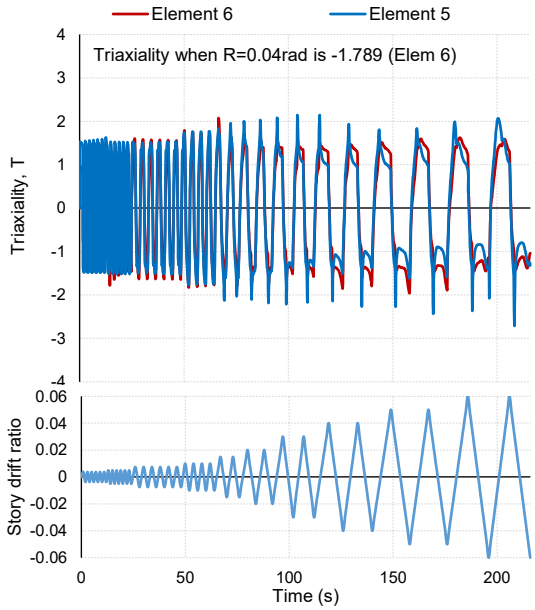

Triaxiality

Simulation 2 cont.

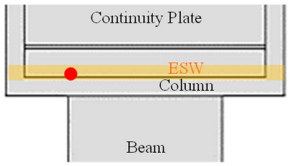

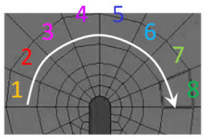

Element 5 and max (1~8)

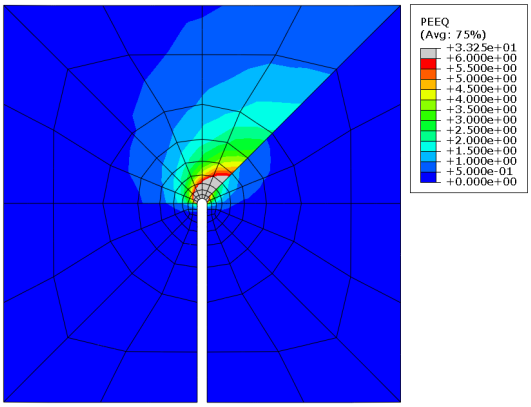

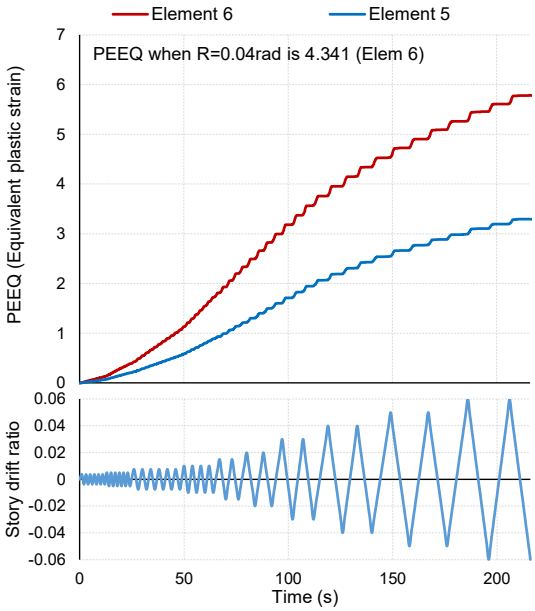

Final state of submodel (PEEQ)

PEEQ

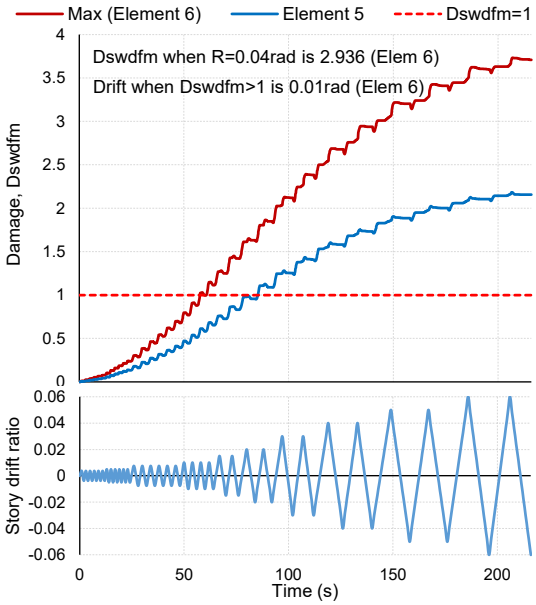

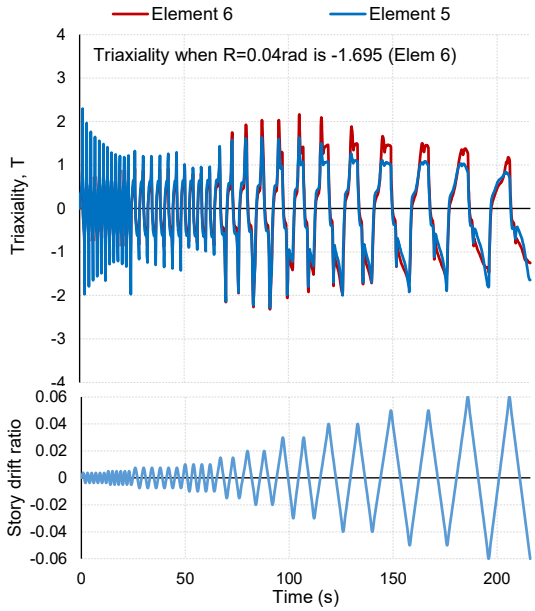

Damage

Triaxiality

Simulation 3

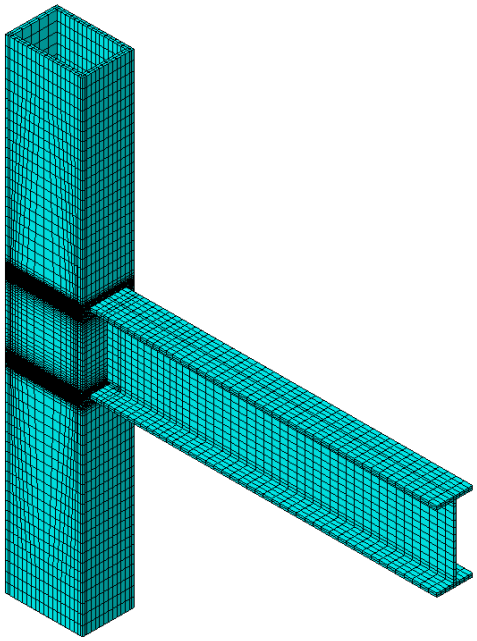

Global model

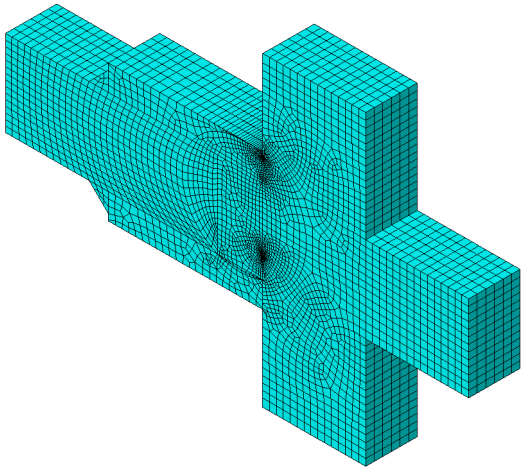

Submodel

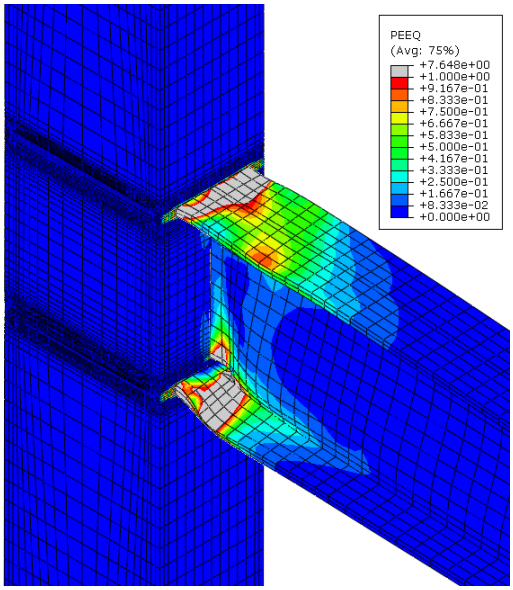

Final state of global model (PEEQ)

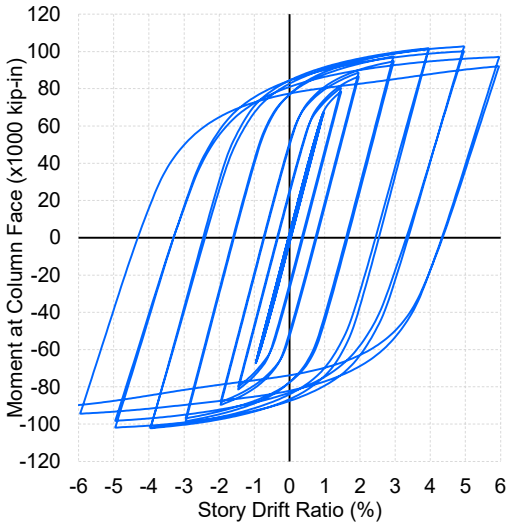

Load-displacement

Simulation 3 cont.

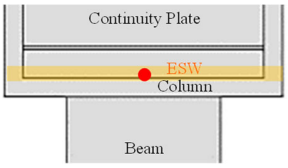

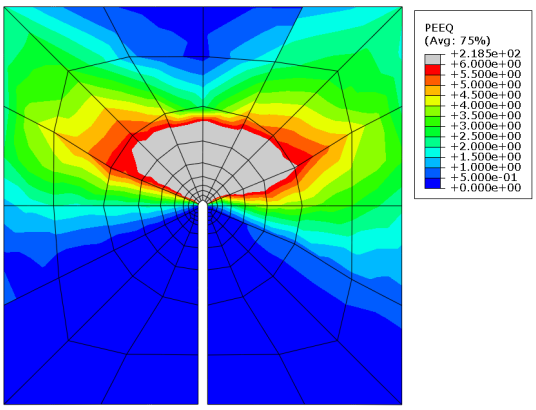

Final state of submodel (PEEQ)

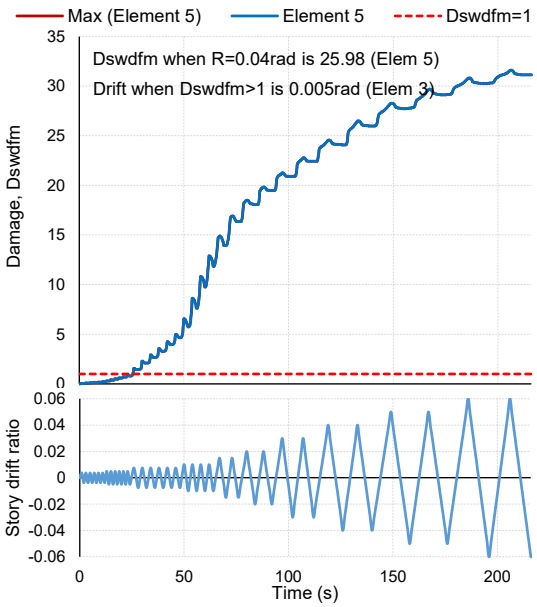

Damage

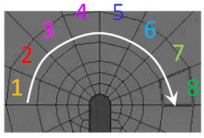

Element 5 and max (1~8)

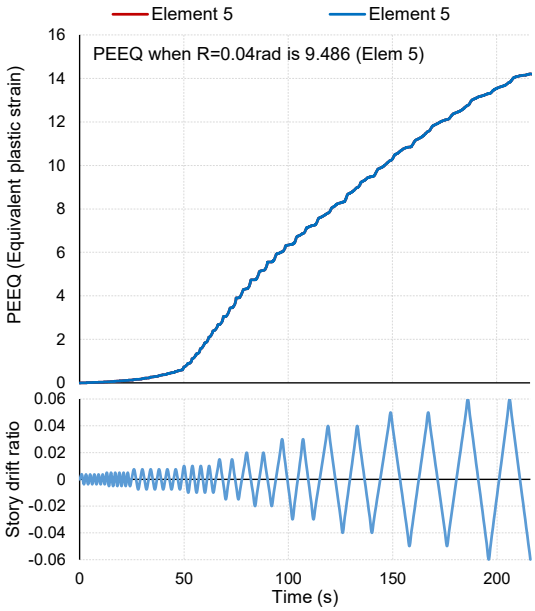

PEEQ

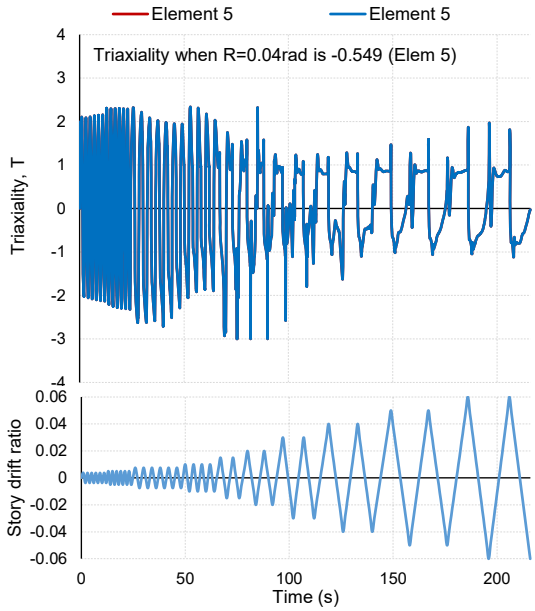

Triaxiality

Simulation 4

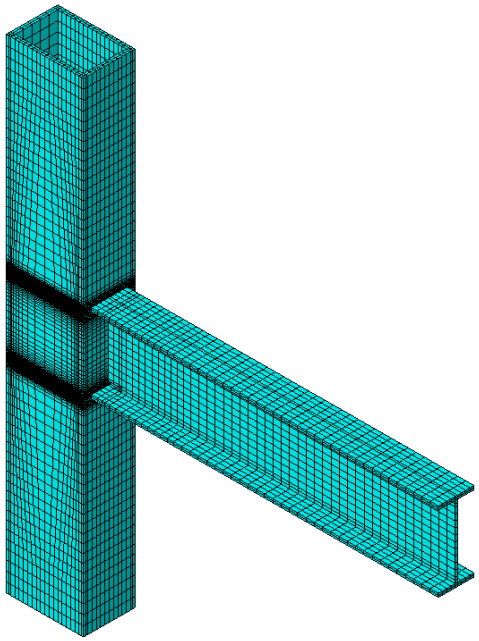

Global model

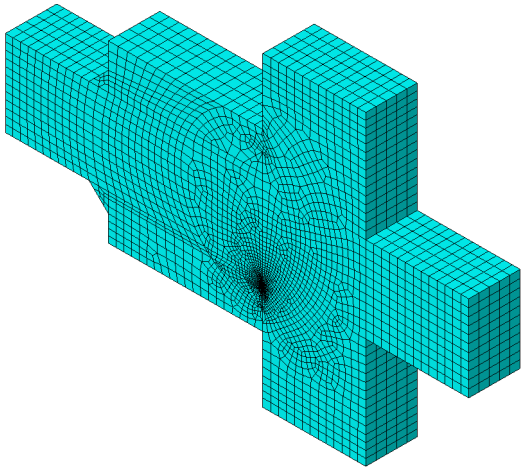

Submodel

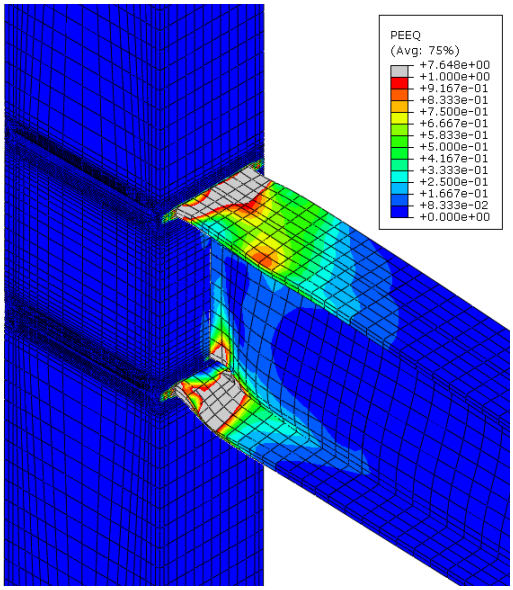

Final state of global model (PEEQ)

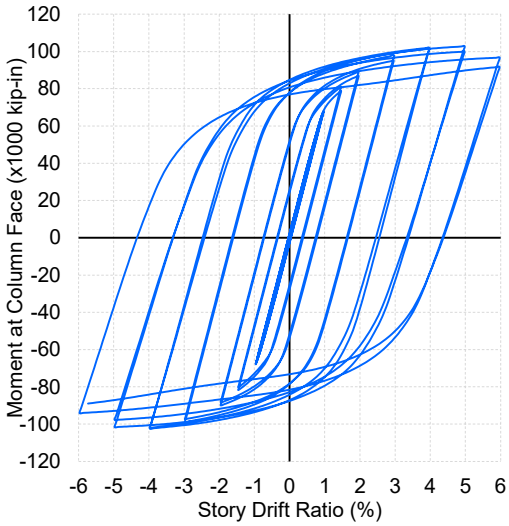

Load-displacement

Simulation 4 cont.

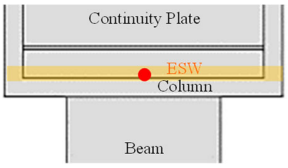

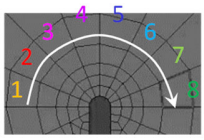

Element 5 and max (1~8)

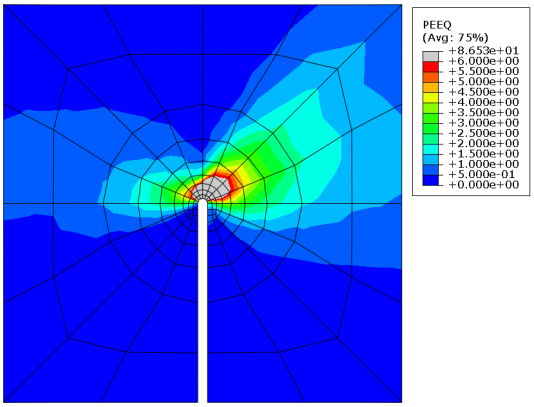

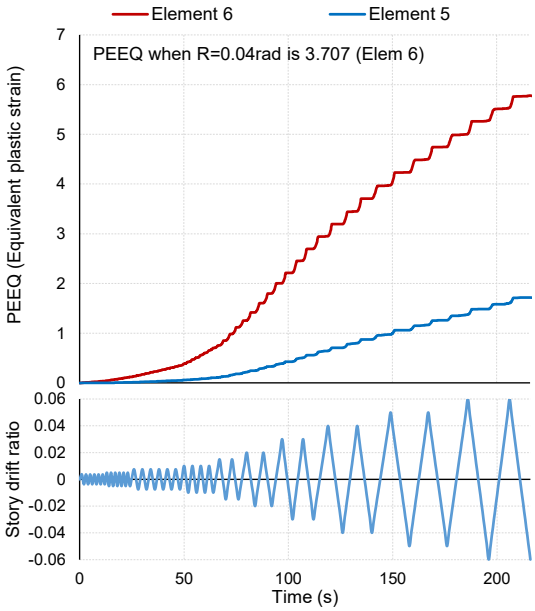

Final state of submodel (PEEQ)

PEEQ

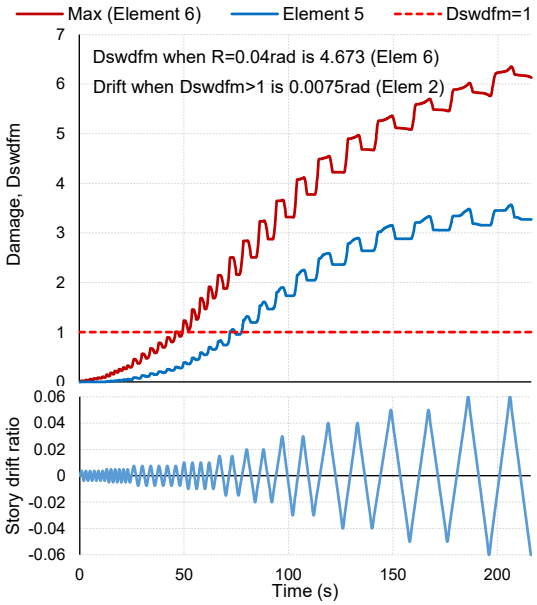

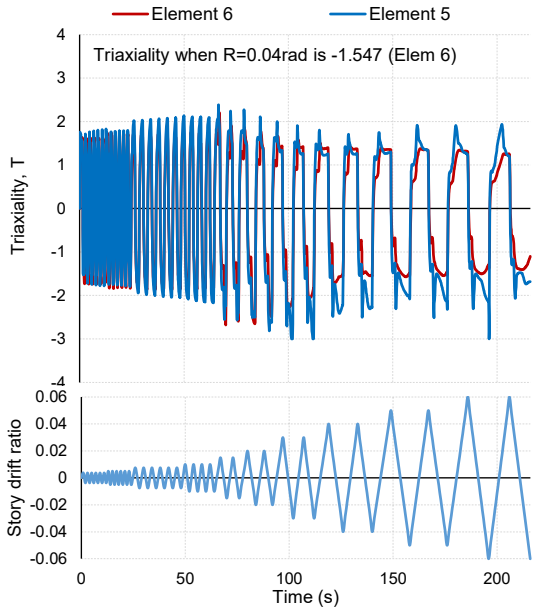

Damage

Triaxiality

Simulation 5

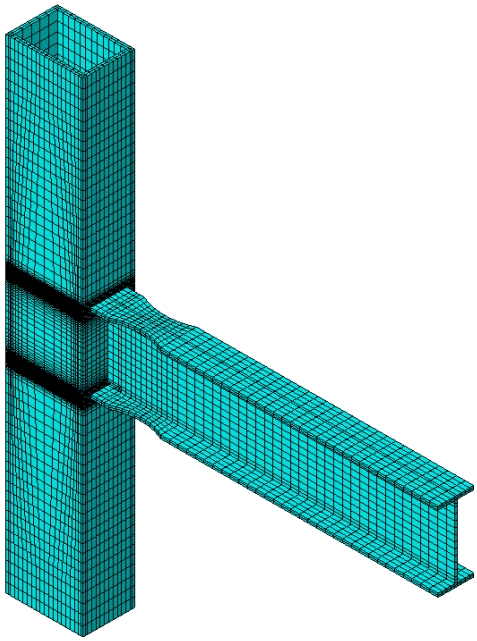

Global model

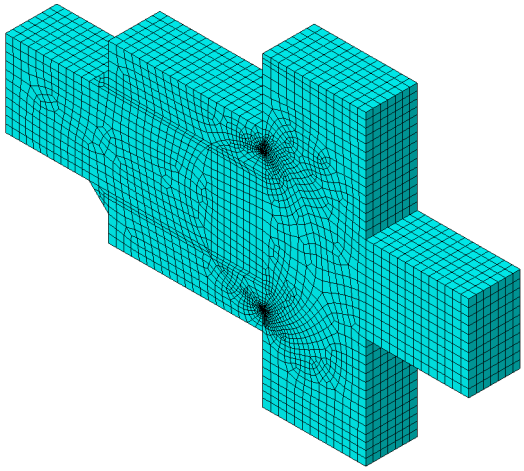

Submodel

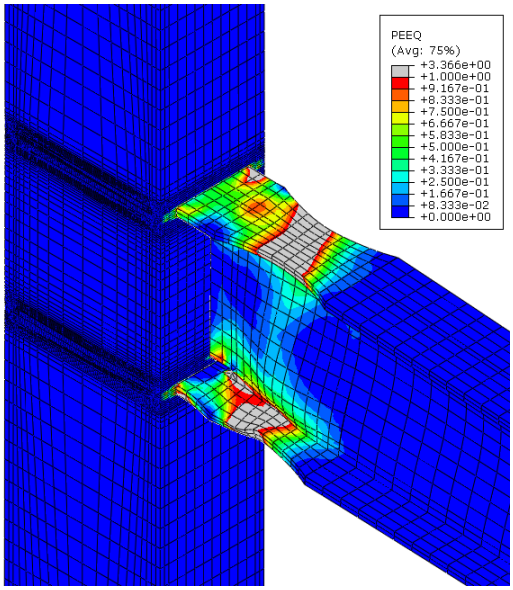

Final state of global model (PEEQ)

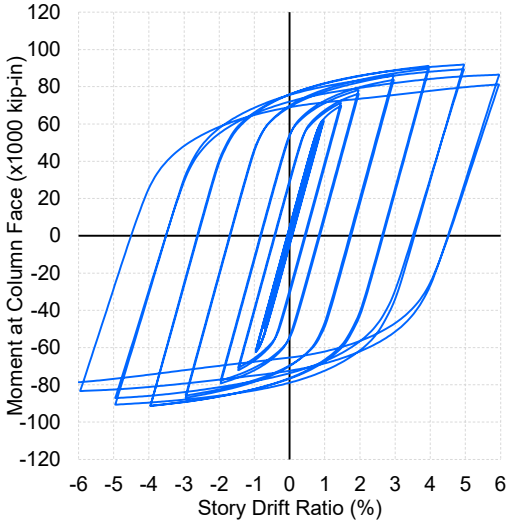

Load-displacement

Simulation 5 cont.

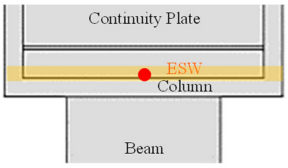

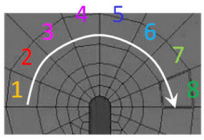

Element 5 and max (1~8)

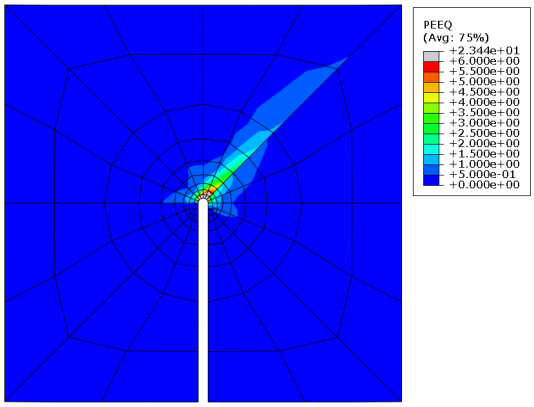

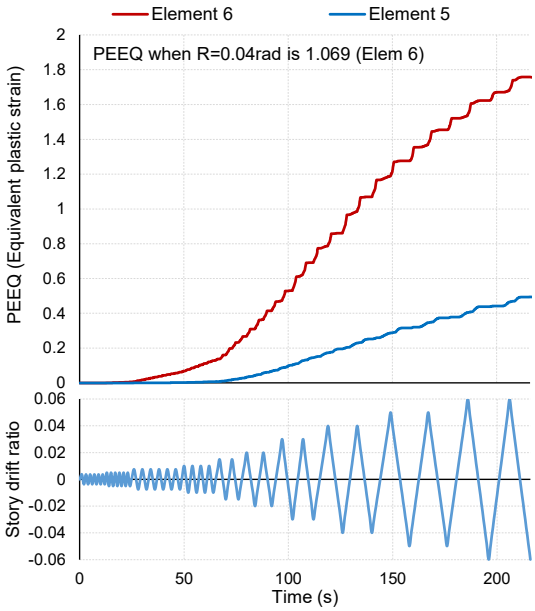

Final state of submodel (PEEQ)

PEEQ

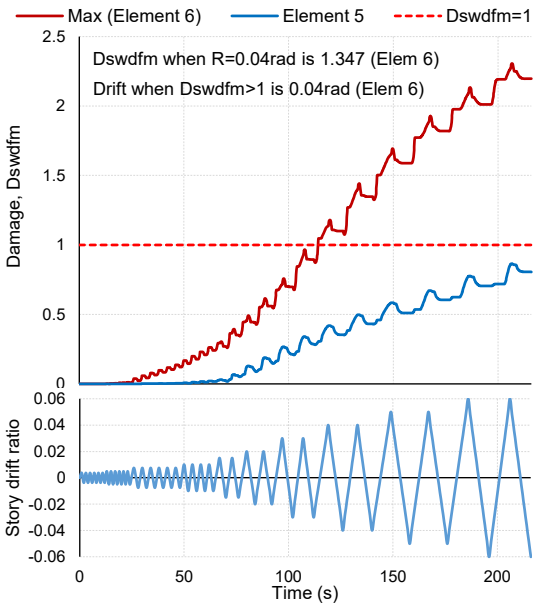

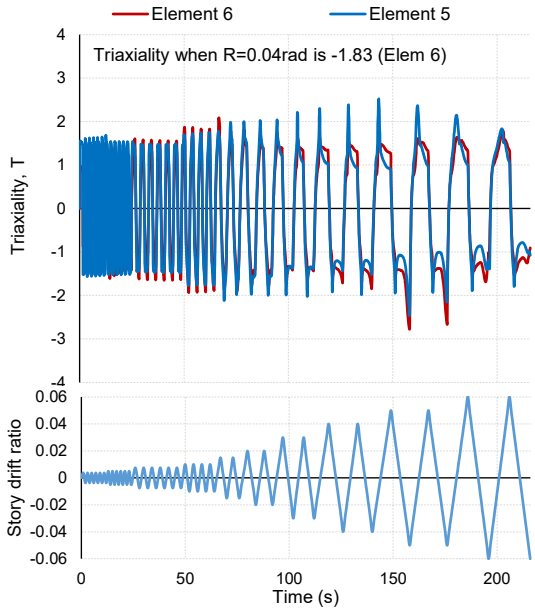

Damage

Triaxiality

Simulation 6

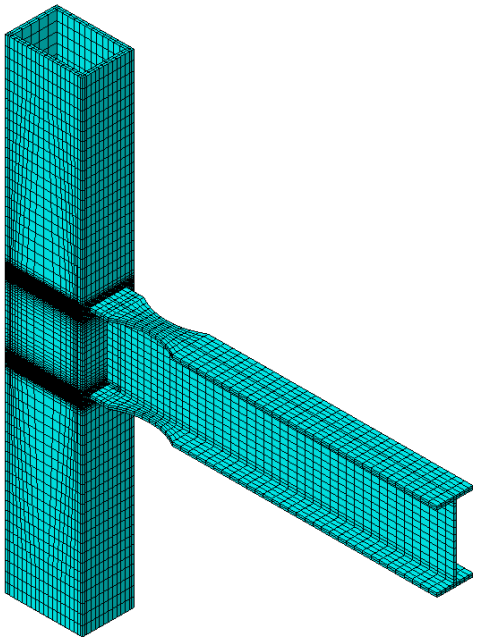

Global model

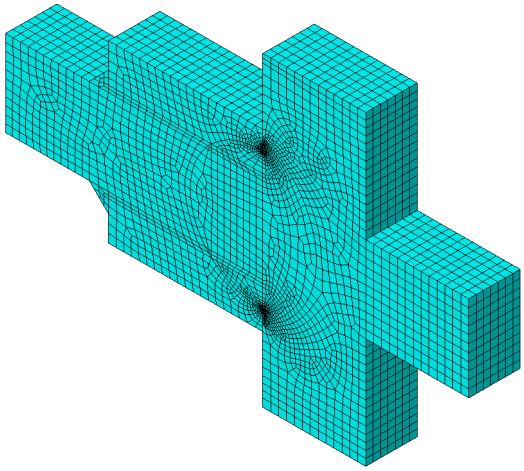

Submodel

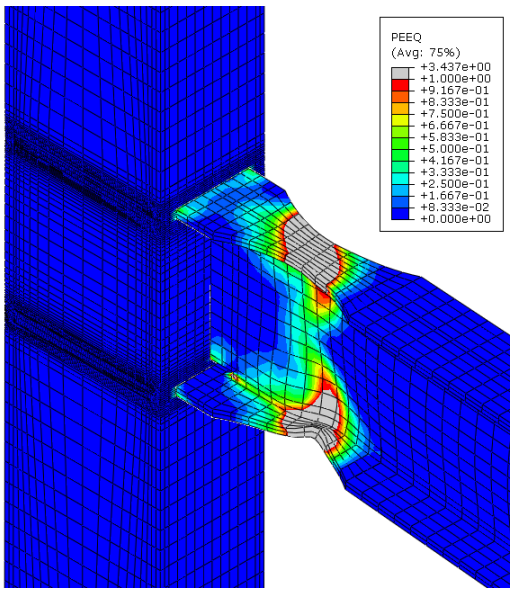

Final state of global model (PEEQ)

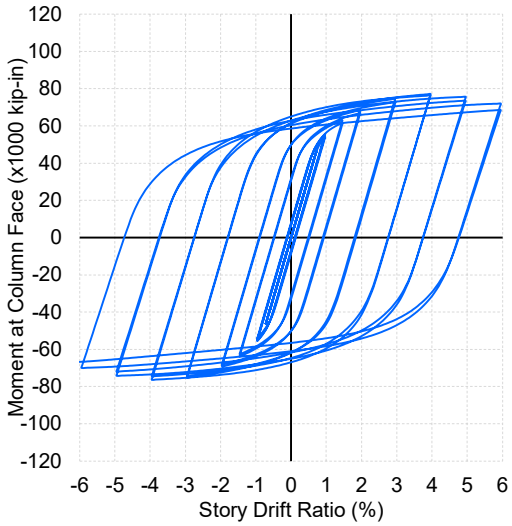

Load-displacement

Simulation 6 cont.

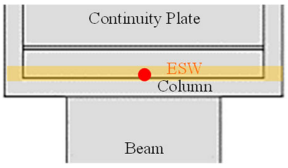

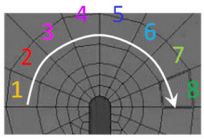

Element 5 and max (1~8)

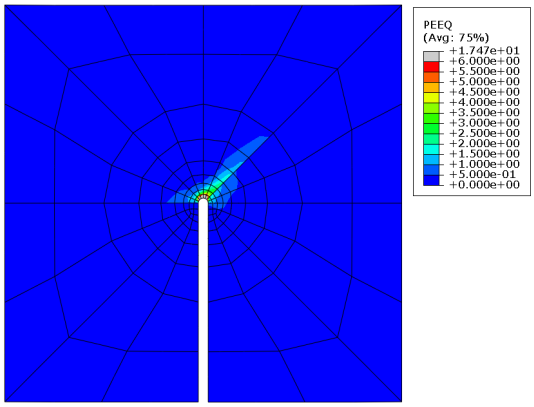

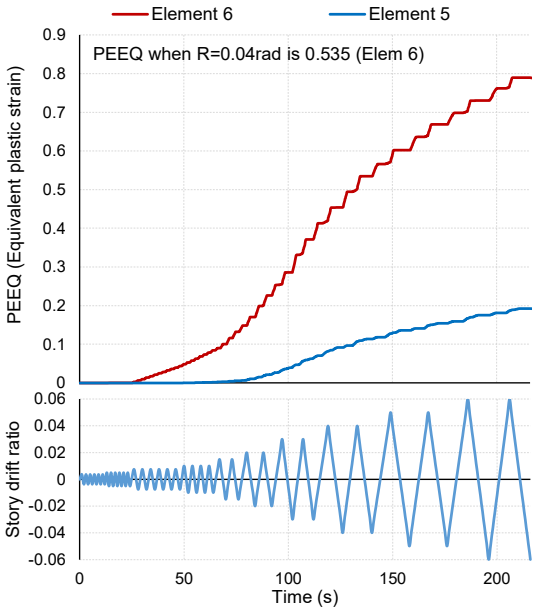

Final state of submodel (PEEQ)

PEEQ

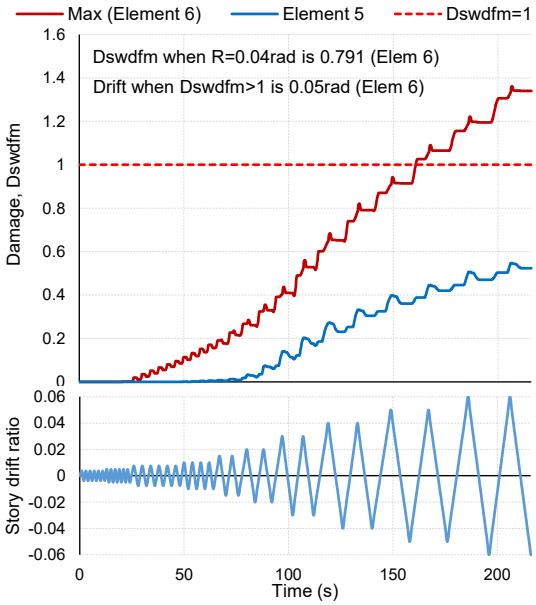

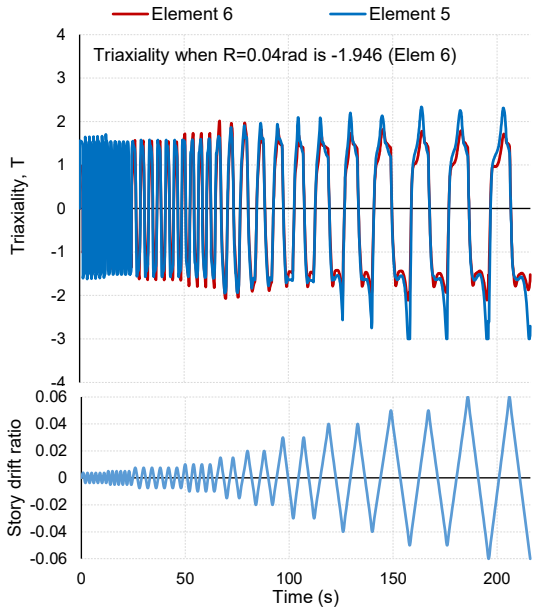

Damage

Triaxiality

Simulation 6 cont.

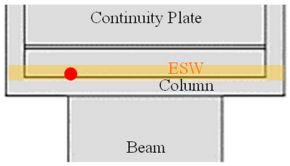

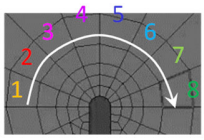

Element 5 and max (1~8)

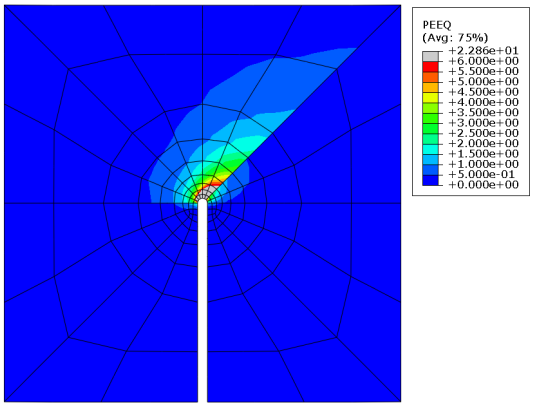

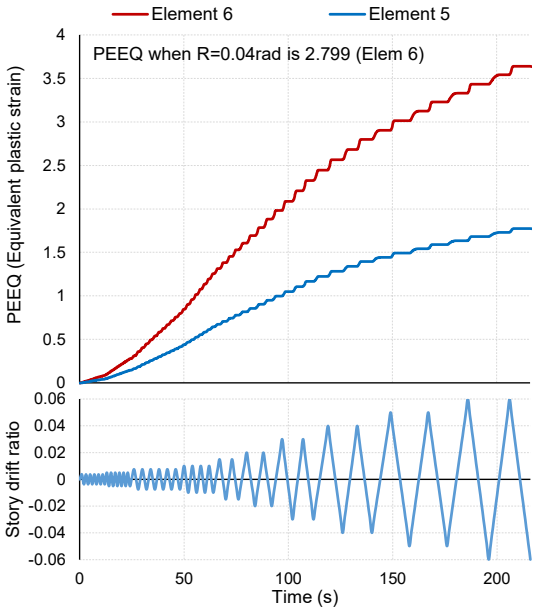

Final state of submodel (PEEQ)

PEEQ

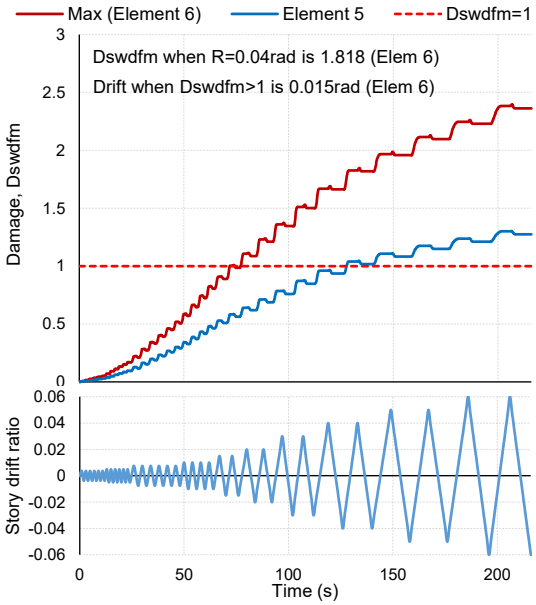

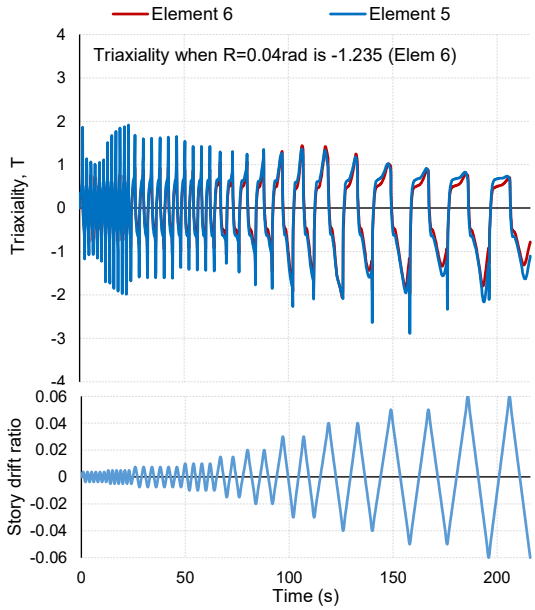

Damage

Triaxiality

Simulation 7

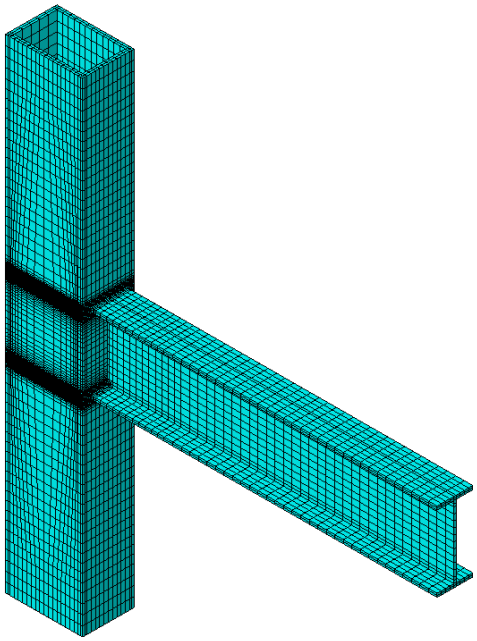

Global model

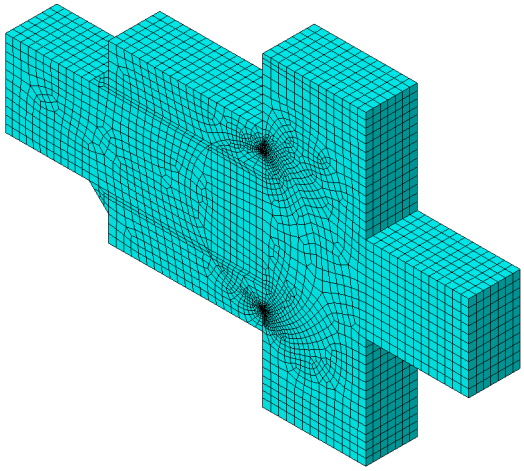

Submodel

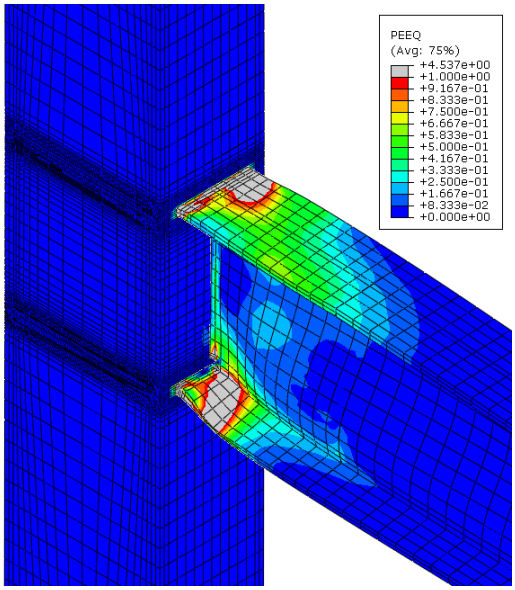

Final state of global model (PEEQ)

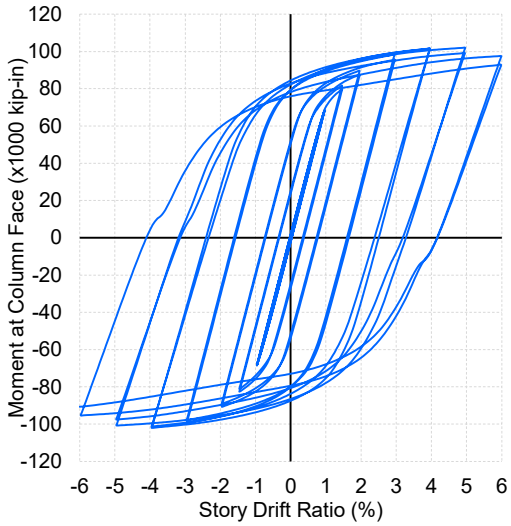

Load-displacement

Simulation 7 cont.

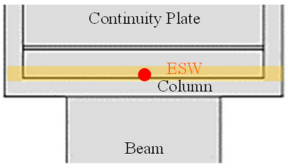

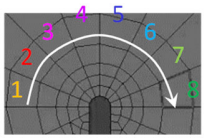

Element 5 and max (1~8)

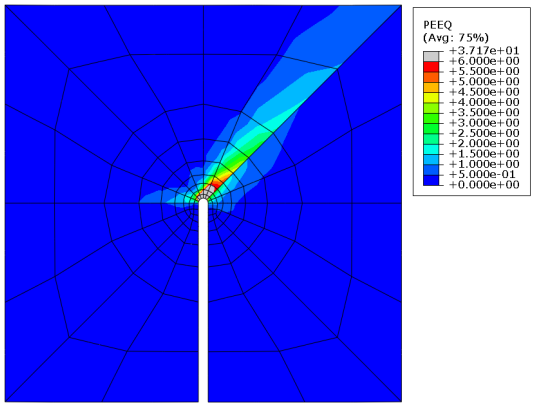

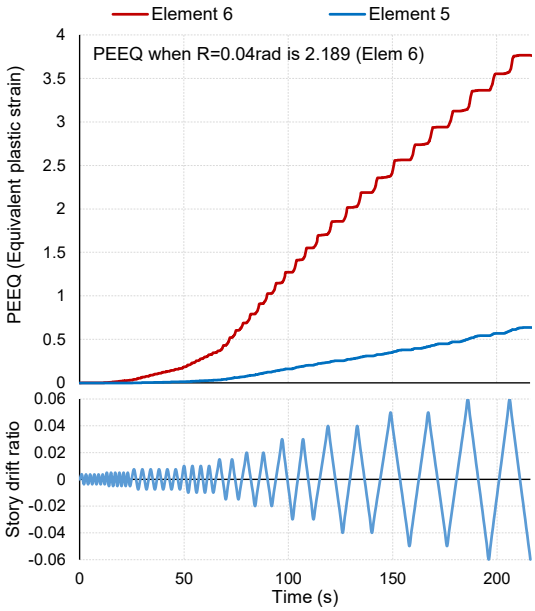

Final state of submodel (PEEQ)

PEEQ

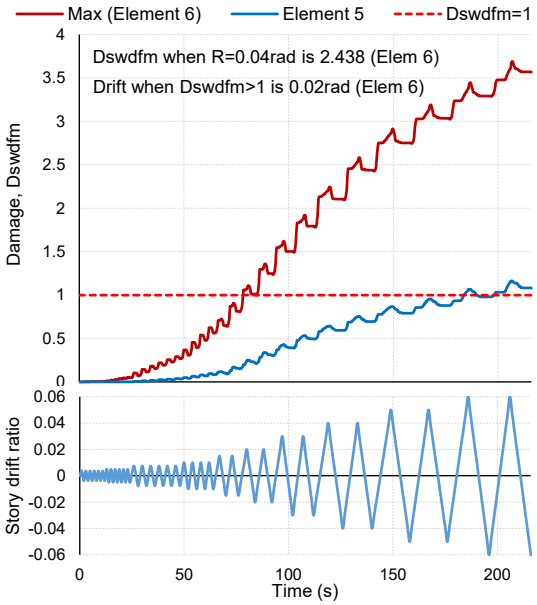

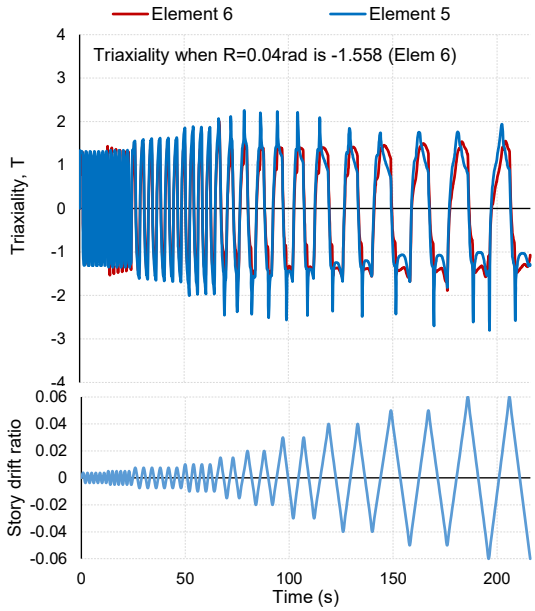

Damage

Triaxiality

Simulation 8

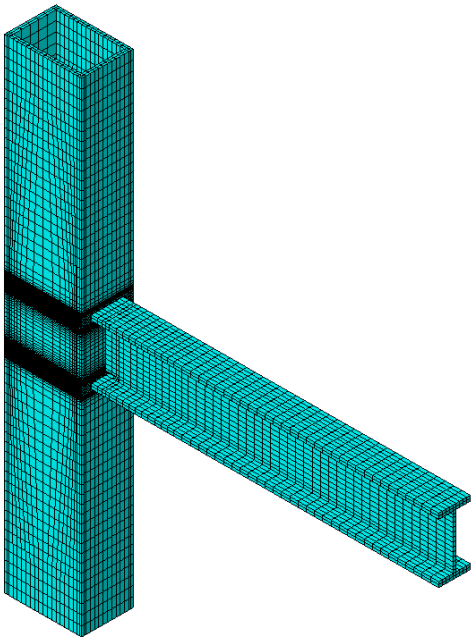

Global model

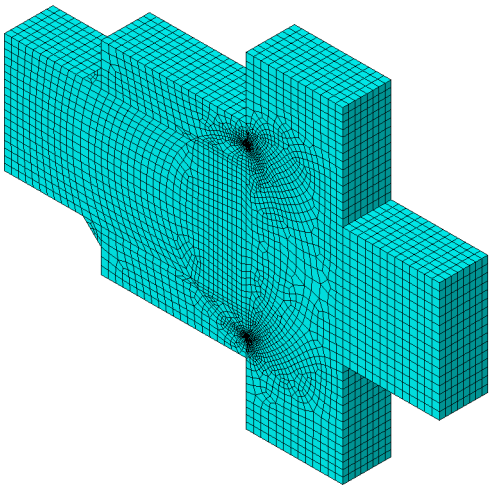

Submodel

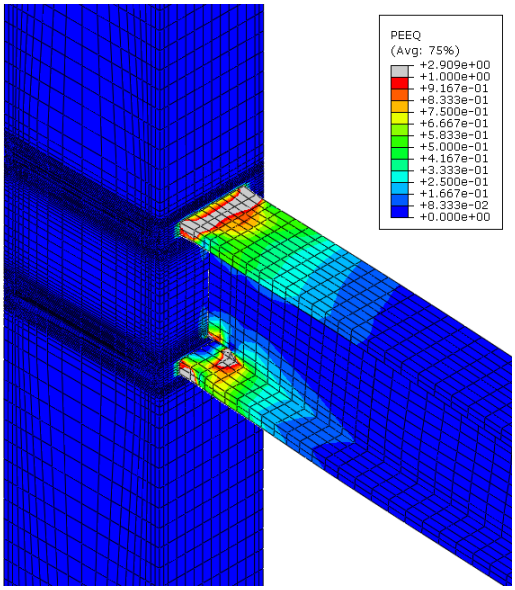

Final state of global model (PEEQ)

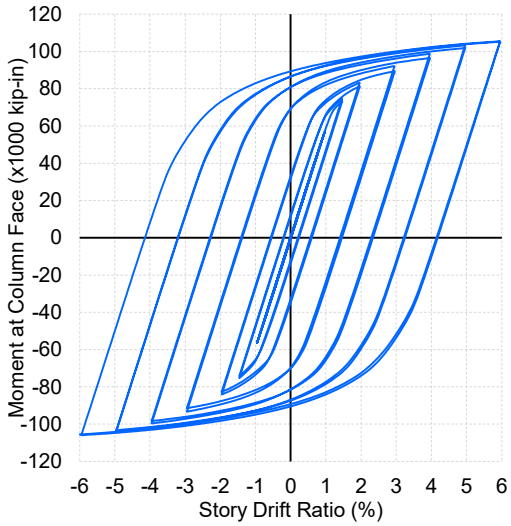

Load-displacement

Simulation 8 cont.

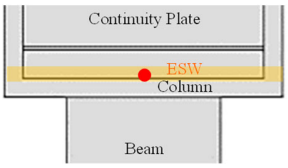

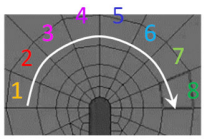

Element 5 and max (1~8)

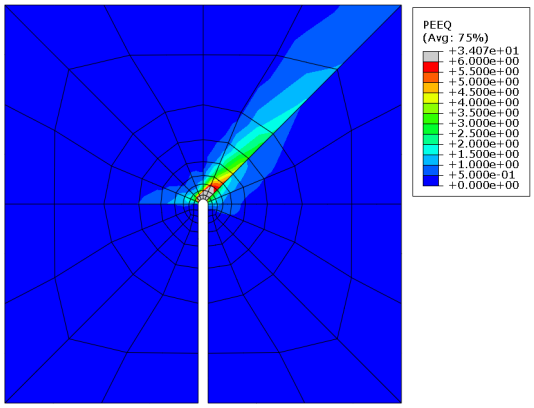

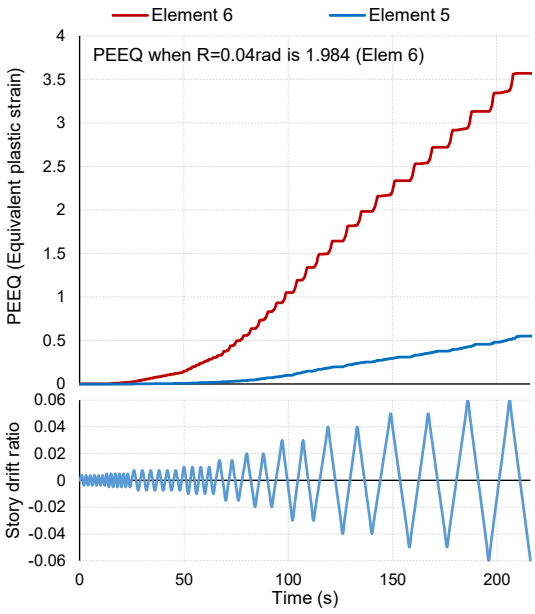

Final state of submodel (PEEQ)

PEEQ

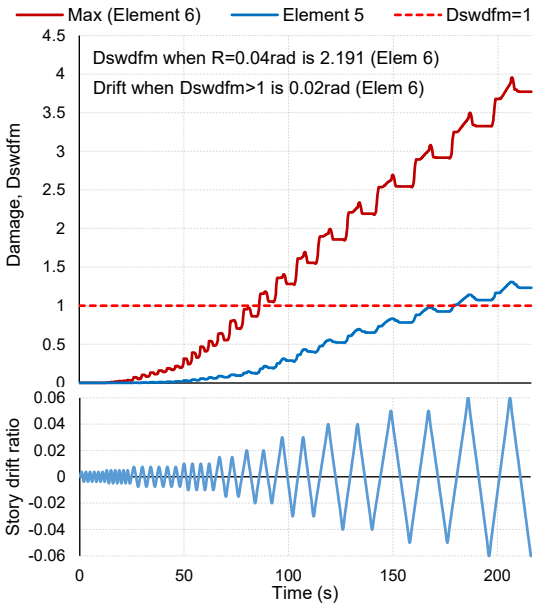

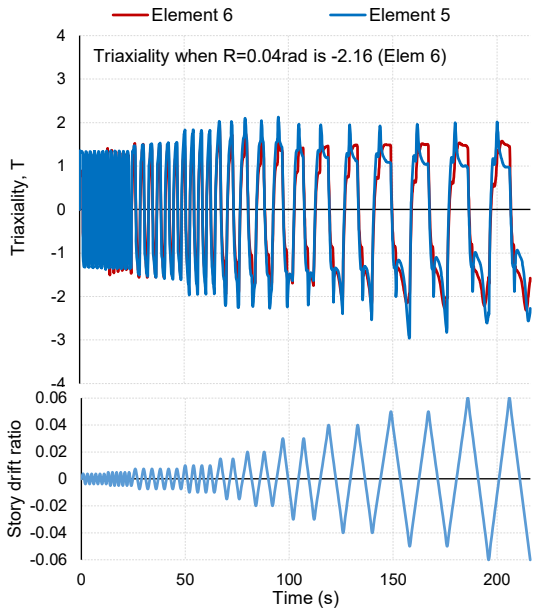

Damage

Triaxiality

Simulation 8 cont.

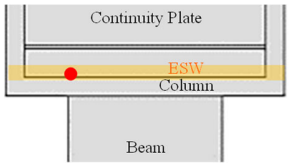

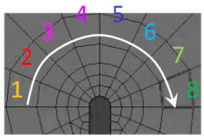

Element 5 and max (1~8)

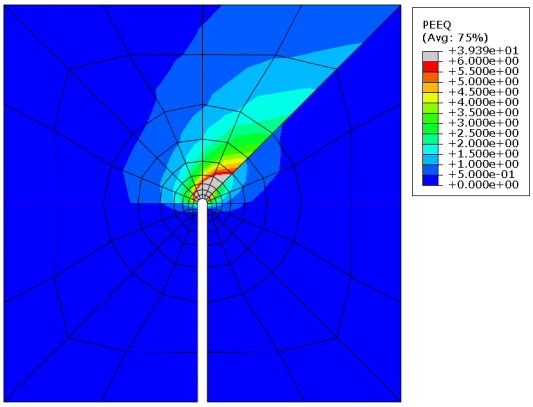

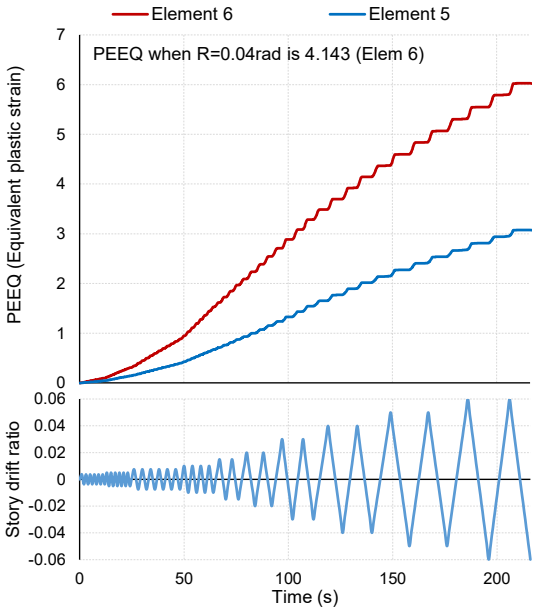

PEEQ

Final state of submodel (PEEQ)

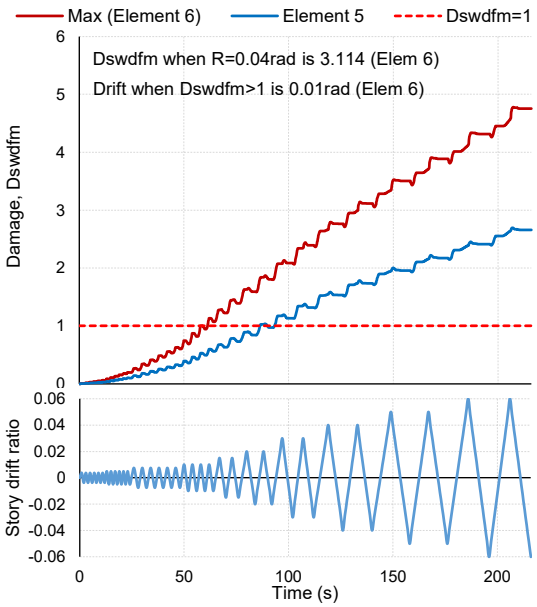

Damage

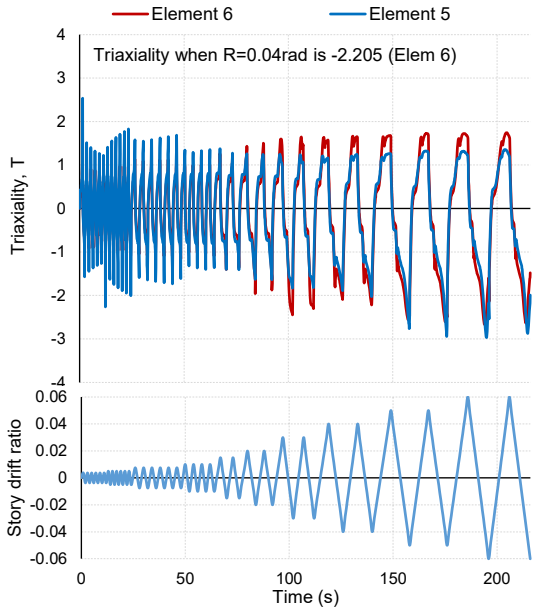

Triaxiality

Simulation 9

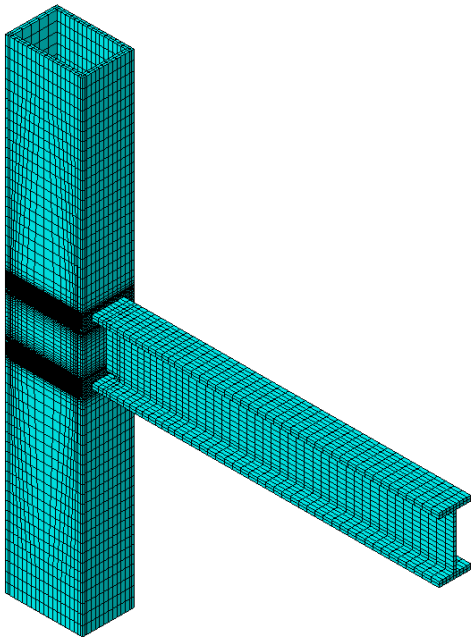

Global model

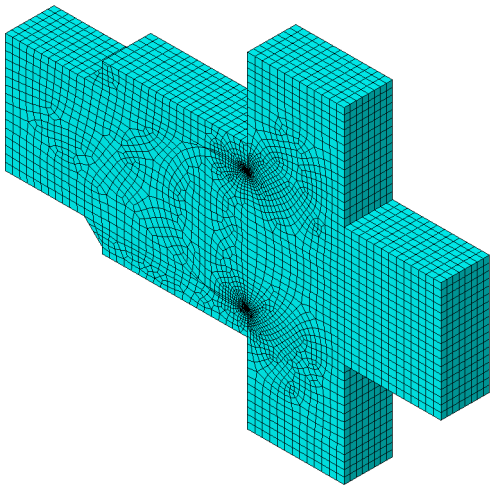

Submodel

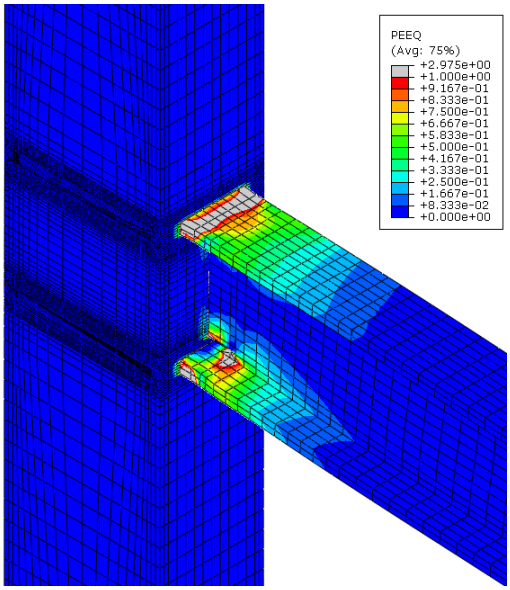

Final state of global model (PEEQ)

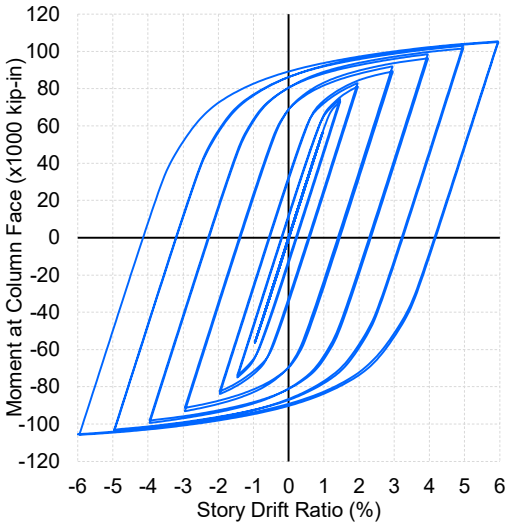

Load-displacement

Simulation 9 cont.

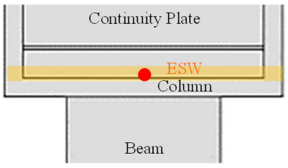

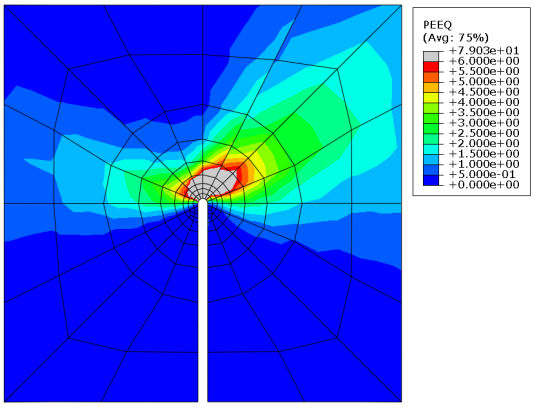

Final state of submodel (PEEQ)

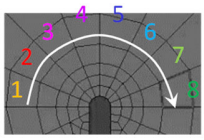

Element 5 and max (1~8)

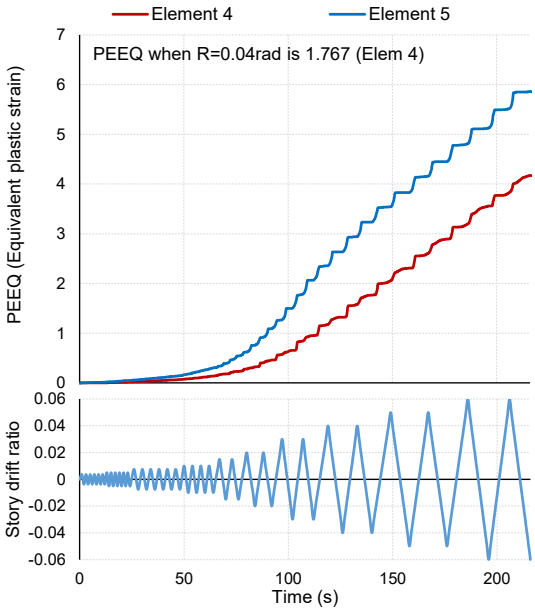

PEEQ

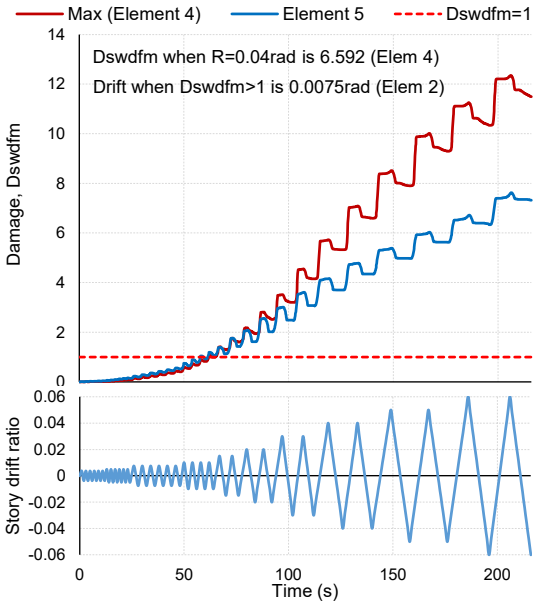

Damage

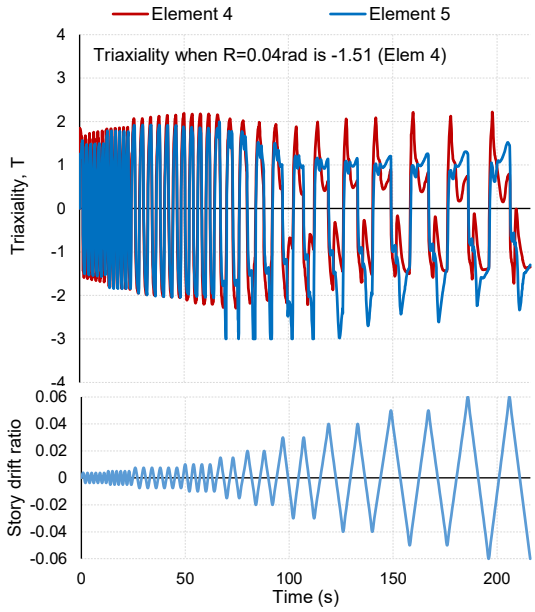

Triaxiality

Simulation 10

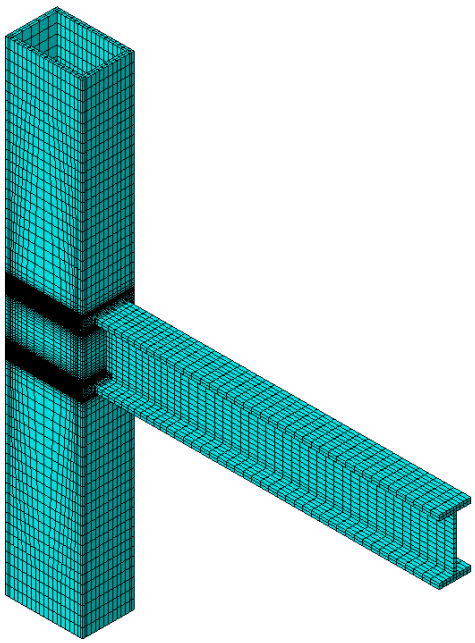

Global model

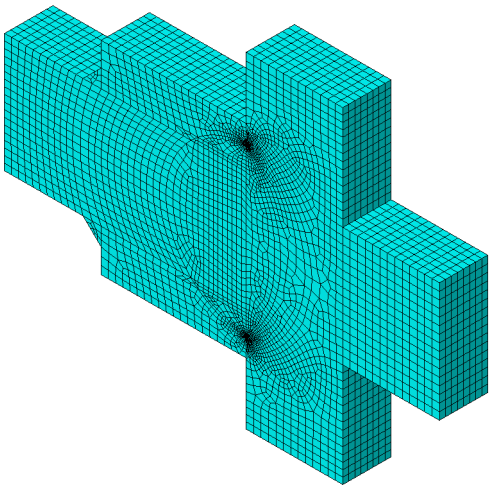

Submodel

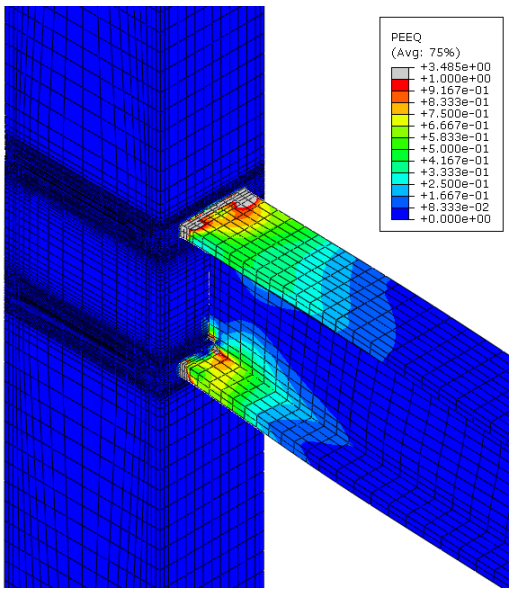

Final state of global model (PEEQ)

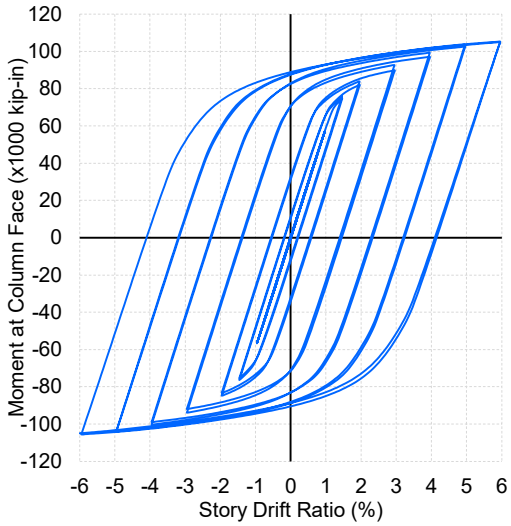

Load-displacement

Simulation 10 cont.

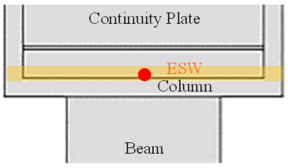

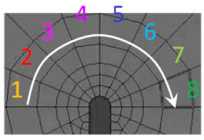

Element 5 and max (1~8)

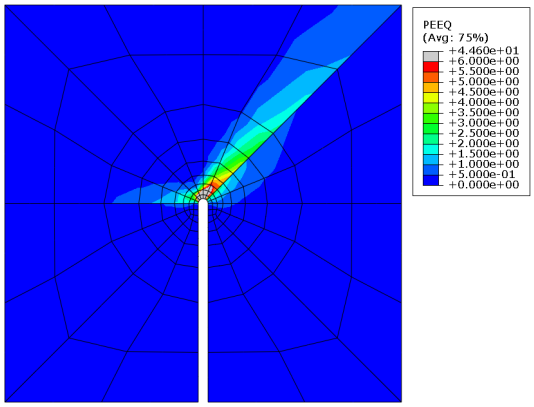

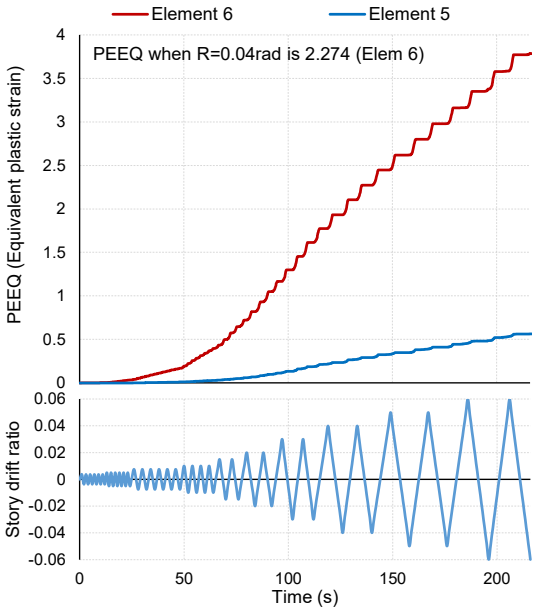

Final state of submodel (PEEQ)

PEEQ

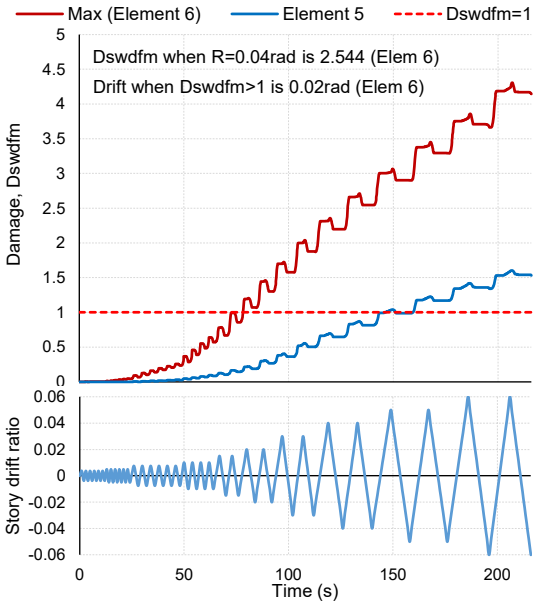

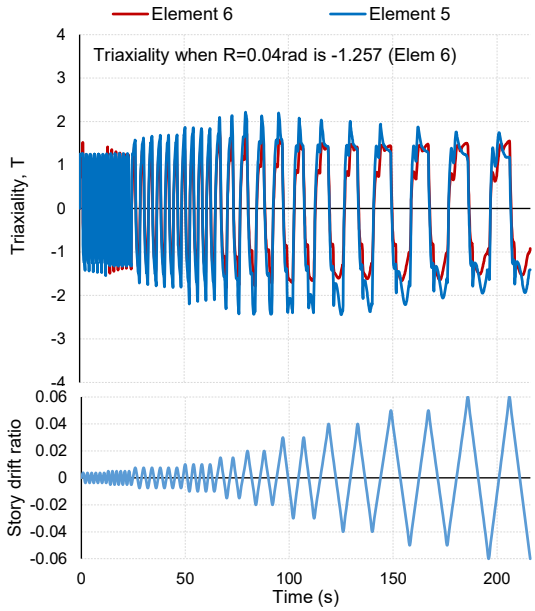

Damage

Triaxiality

Simulation 11

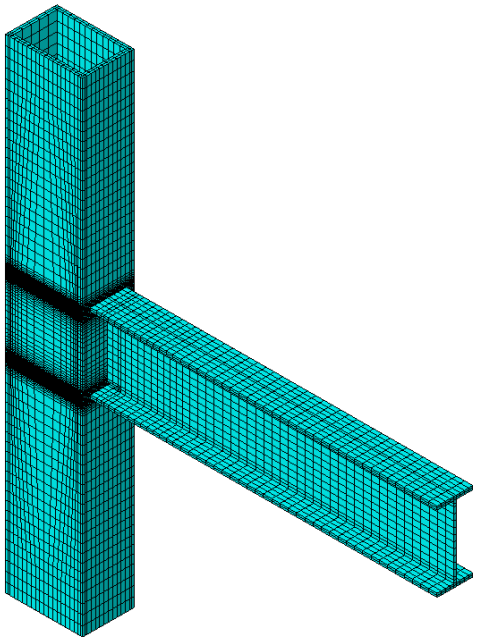

Global model

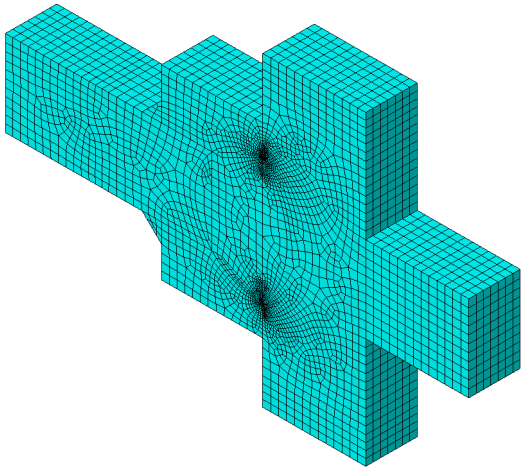

Submodel

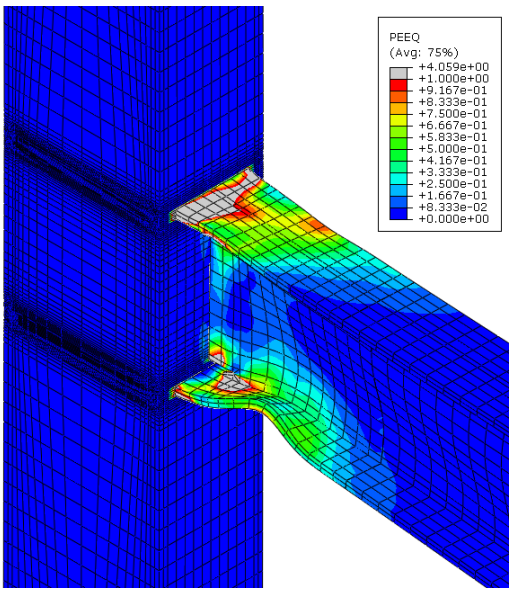

Final state of global model (PEEQ)

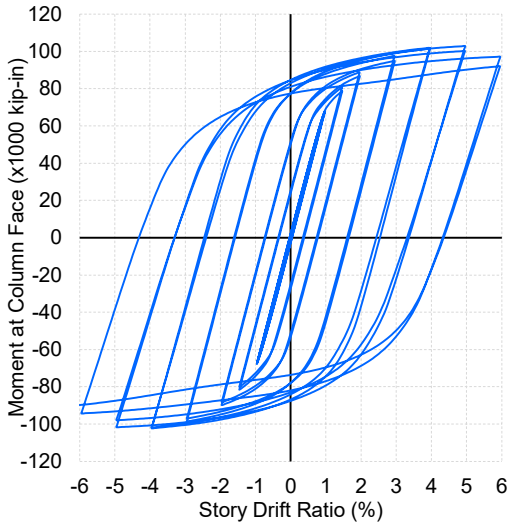

Load-displacement

Simulation 11 cont.

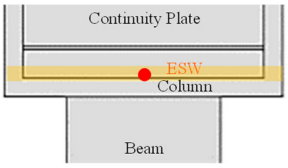

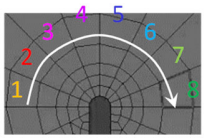

Element 5 and max (1~8)

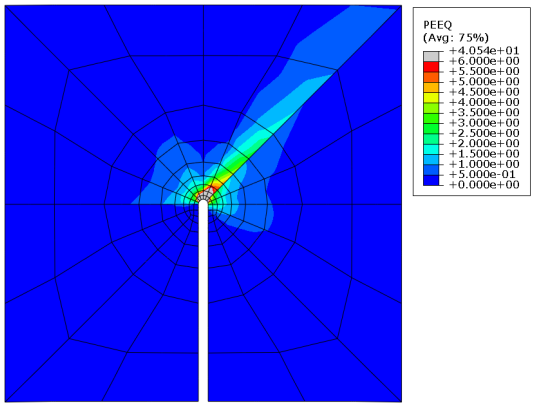

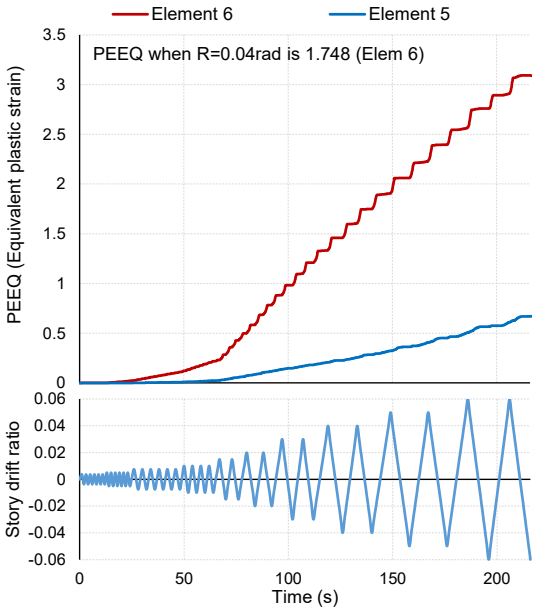

Final state of submodel (PEEQ)

PEEQ

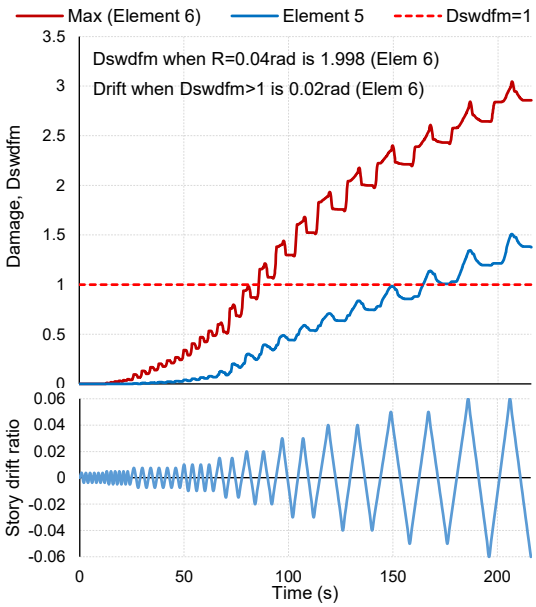

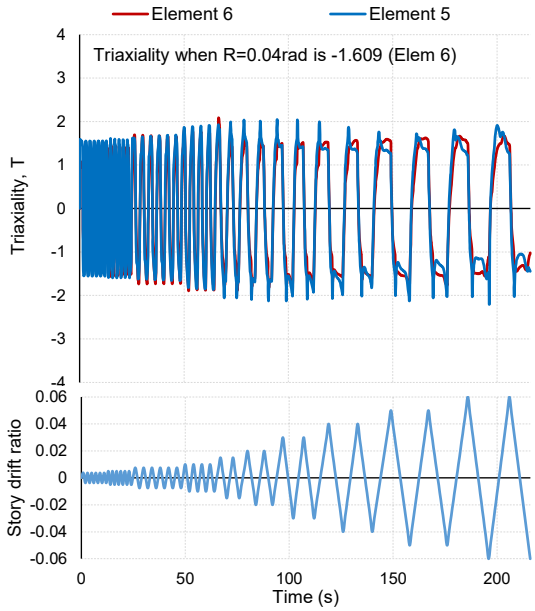

Damage

Triaxiality

Simulation 12

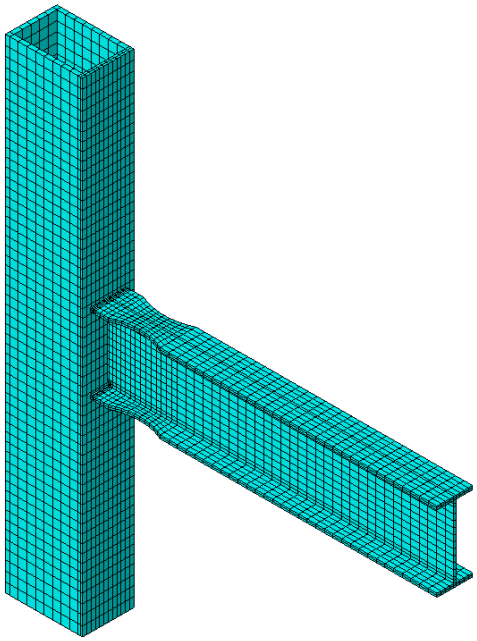

Global model

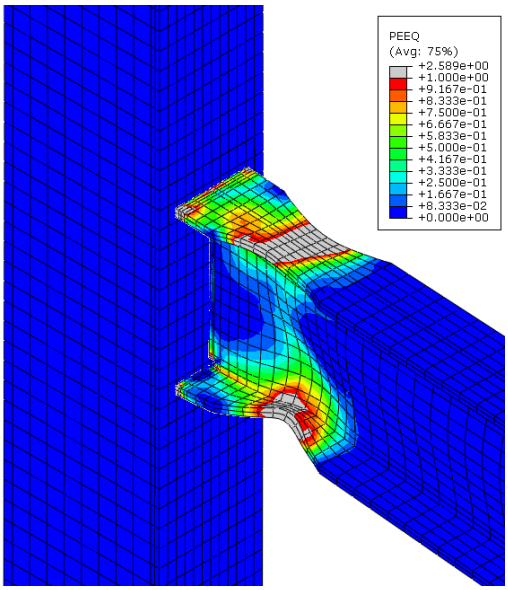

Final state of global model (PEEQ)

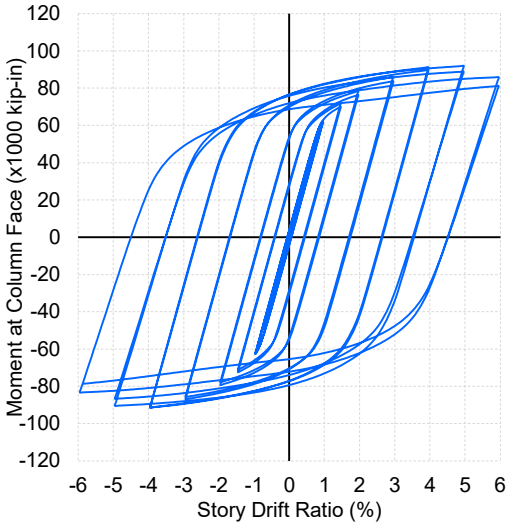

Load-displacement

Simulation 6-2

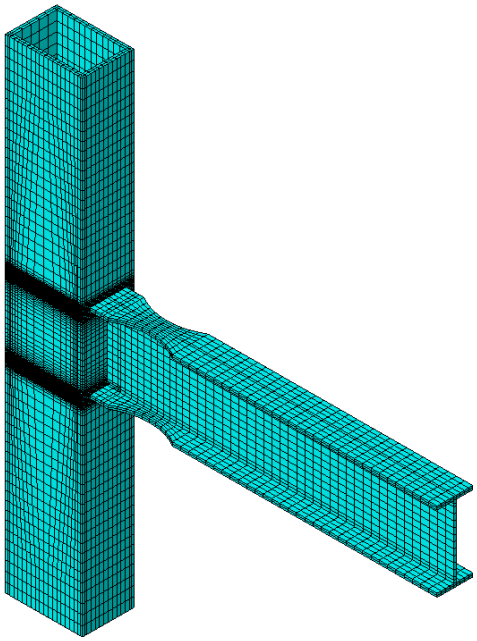

Global model

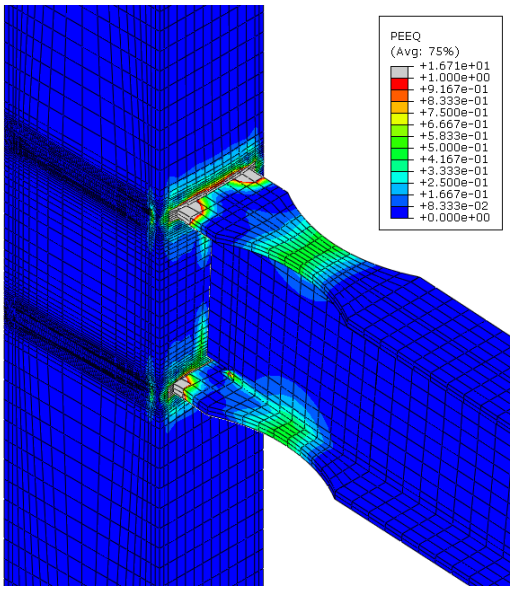

Final state of global model (PEEQ)

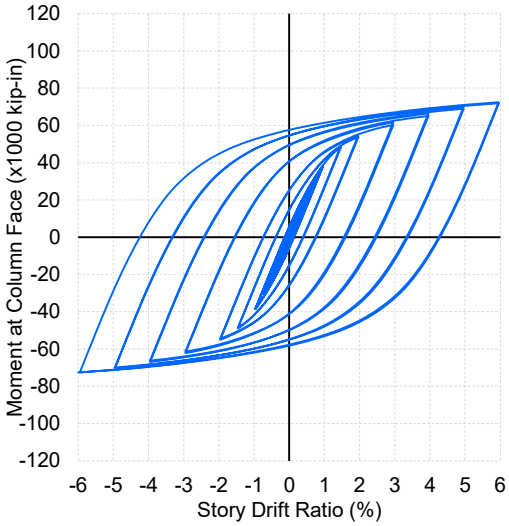

Load-displacement

Simulation 12-2

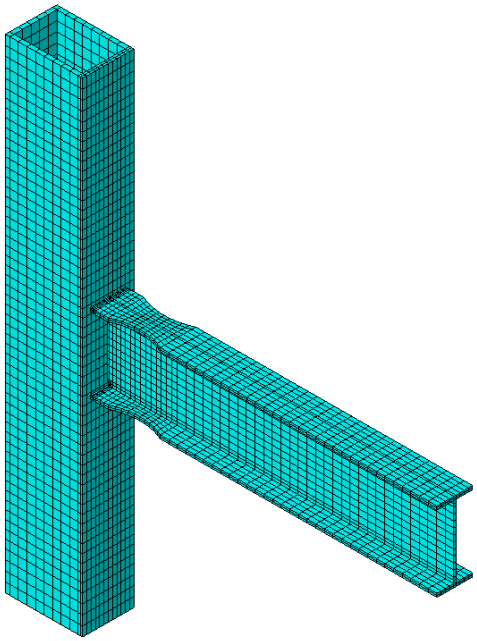

Global model

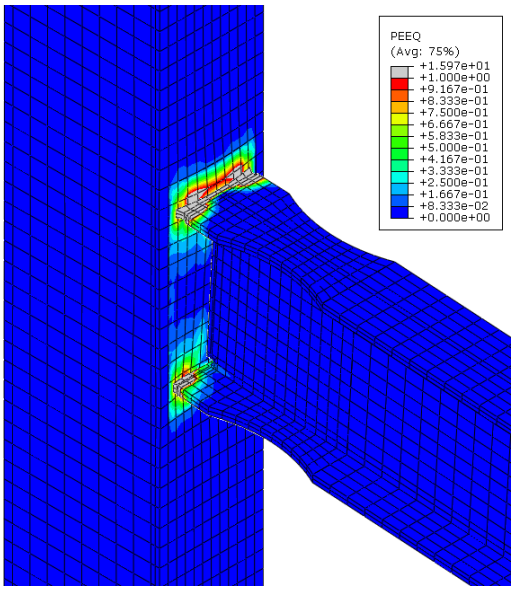

Final state of global model (PEEQ)

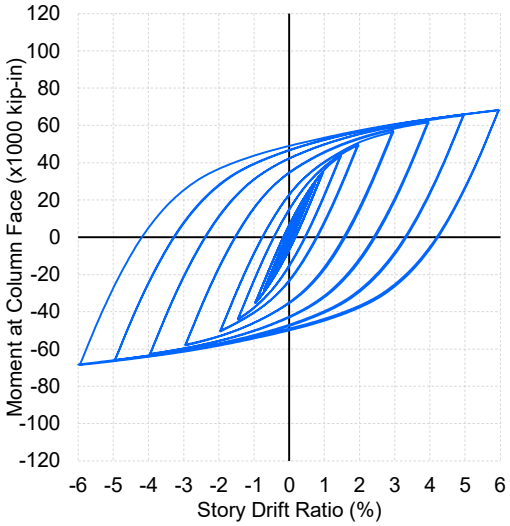

Load-displacement

Simulation 13

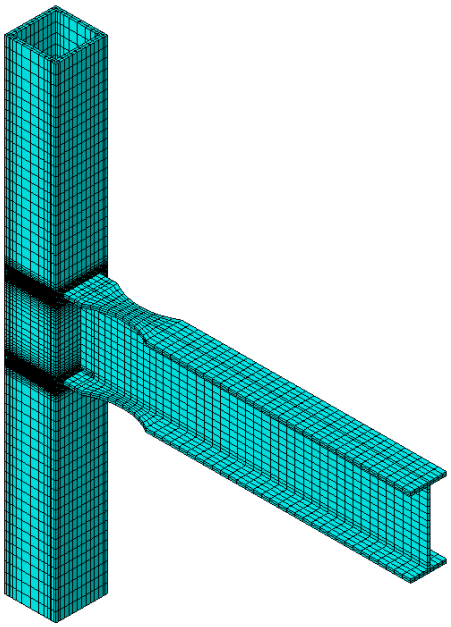

Global model

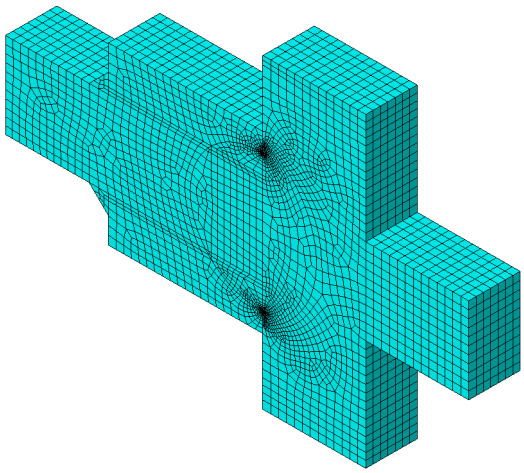

Submodel

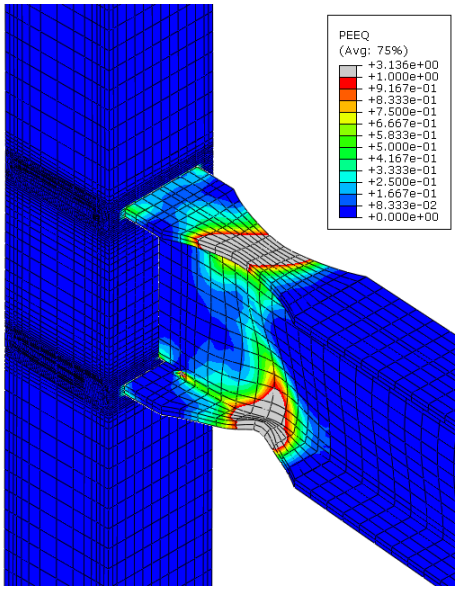

Final state of global model (PEEQ)

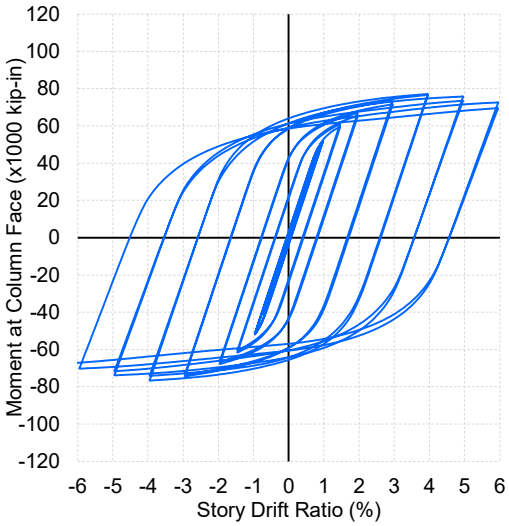

Load-displacement

Simulation 13 cont.

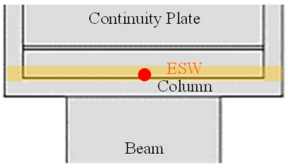

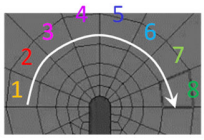

Element 5 and max (1~8)

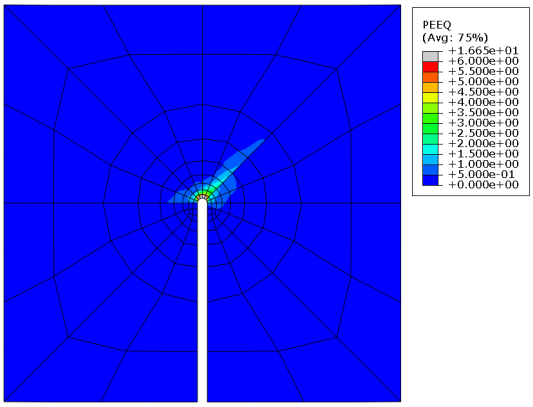

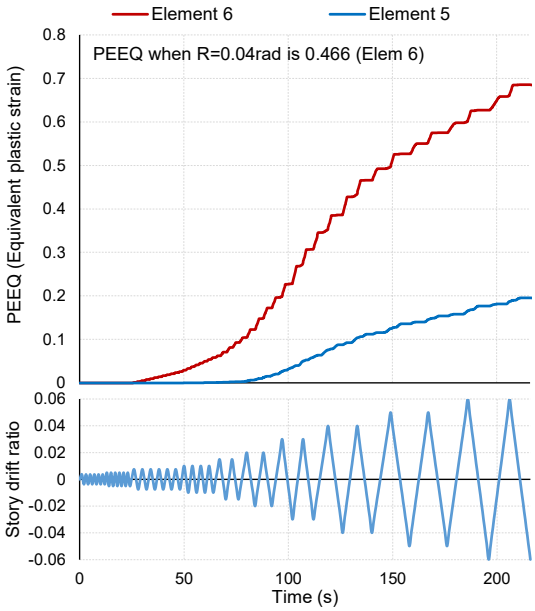

Final state of submodel (PEEQ)

PEEQ

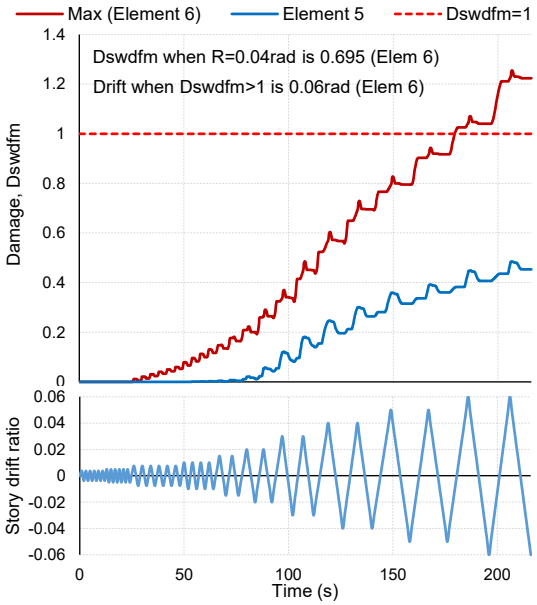

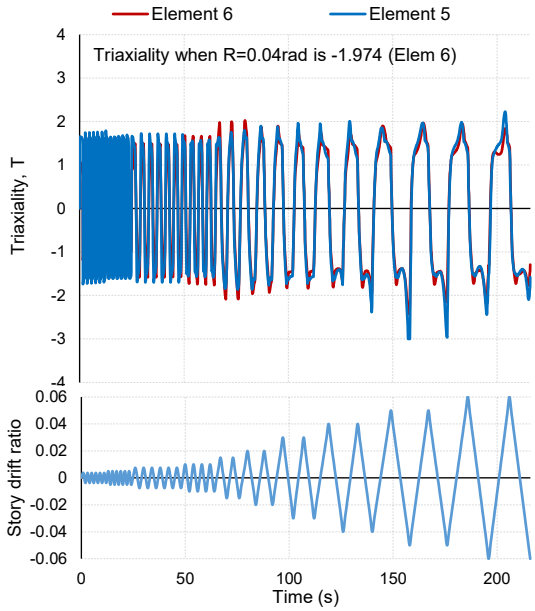

Damage

Triaxiality

Simulation 13 cont.

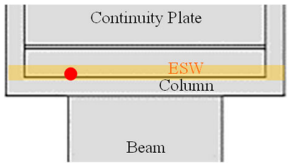

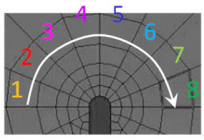

Element 5 and max (1~8)

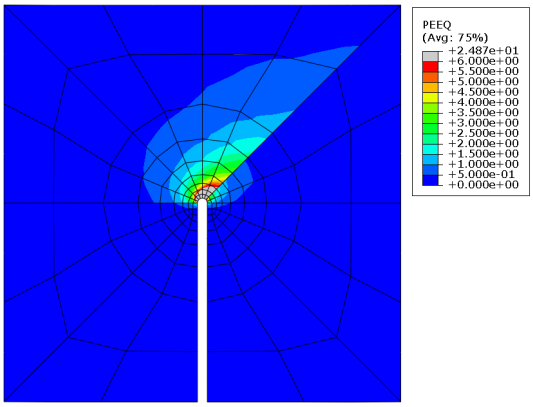

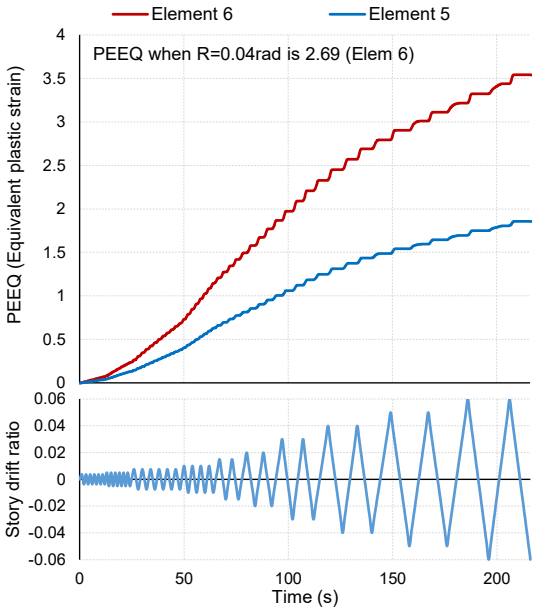

Final state of submodel (PEEQ)

PEEQ

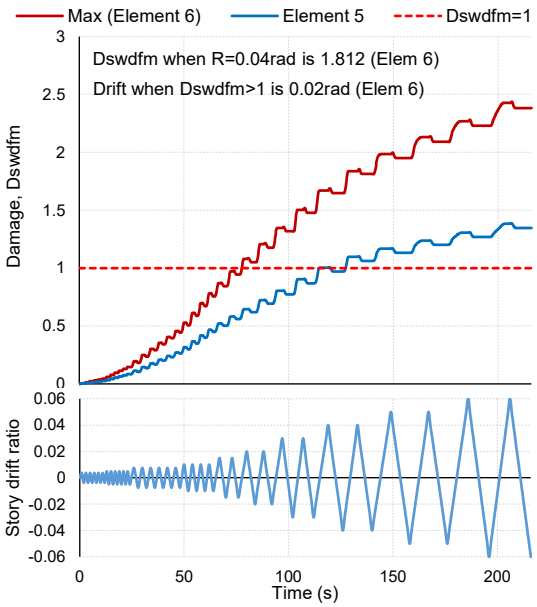

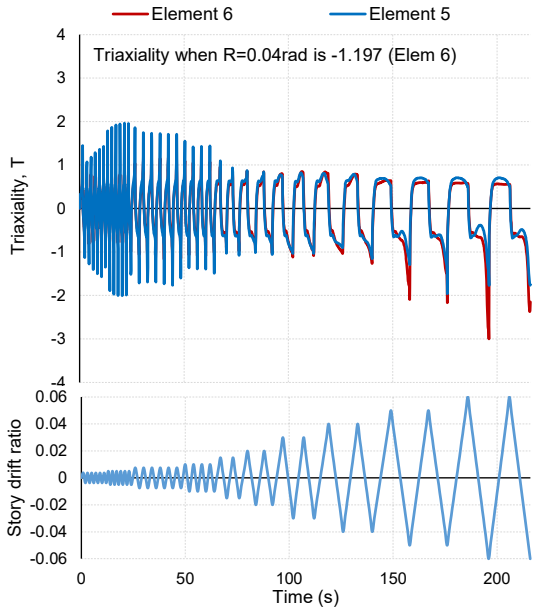

Damage

Triaxiality

Simulation 14

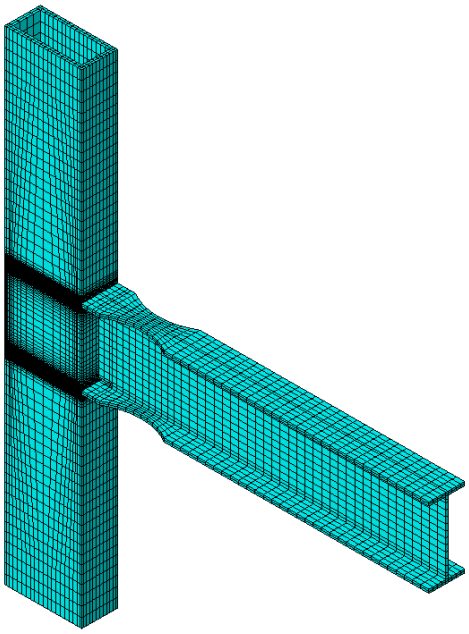

Global model

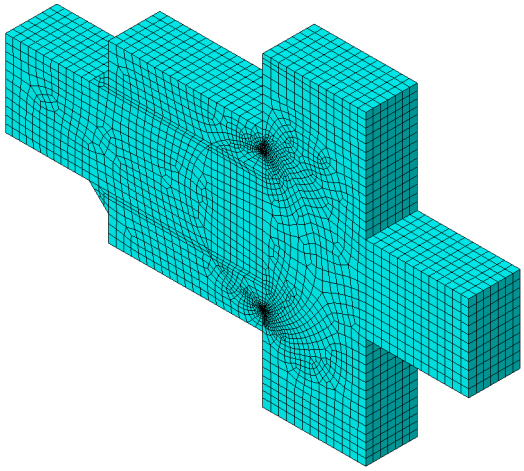

Submodel

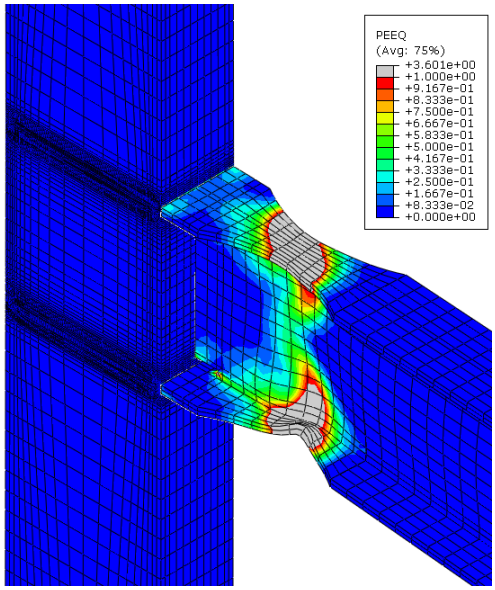

Final state of global model (PEEQ)

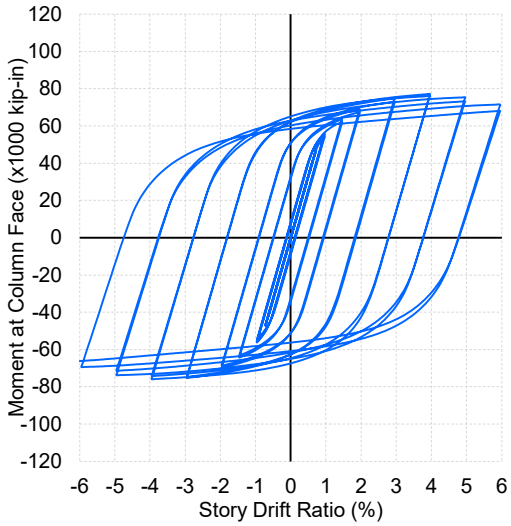

Load-displacement

Simulation 14 cont.

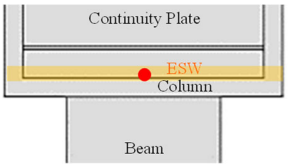

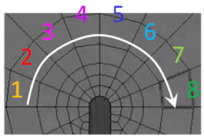

Element 5 and max (1~8)

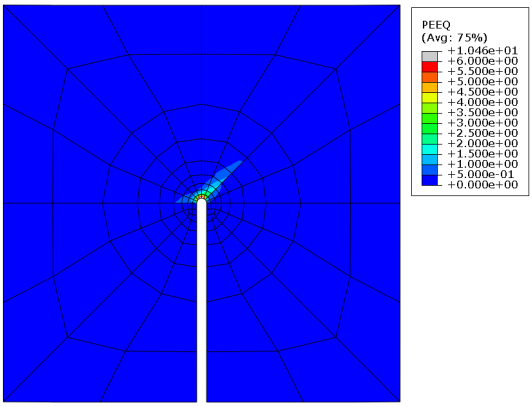

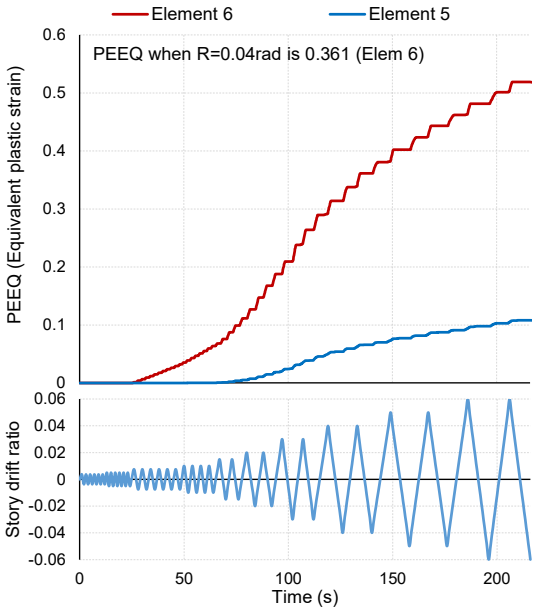

Final state of submodel (PEEQ)

PEEQ

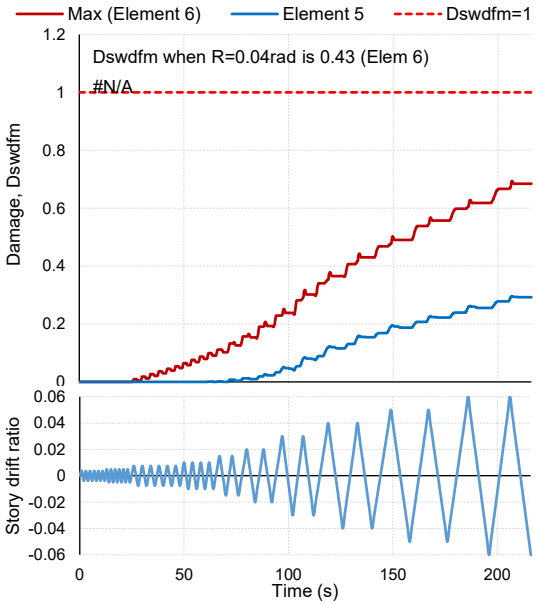

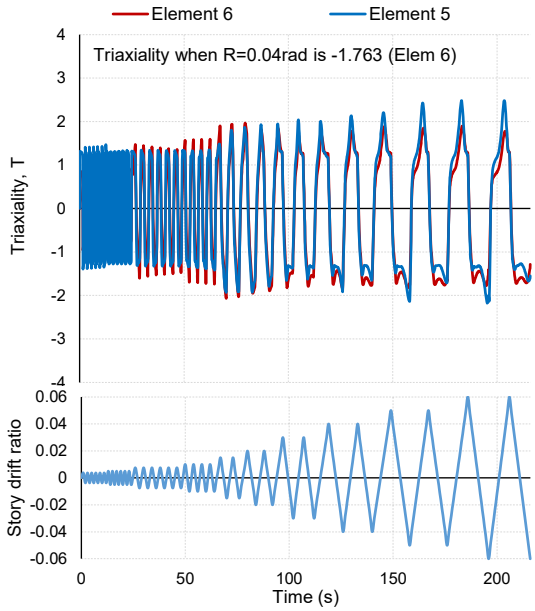

Damage

Triaxiality

Simulation 14 cont.

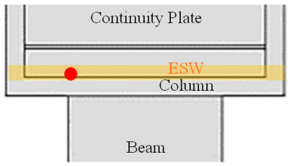

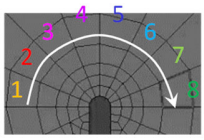

Element 5 and max (1~8)

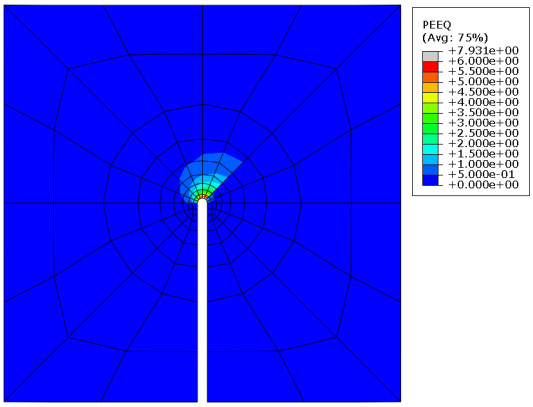

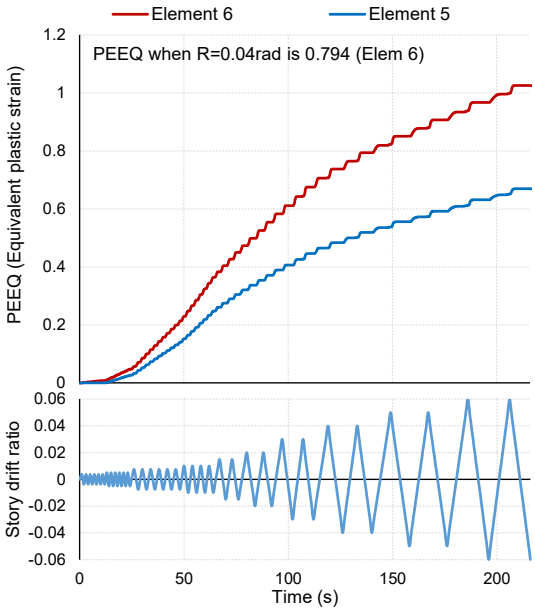

Final state of submodel (PEEQ)

PEEQ

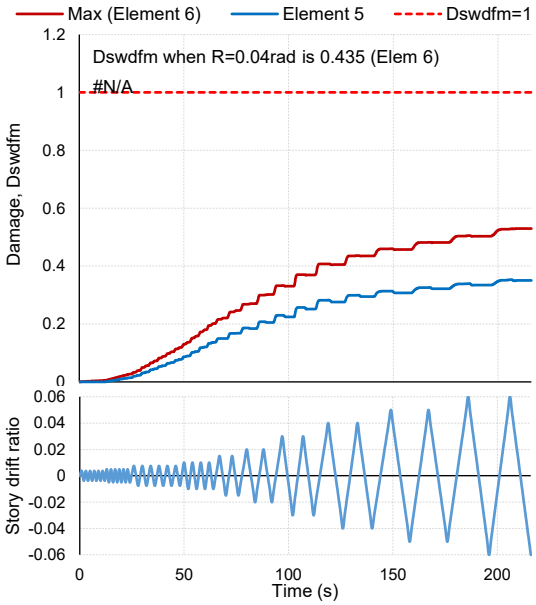

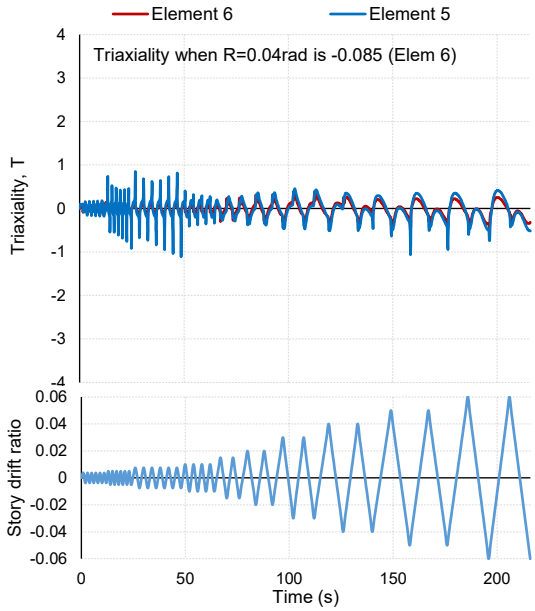

Damage

Triaxiality

Simulation 15

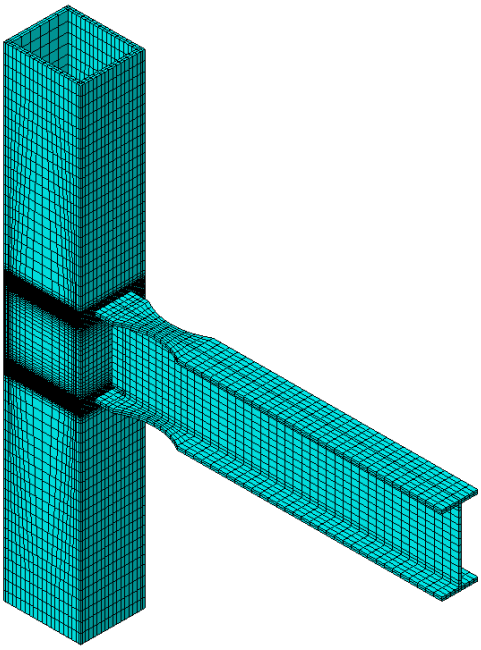

Global model

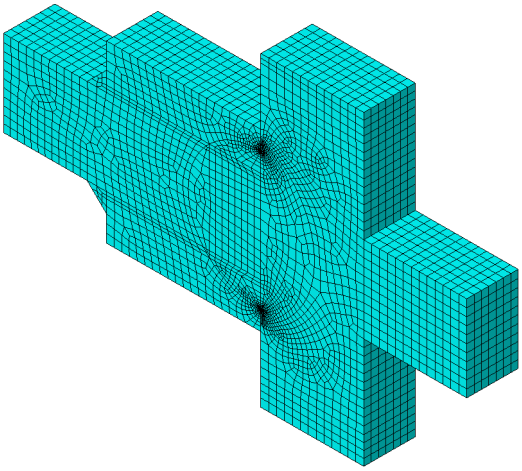

Submodel

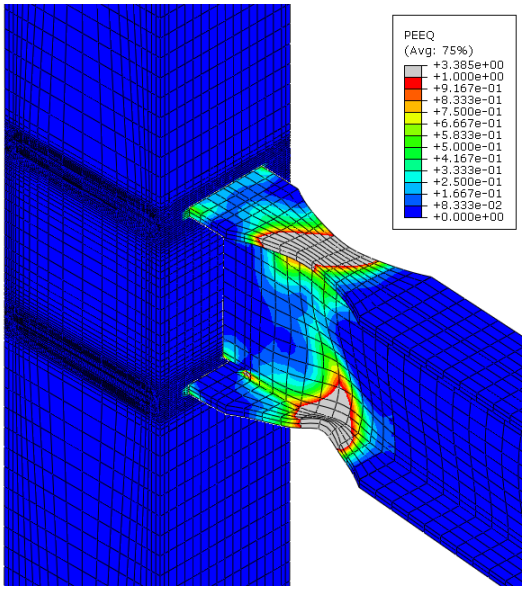

Final state of global model (PEEQ)

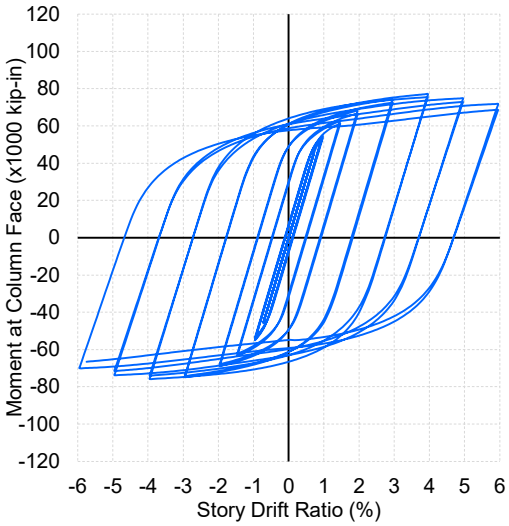

Load-displacement

Simulation 15 cont.

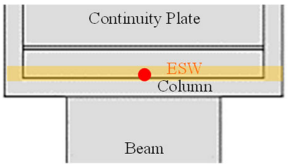

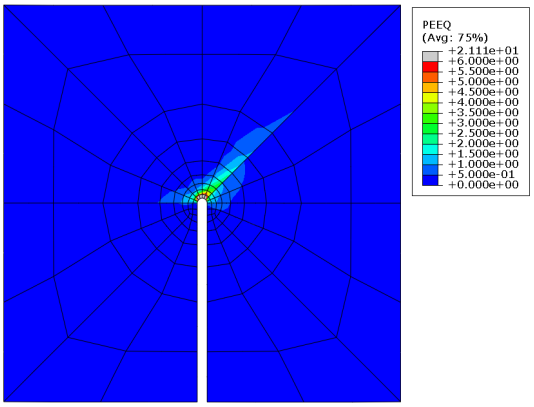

Final state of submodel (PEEQ)

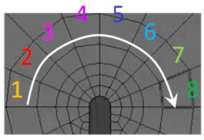

Element 5 and max (1~8)

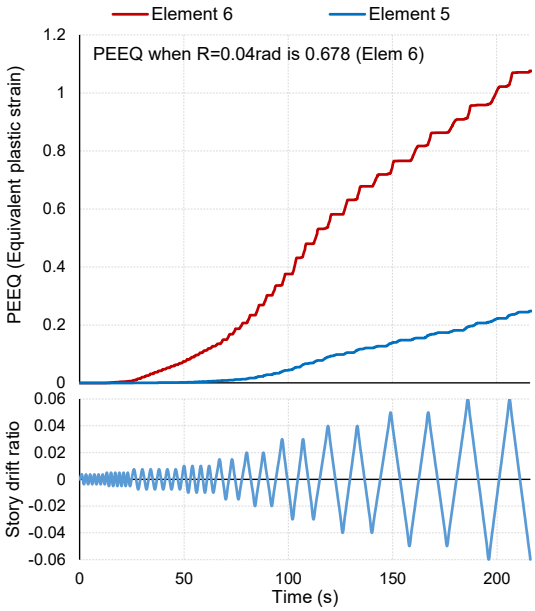

PEEQ

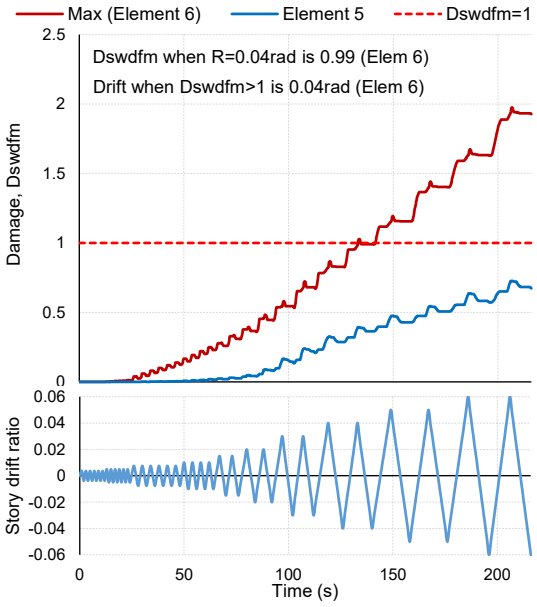

Damage

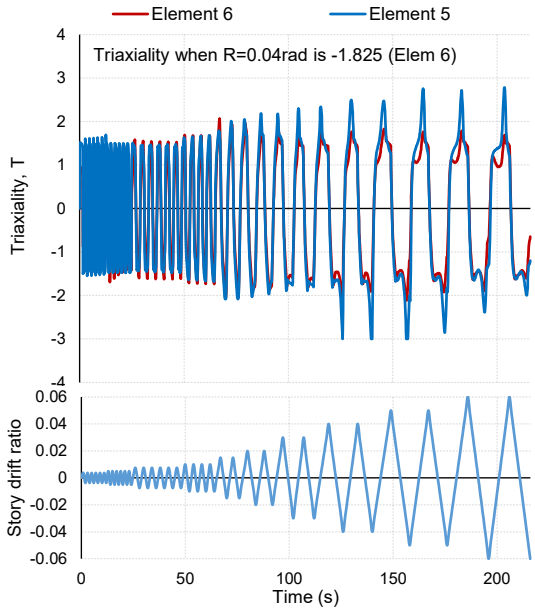

Triaxiality

Simulation 15 cont.

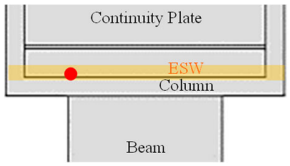

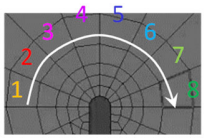

Element 5 and max (1~8)

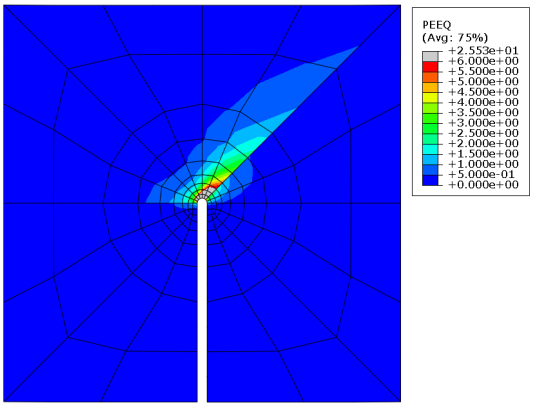

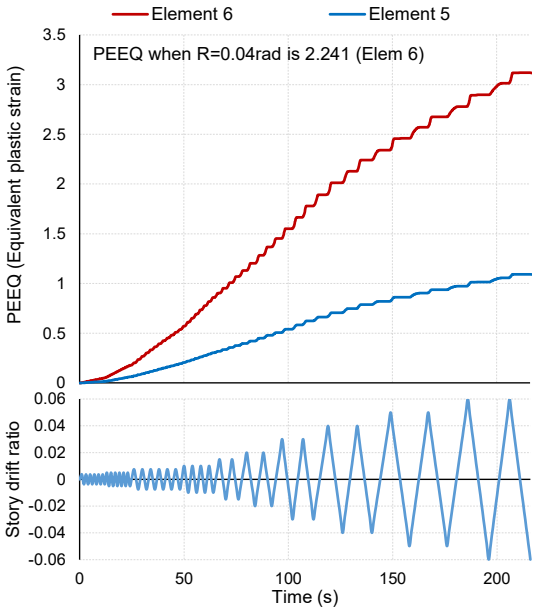

Final state of submodel (PEEQ)

PEEQ

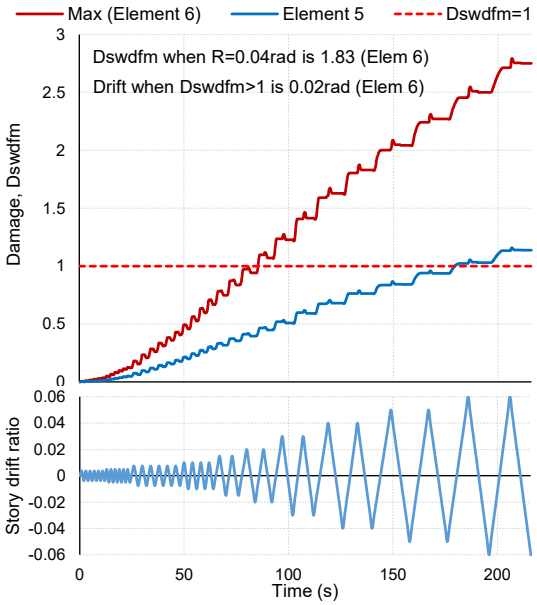

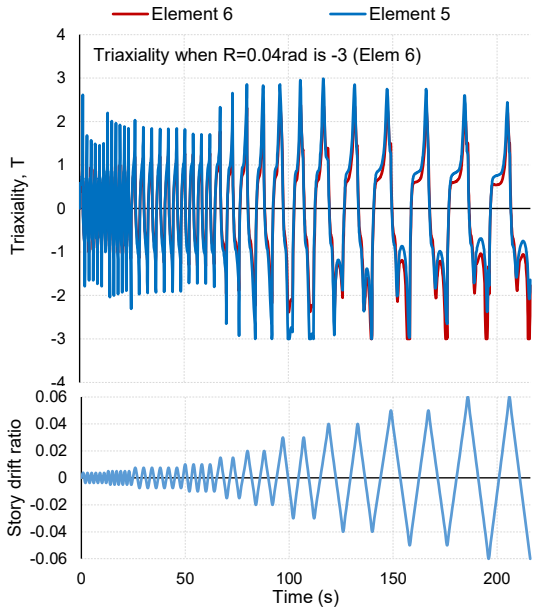

Damage

Triaxiality

Simulation 15 cont.

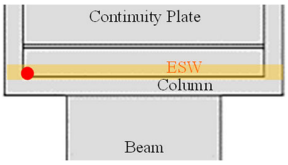

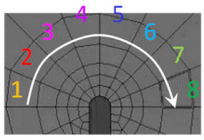

Element 5 and max (1~8)

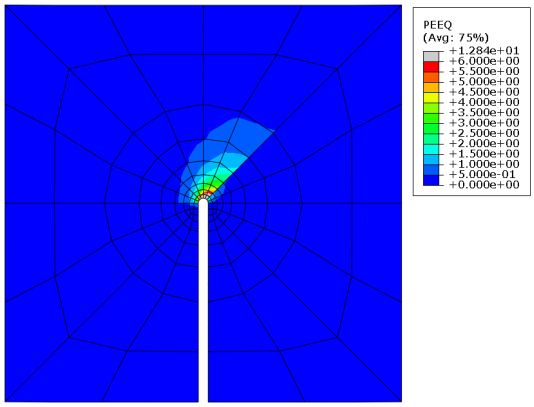

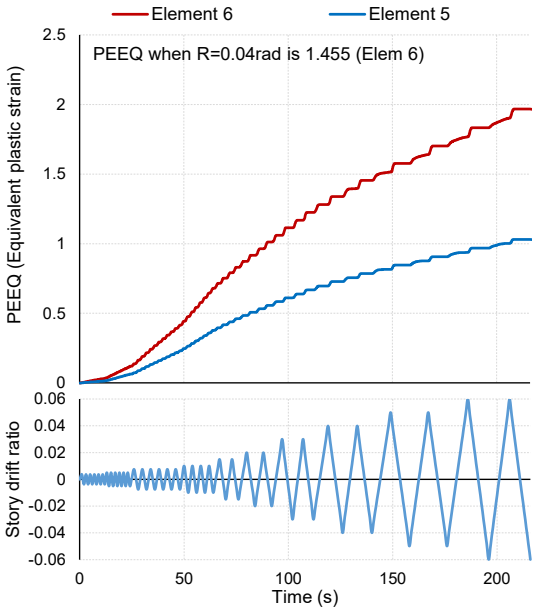

Final state of submodel (PEEQ)

PEEQ

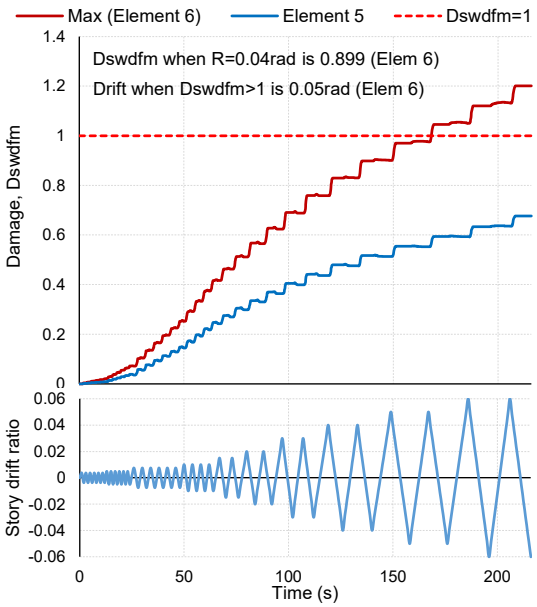

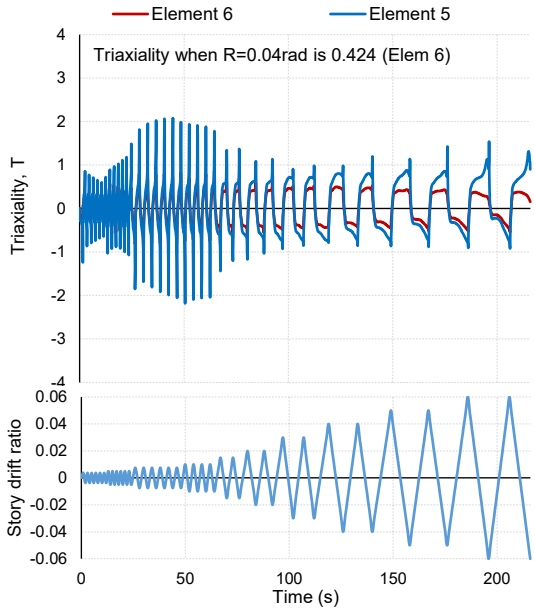

Damage

Triaxiality

Simulation 16

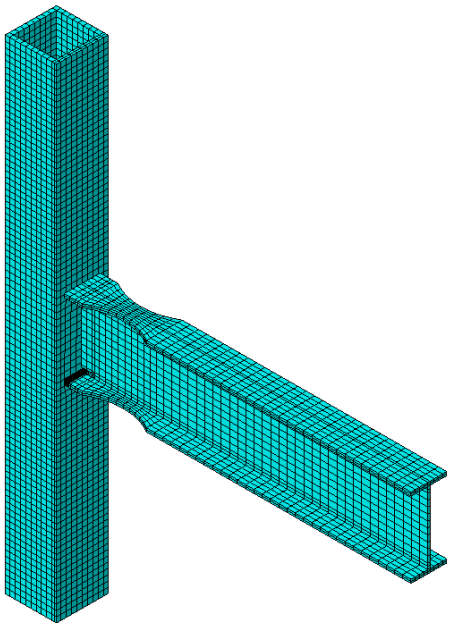

Global model

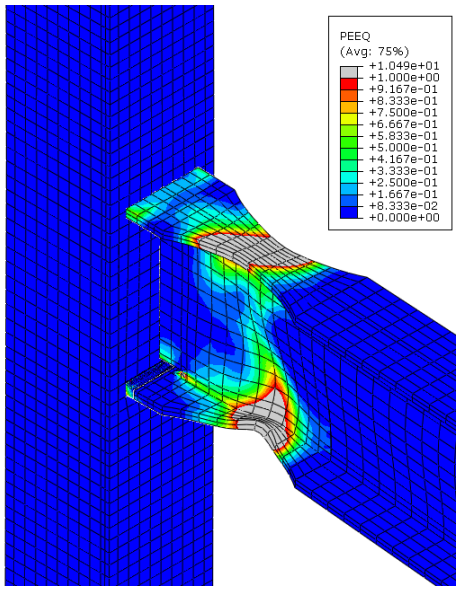

Final state of global model (PEEQ)

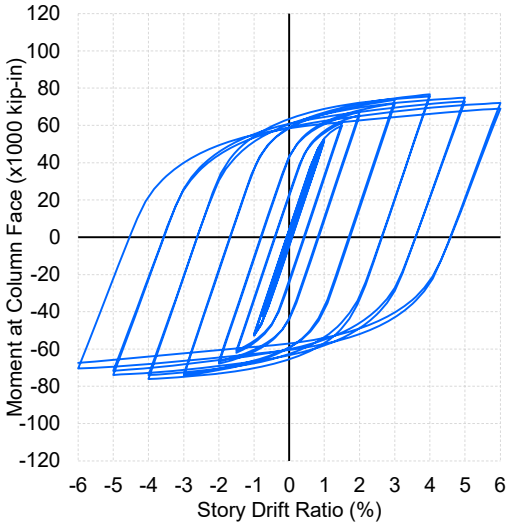

Load-displacement

Simulation 16 cont.

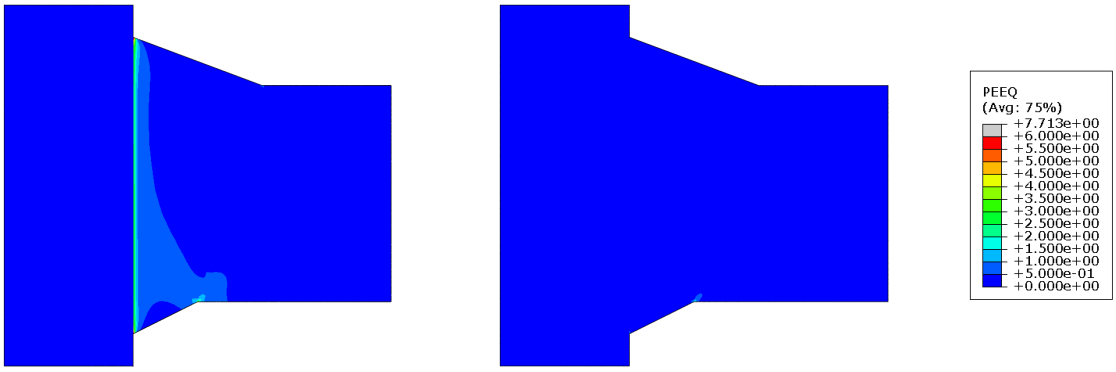

Edge Center

PEEQ at *R*=0.04 rad

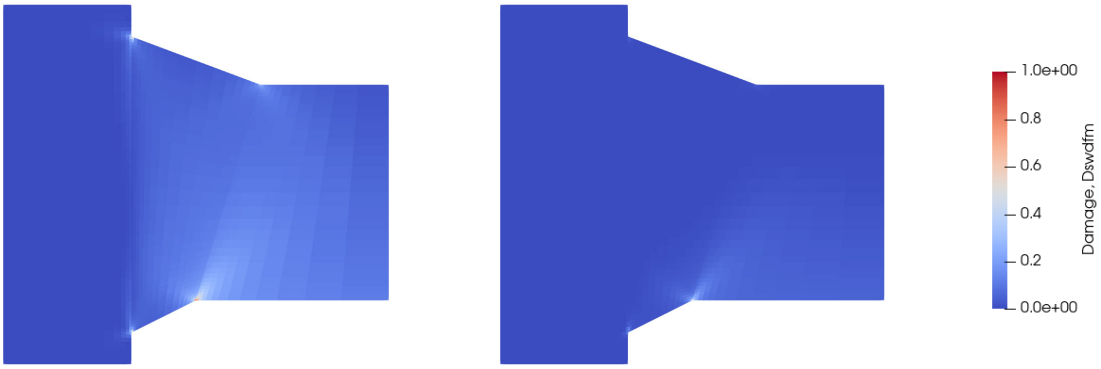

Edge Center

Damage at *R*=0.04 rad

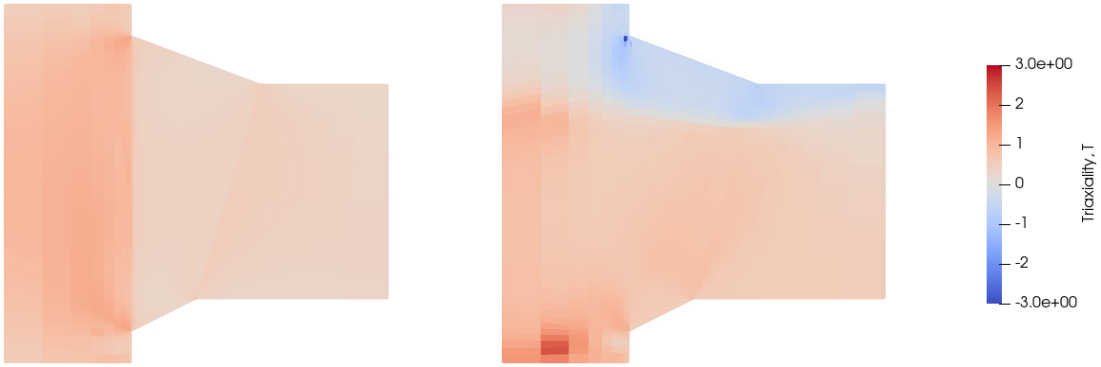

Edge Center

Triaxiality at *R*=0.04 rad (Time =133s, flange in tension)

Simulation 17

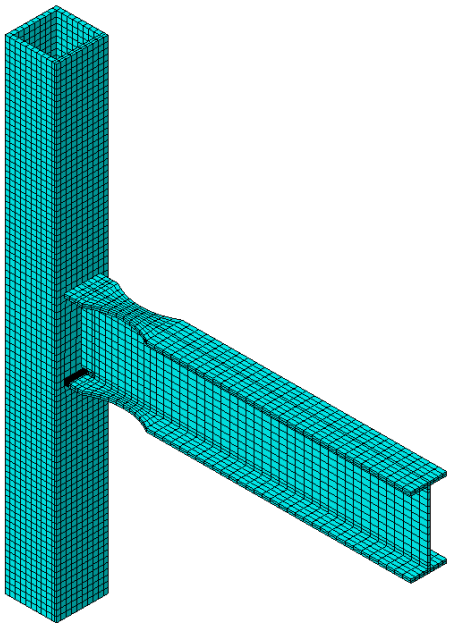

Global model

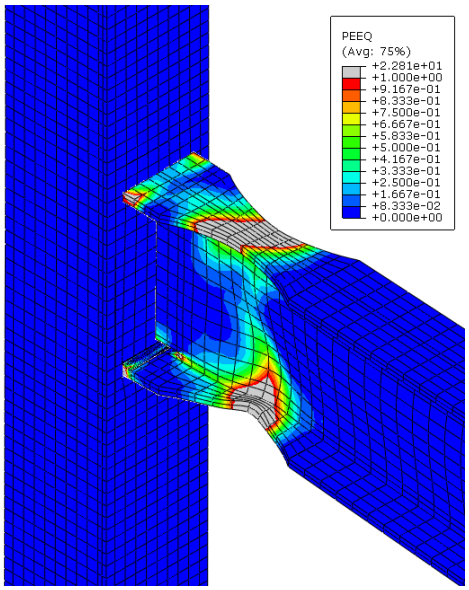

Final state of global model (PEEQ)

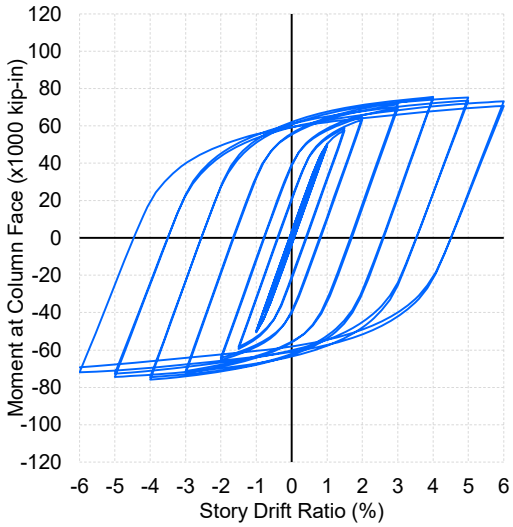

Load-displacement

Simulation 17 cont.

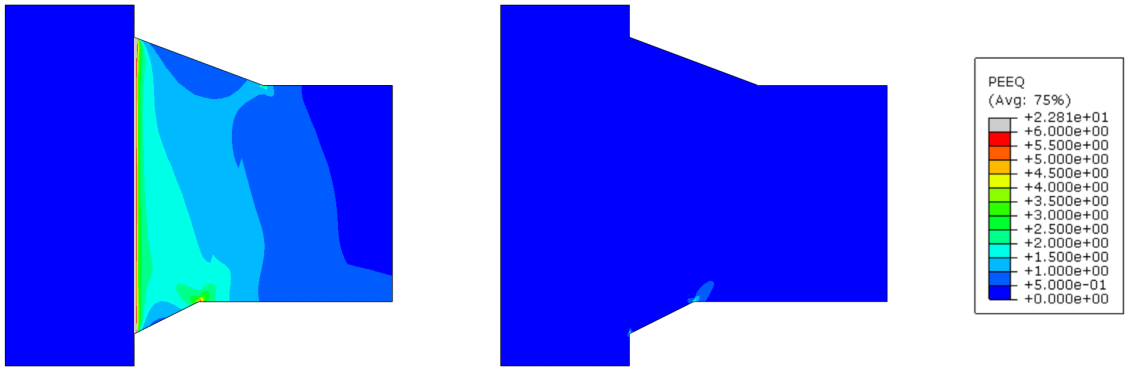

Edge Center

PEEQ at *R*=0.04 rad

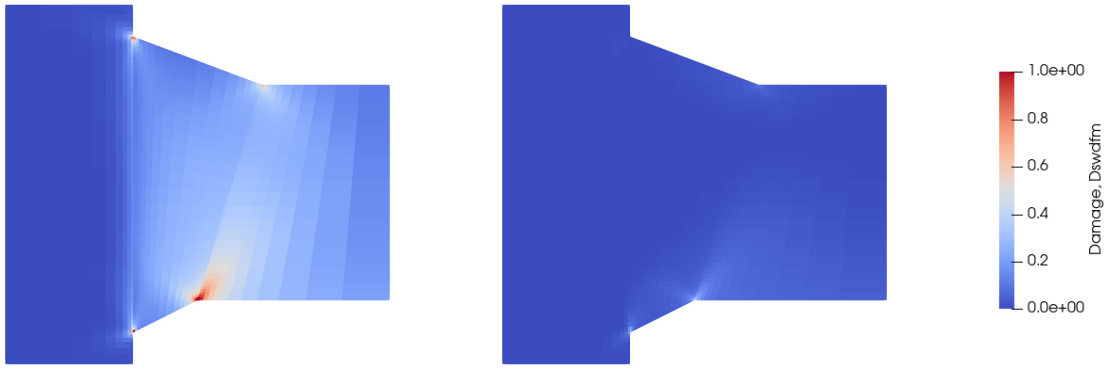

Edge Center

Damage at *R*=0.04 rad

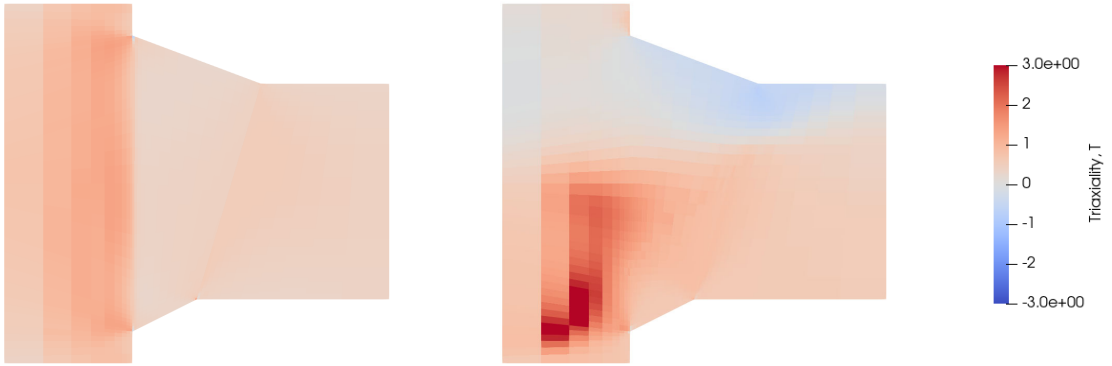

Edge Center

Triaxiality at *R*=0.04 rad (Time =133s, flange in tension)

Simulation 18

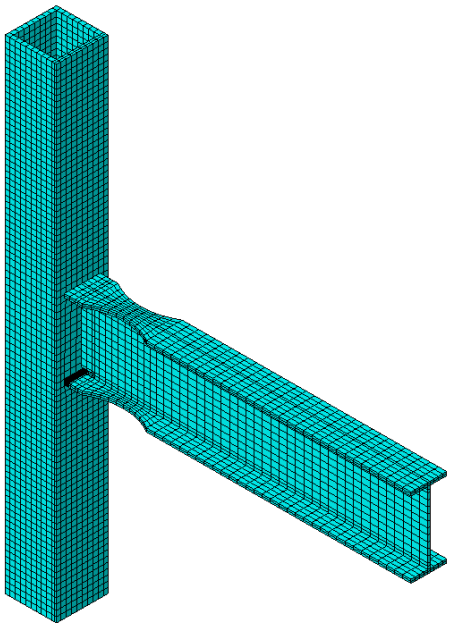

Global model

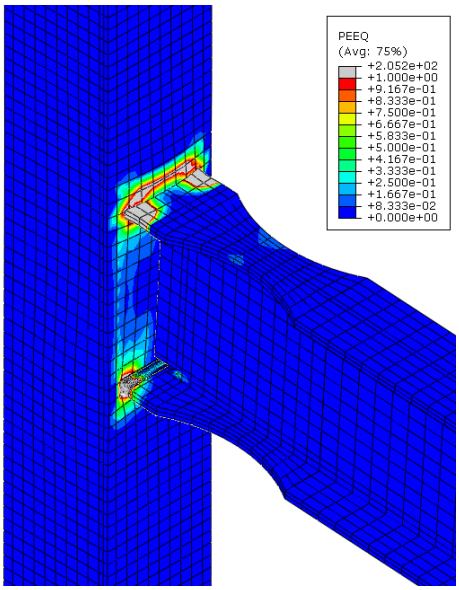

Final state of global model (PEEQ)

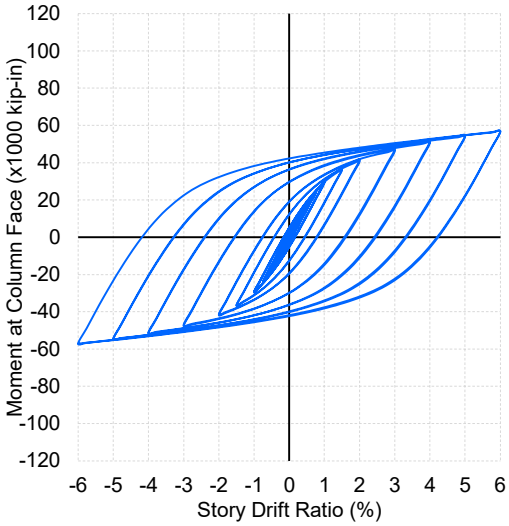

Load-displacement

Simulation 18 cont.

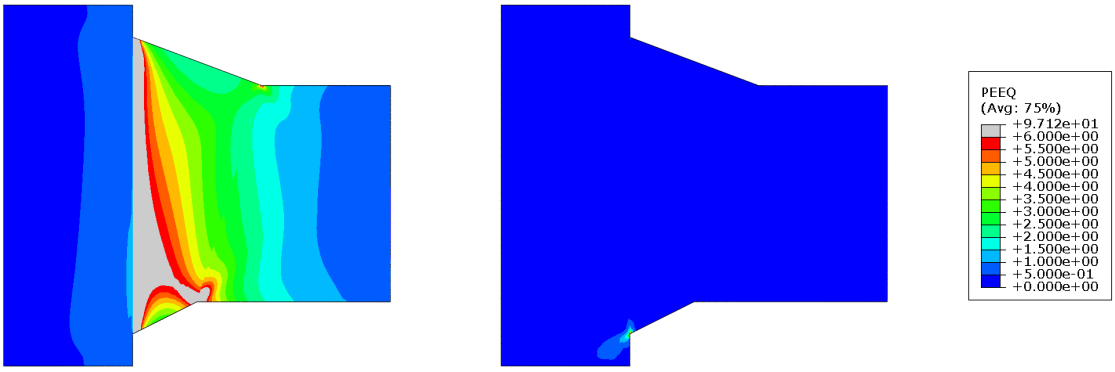

Edge Center

PEEQ at R=0.04 rad

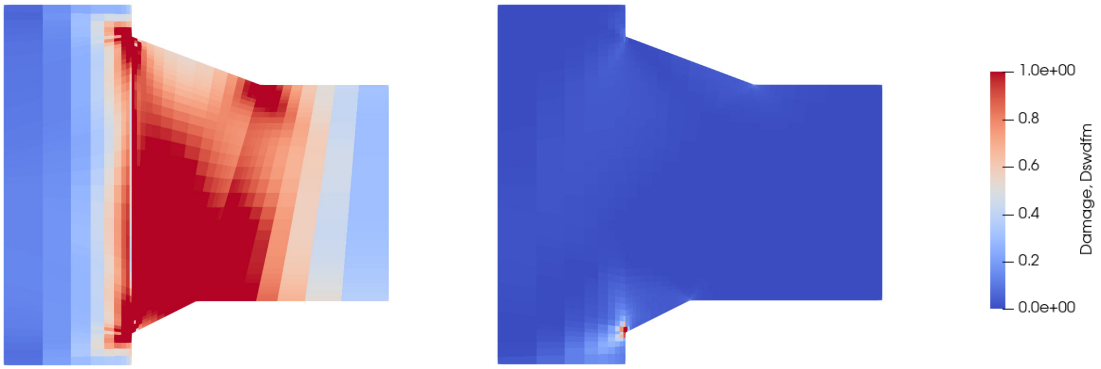

Edge Center

Damage at R=0.04 rad

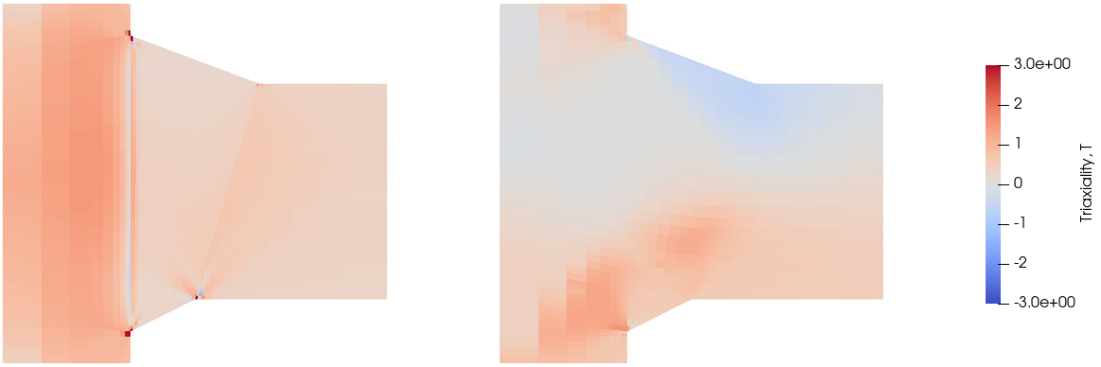

Edge Center

Triaxiality at R=0.04 rad (Time =133s, flange in tension)

Simulation 19

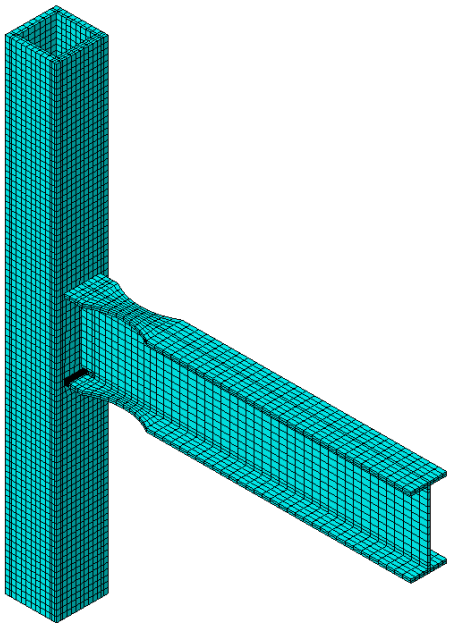

Global model

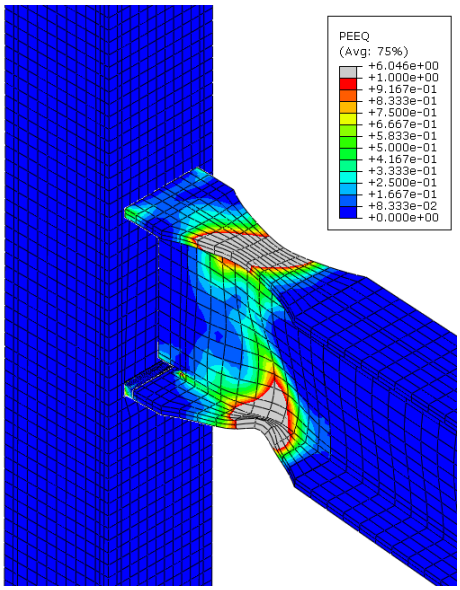

Final state of global model (PEEQ)

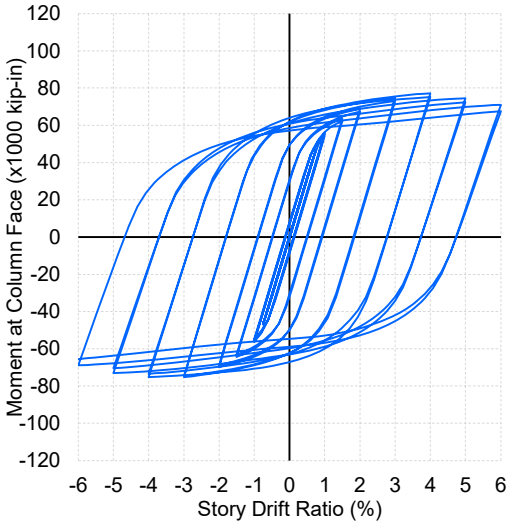

Load-displacement

Simulation 19 cont.

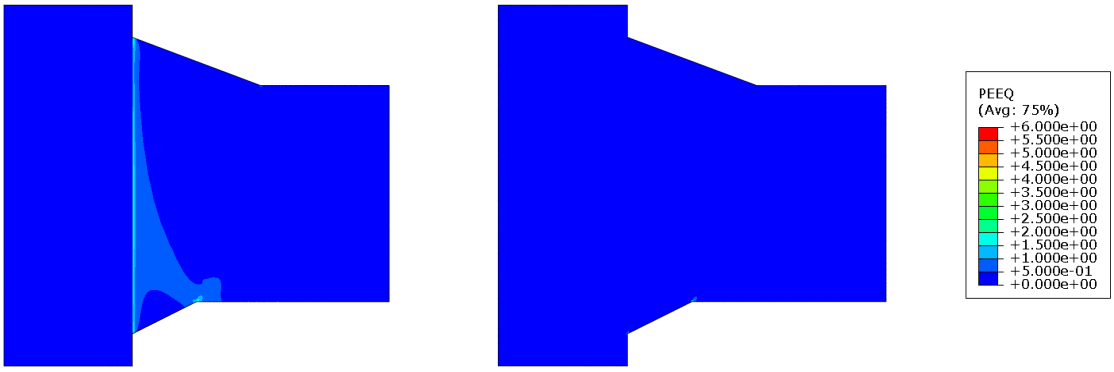

Edge Center

PEEQ at *R*=0.04 rad

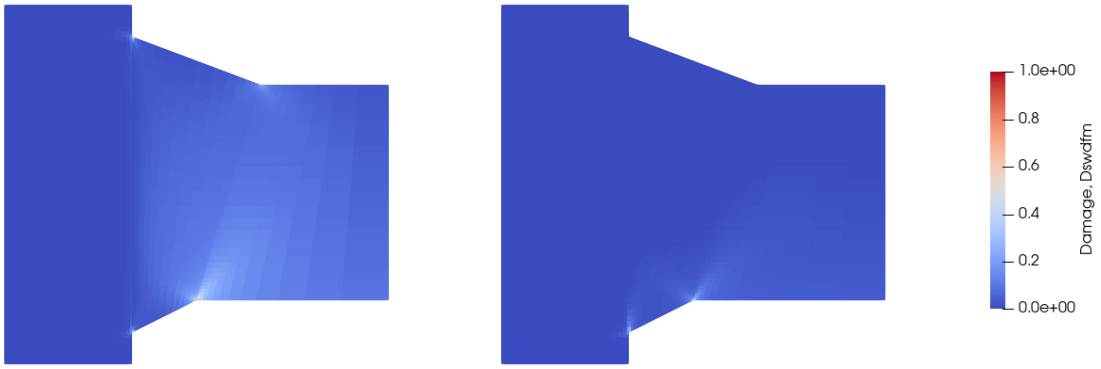

Edge Center

Damage at *R*=0.04 rad

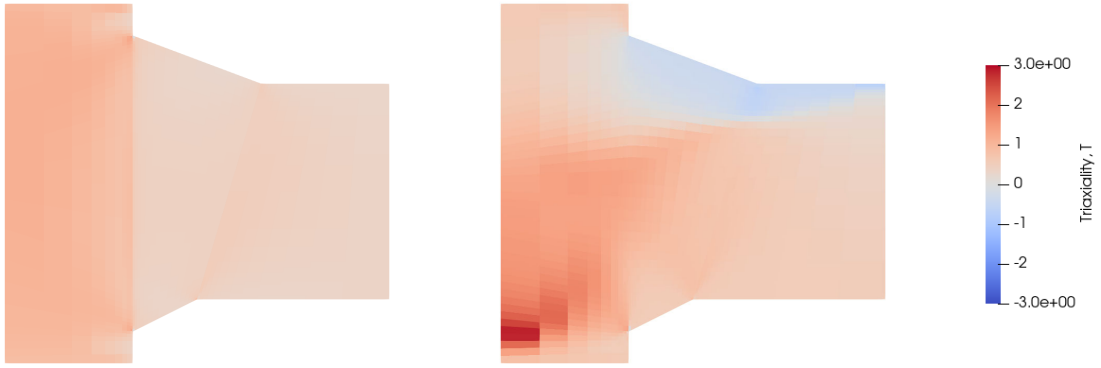

Edge Center

Triaxiality at *R*=0.04 rad (Time =133s, flange in tension)

Simulation 20

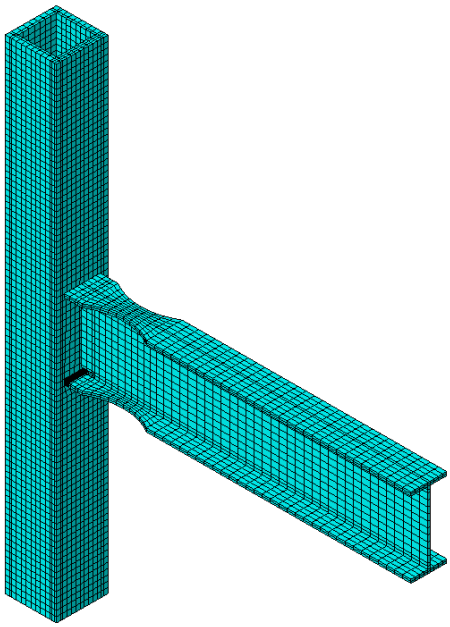

Global model

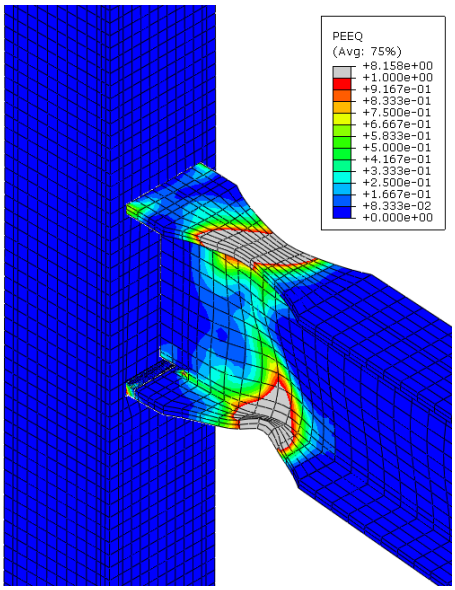

Final state of global model (PEEQ)

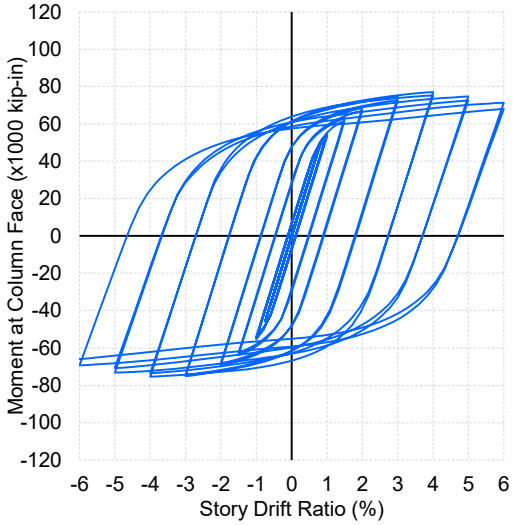

Load-displacement

Simulation 20 cont.

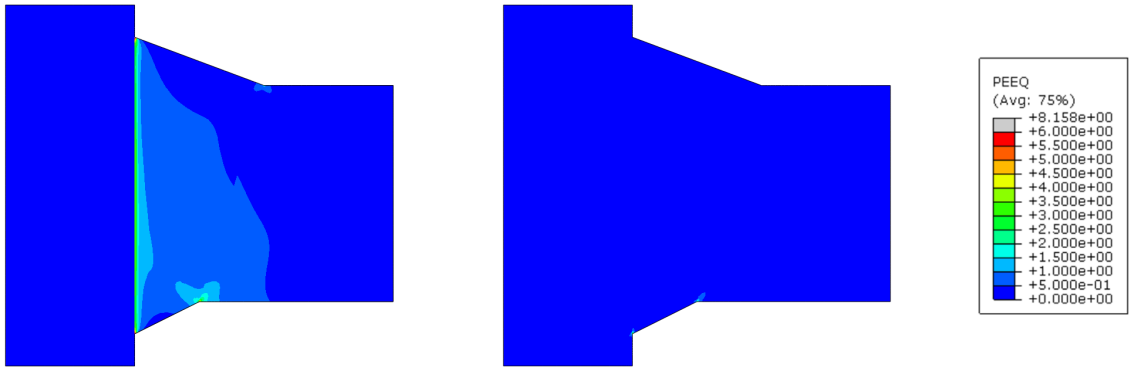

Edge Center

PEEQ at *R*=0.04 rad

Edge Center

Damage at *R*=0.04 rad

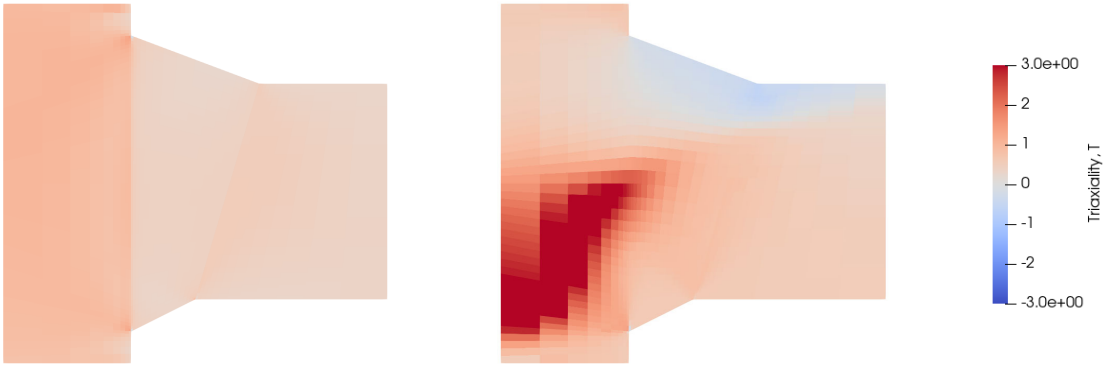

Edge Center

Triaxiality at *R*=0.04 rad (Time =133s, flange in tension)

Simulation 21

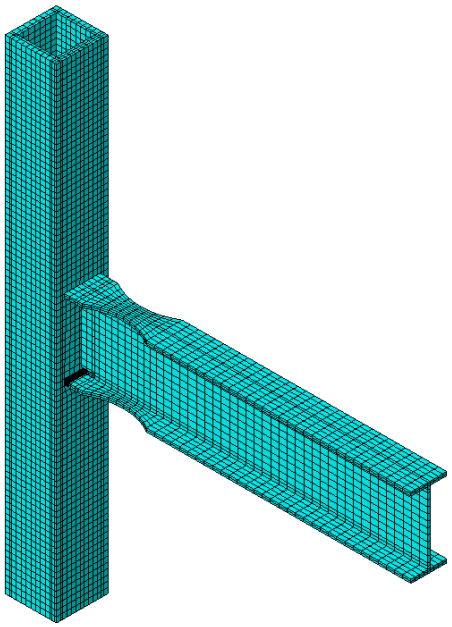

Global model

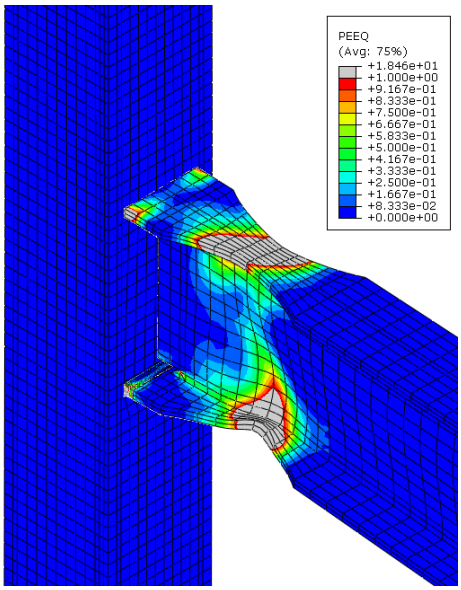

Final state of global model (PEEQ)

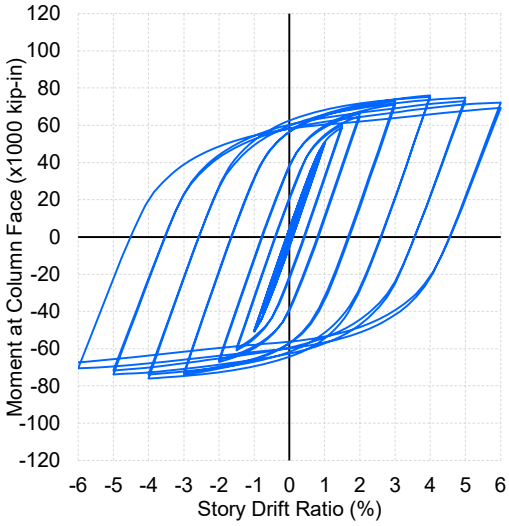

Load-displacement

Simulation 21 cont.

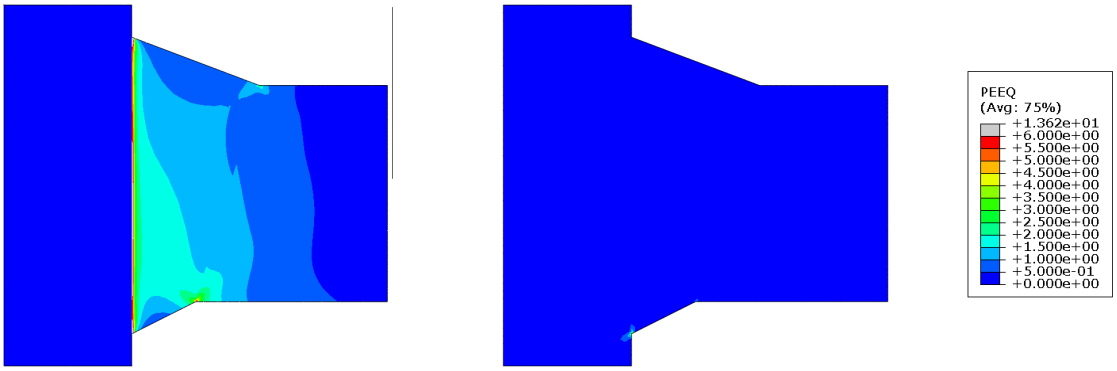

Edge Center

PEEQ at *R*=0.04 rad

Edge Center

Damage at *R*=0.04 rad

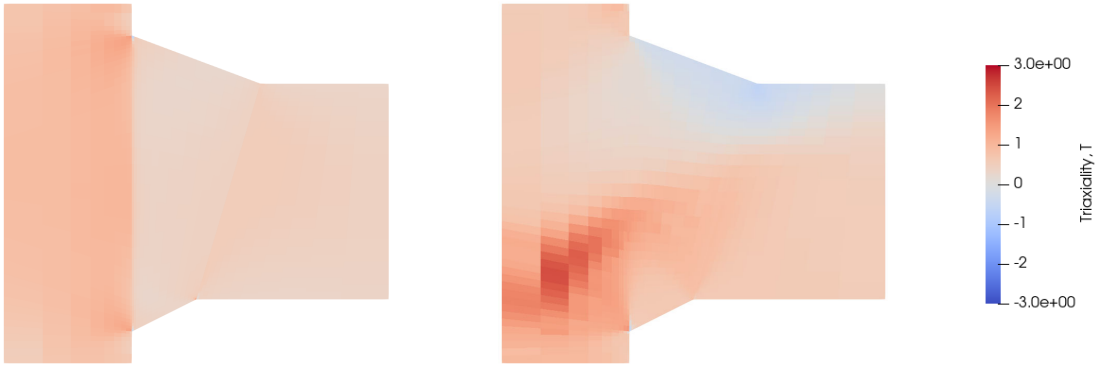

Edge Center

Triaxiality at *R*=0.04 rad (Time =133s, flange in tension)

Simulation 22

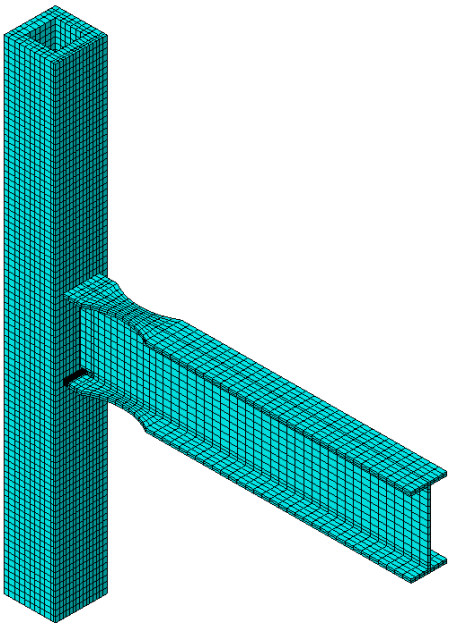

Global model

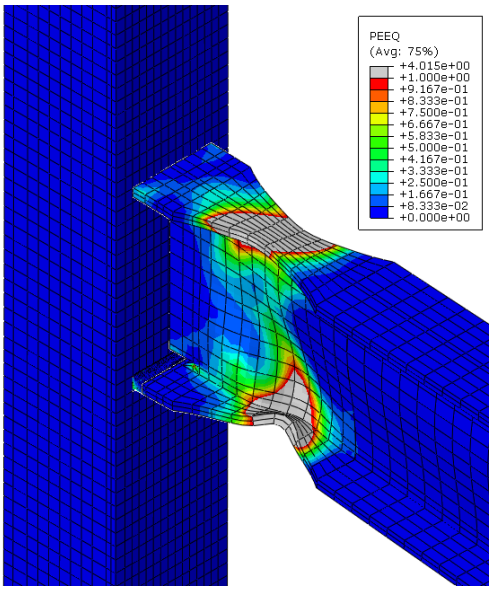

Final state of global model (PEEQ)

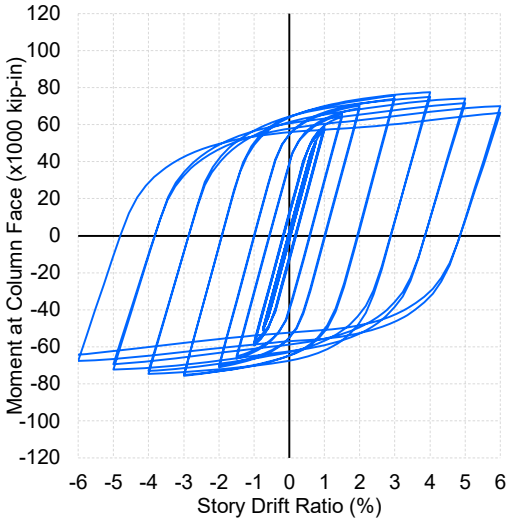

Load-displacement

Simulation 22 cont.

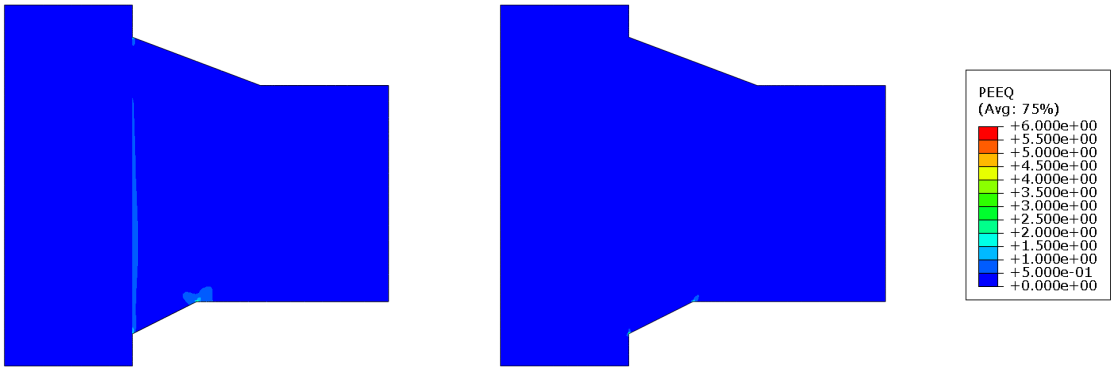

Edge Center

PEEQ at *R*=0.04 rad

Edge Center

Damage at *R*=0.04 rad

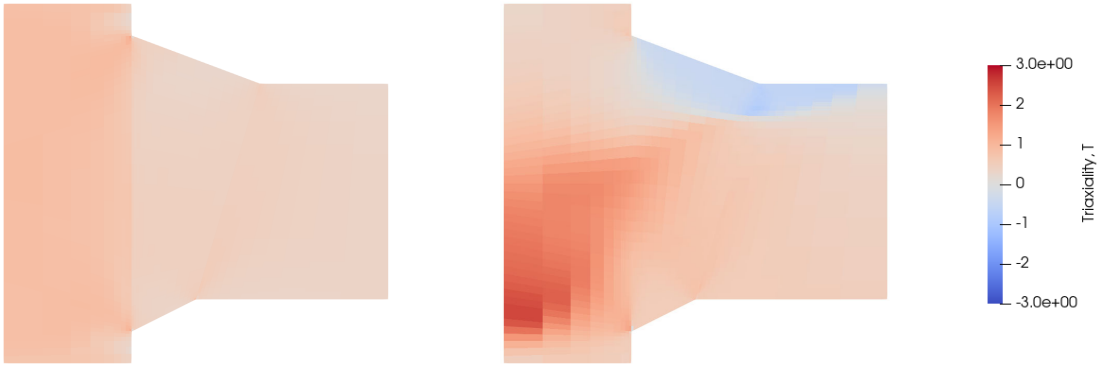

Edge Center

Triaxiality at *R*=0.04 rad (Time =133s, flange in tension)

Simulation 23

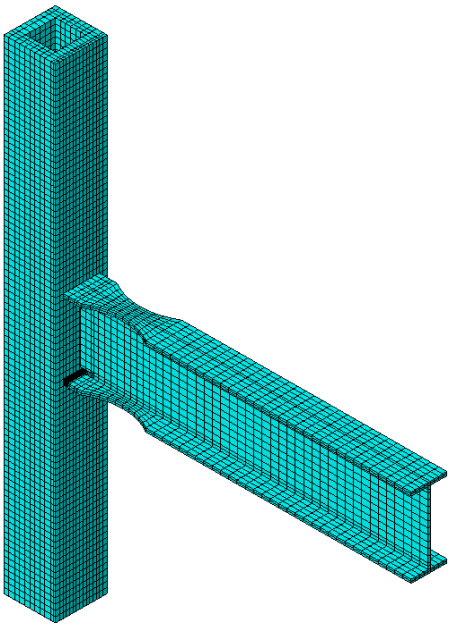

Global model

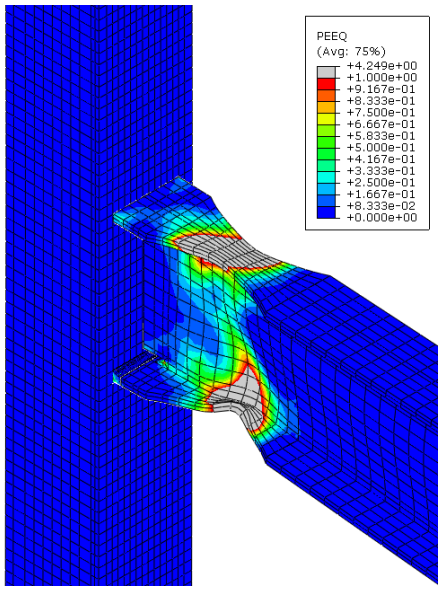

Final state of global model (PEEQ)

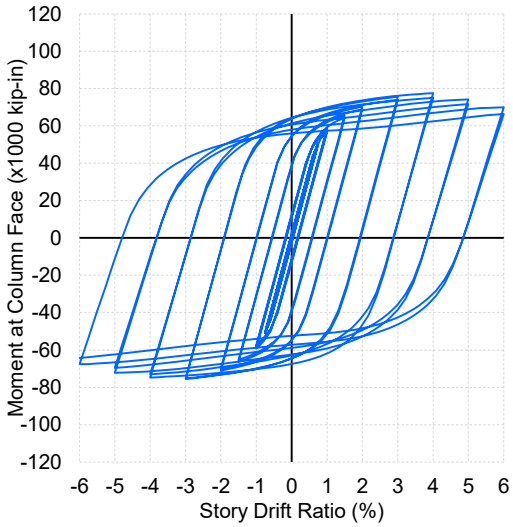

Load-displacement

Simulation 23 cont.

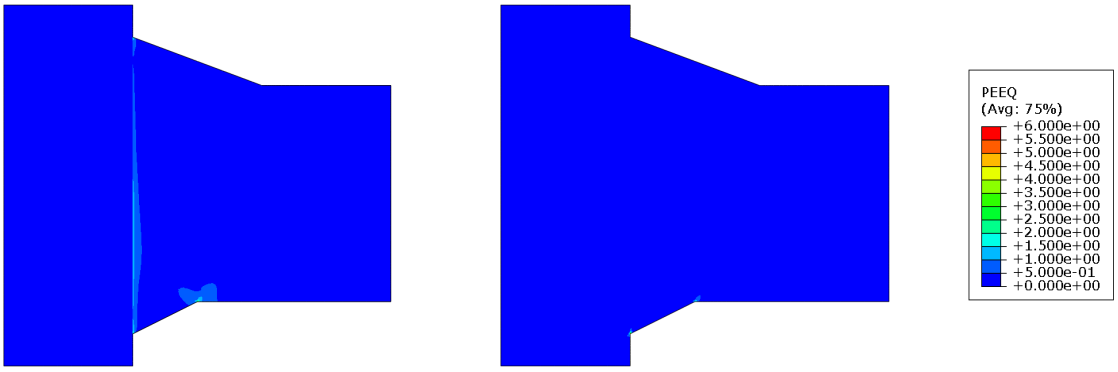

Edge Center

PEEQ at R=0.04 rad

Edge Center

Damage at R=0.04 rad

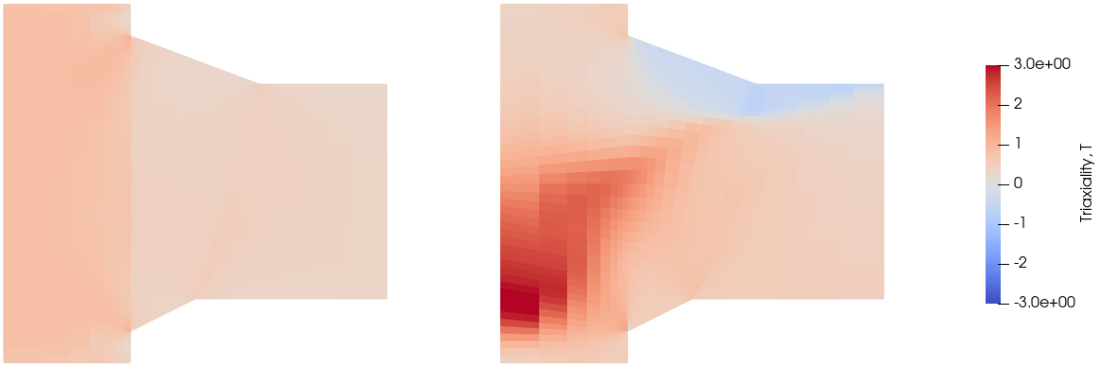

Edge Center

Triaxiality at R=0.04 rad (Time =133s, flange in tension)

Simulation 24

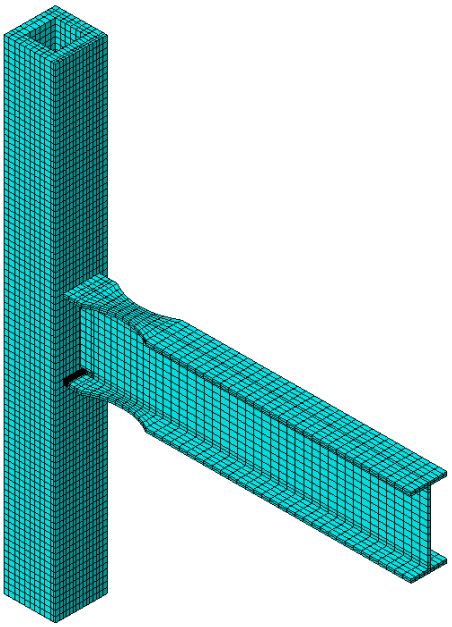

Global model

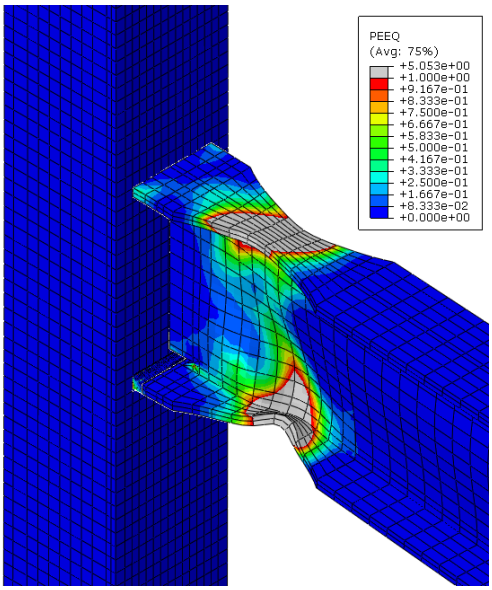

Final state of global model (PEEQ)

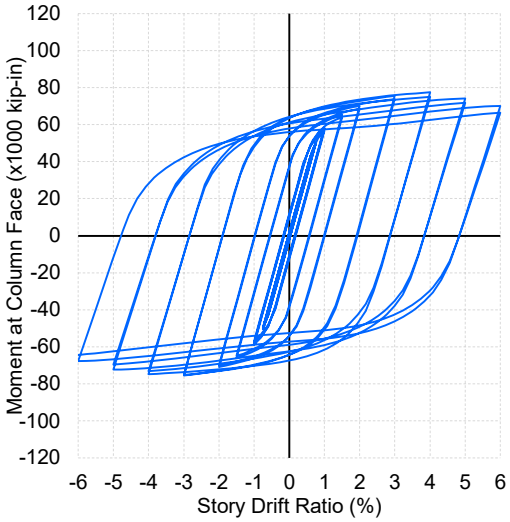

Load-displacement

Simulation 24 cont.

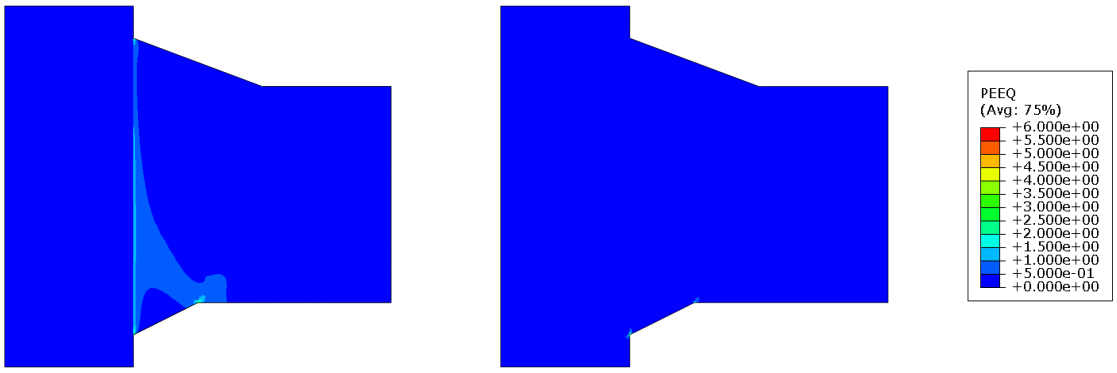

Edge Center

PEEQ at R=0.04 rad

Edge Center

Damage at R=0.04 rad

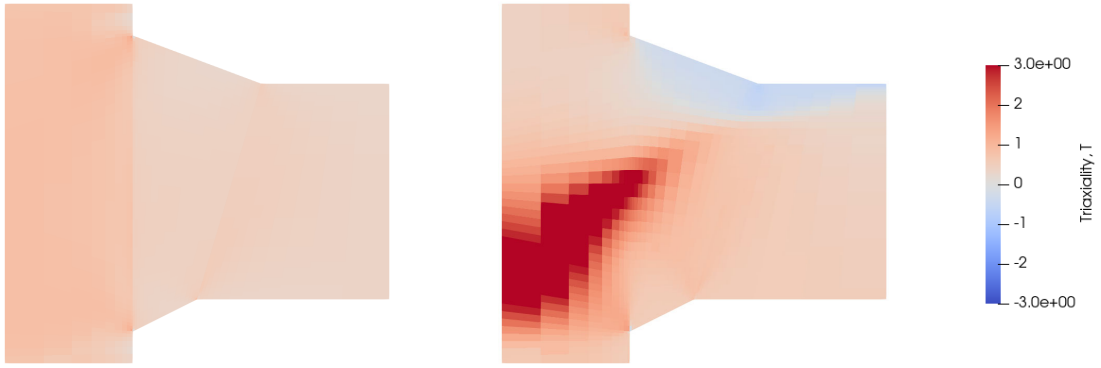

Edge Center

Triaxiality at R=0.04 rad (Time =133s, flange in tension)

Simulation 25

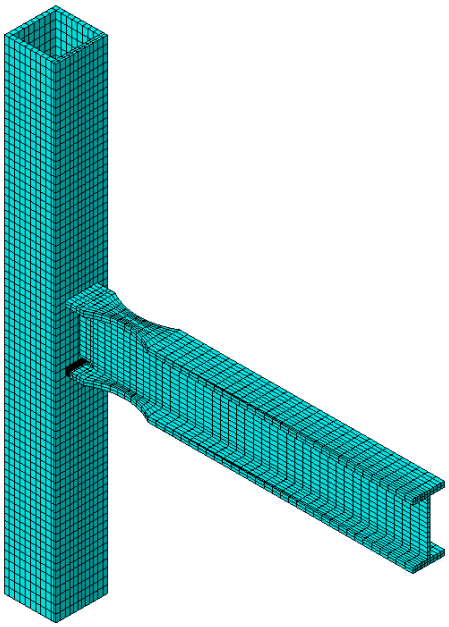

Global model

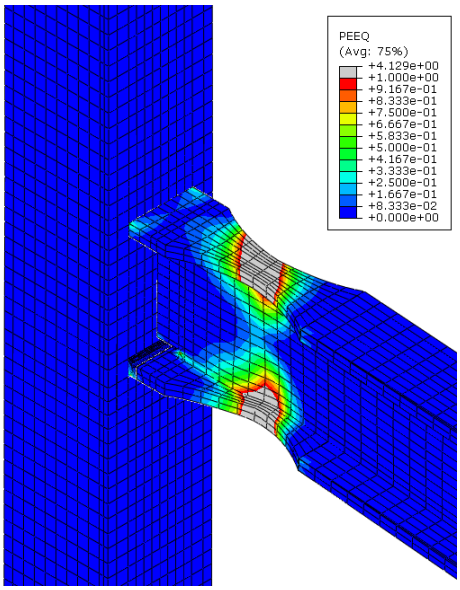

Final state of global model (PEEQ)

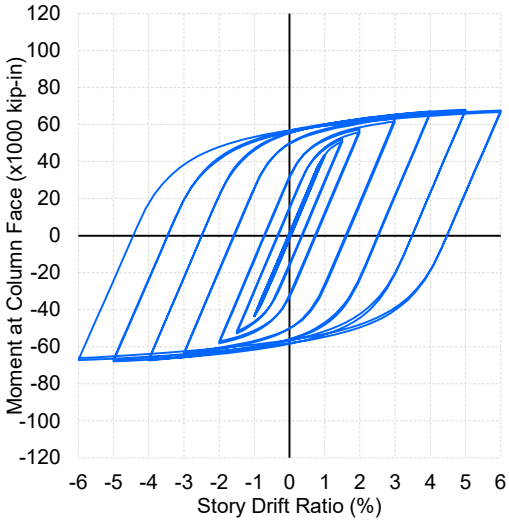

Load-displacement

Simulation 25 cont.

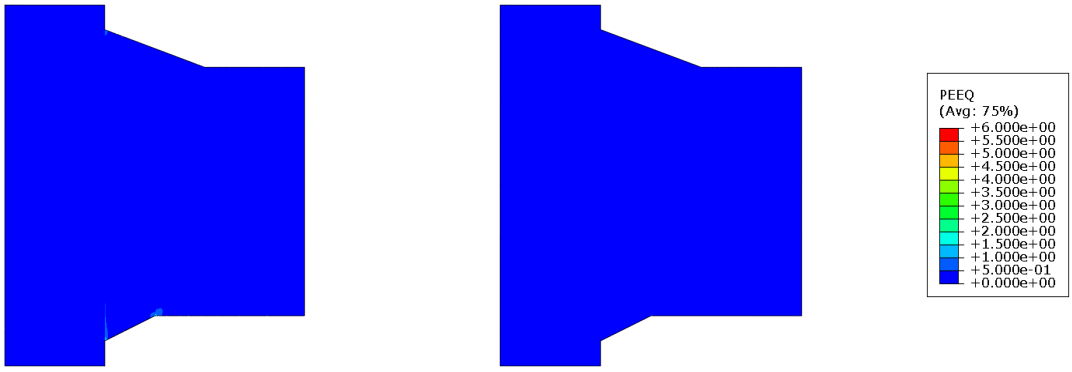

Edge Center

PEEQ at *R*=0.04 rad

Edge Center

Damage at *R*=0.04 rad

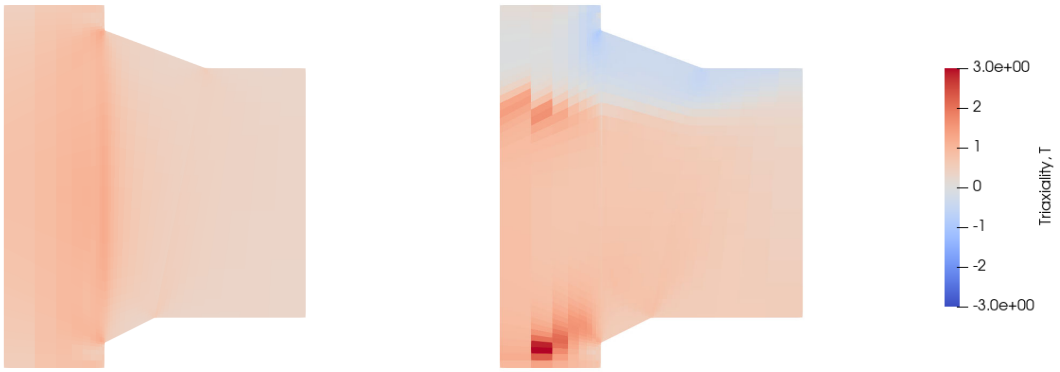

Edge Center

Triaxiality at *R*=0.04 rad (Time =133s, flange in tension)

Simulation 26

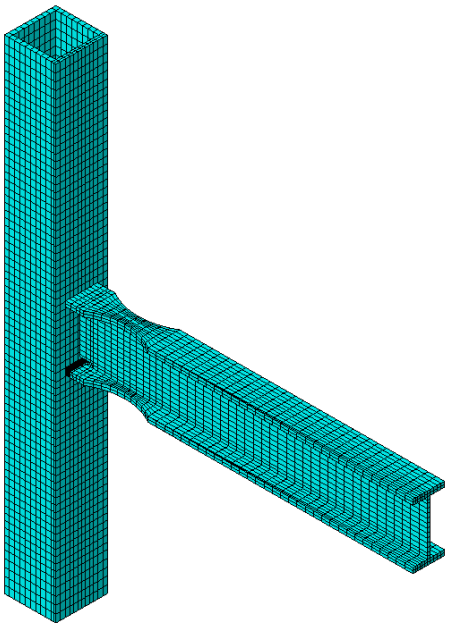

Global model

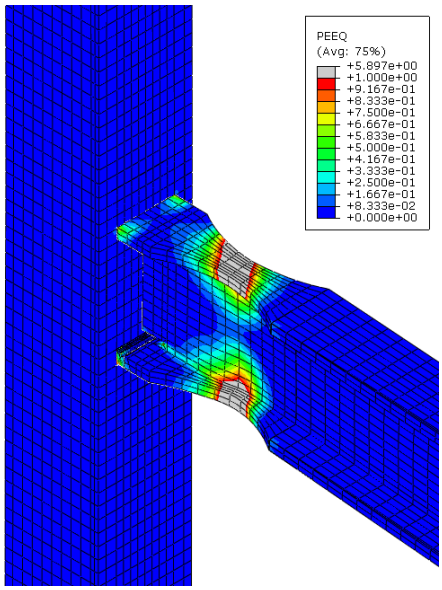

Final state of global model (PEEQ)

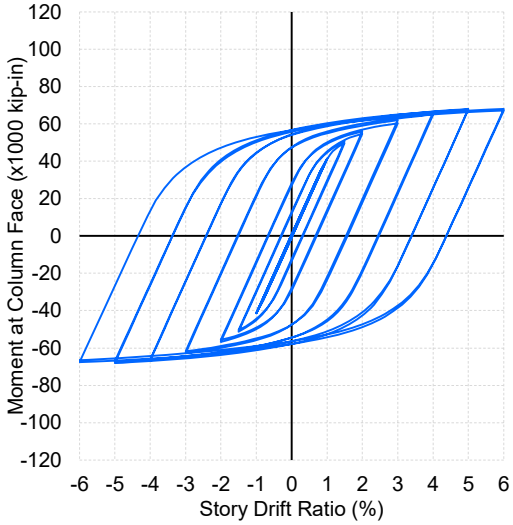

Load-displacement

Simulation 26 cont.

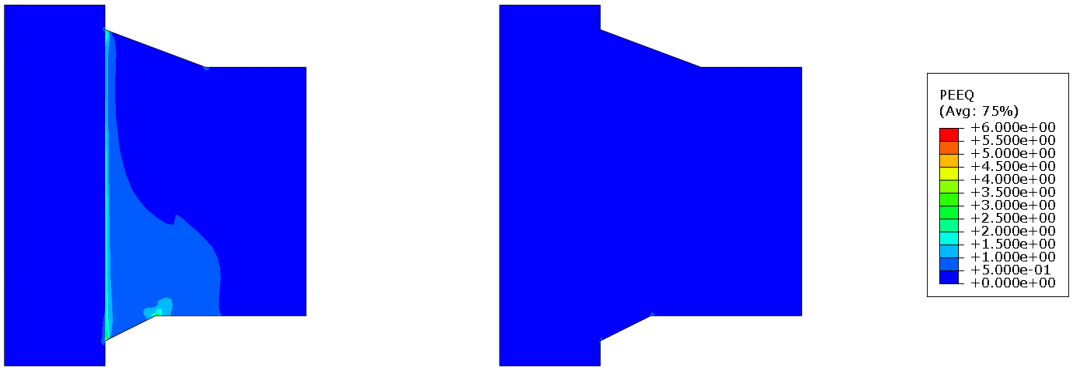

Edge Center

PEEQ at R=0.04 rad

Edge Center

Damage at R=0.04 rad

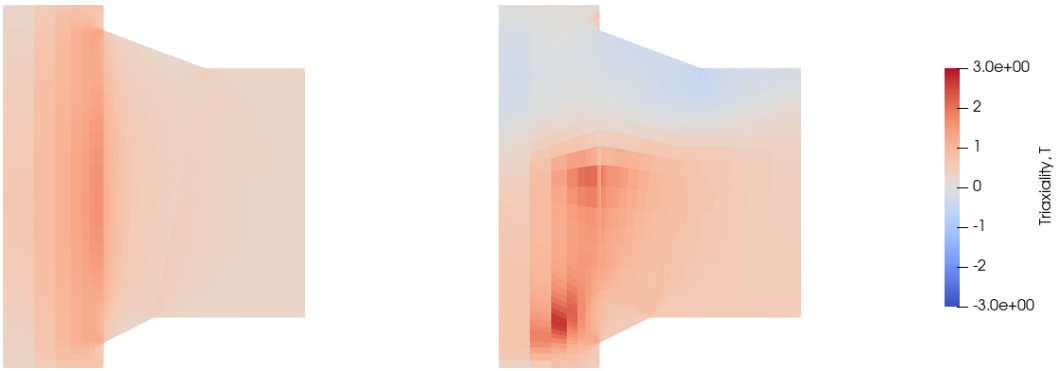

Edge Center

Triaxiality at R=0.04 rad (Time =133s, flange in tension)

Simulation 27

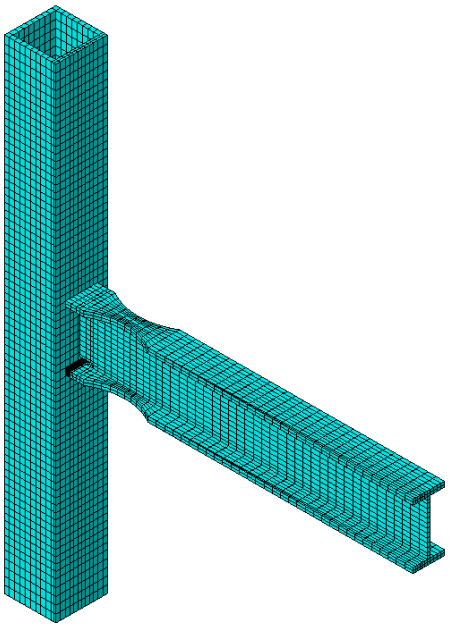

Global model

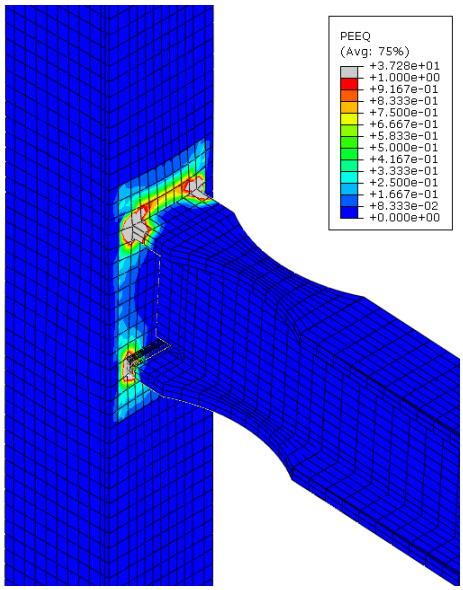

Final state of global model (PEEQ)

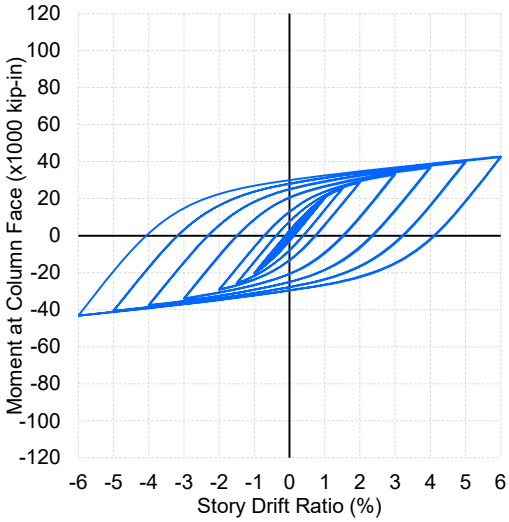

Load-displacement

Simulation 27 cont.

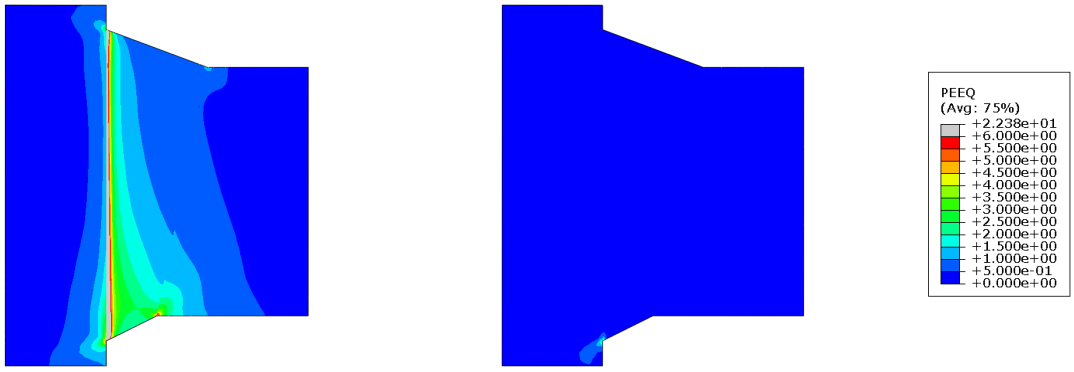

Edge Center

PEEQ at *R*=0.04 rad

Edge Center

Damage at *R*=0.04 rad

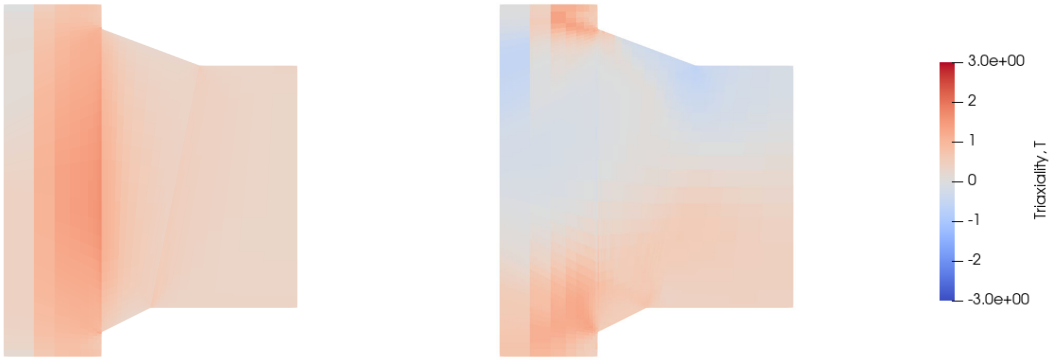

Edge Center

Triaxiality at *R*=0.04 rad (Time =133s, flange in tension)

Simulation 28

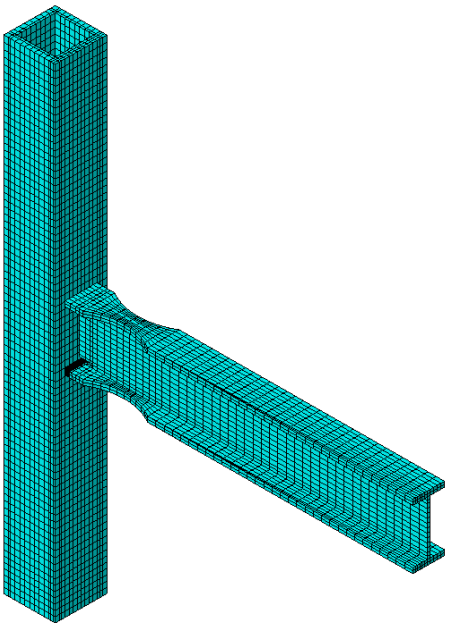

Global model

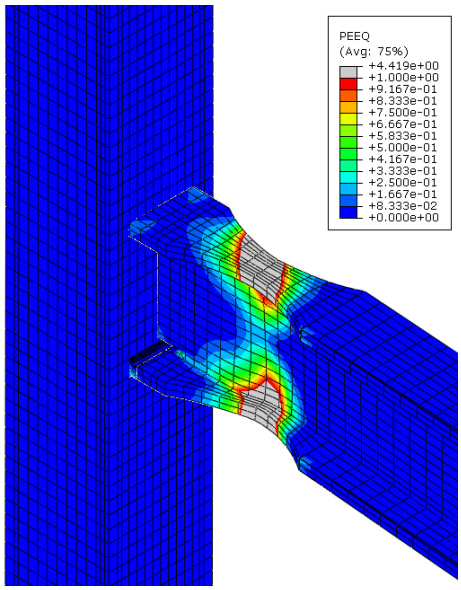

Final state of global model (PEEQ)

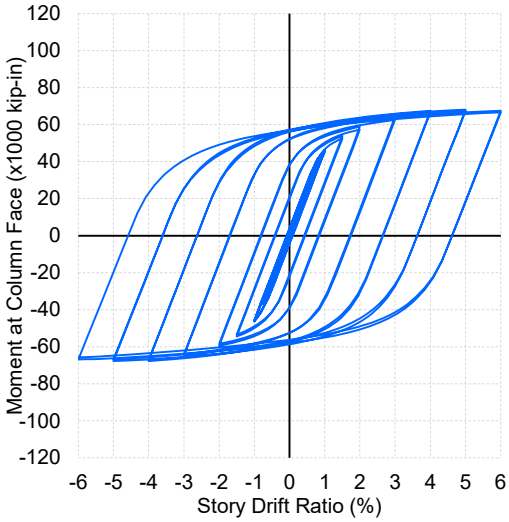

Load-displacement

Simulation 28 cont.

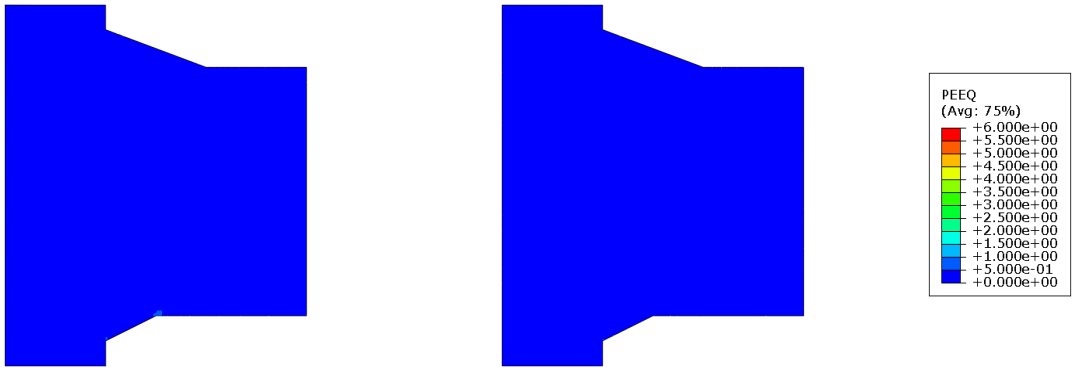

Edge Center

PEEQ at R=0.04 rad

Edge Center

Damage at R=0.04 rad

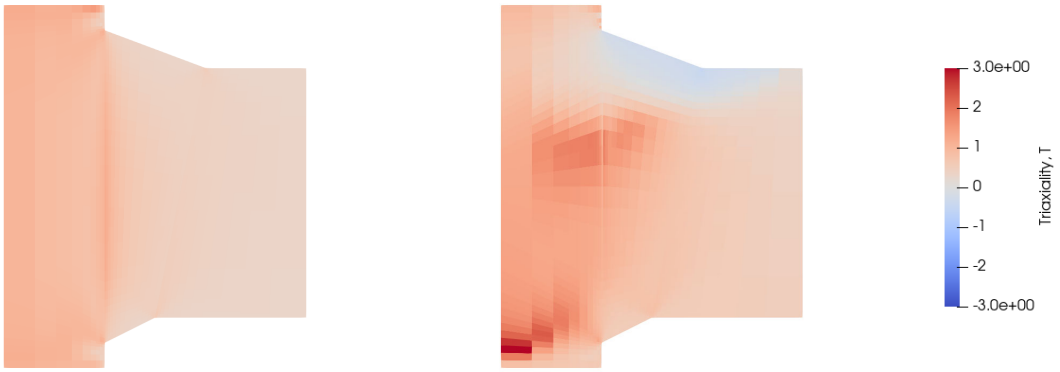

Edge Center

Triaxiality at R=0.04 rad (Time =133s, flange in tension)

Simulation 29

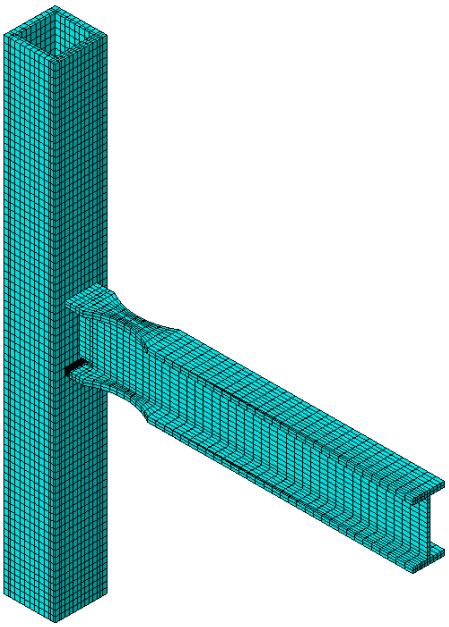

Global model

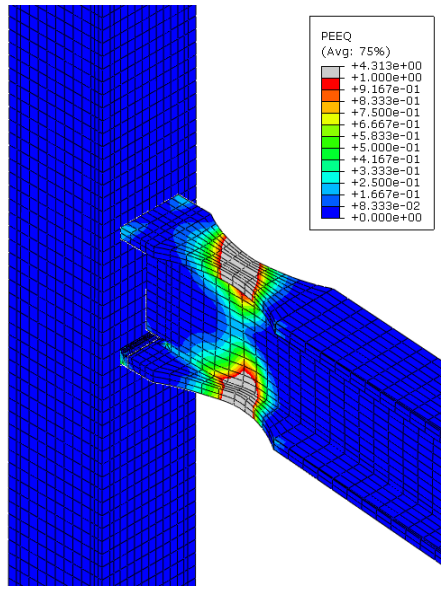

Final state of global model (PEEQ)

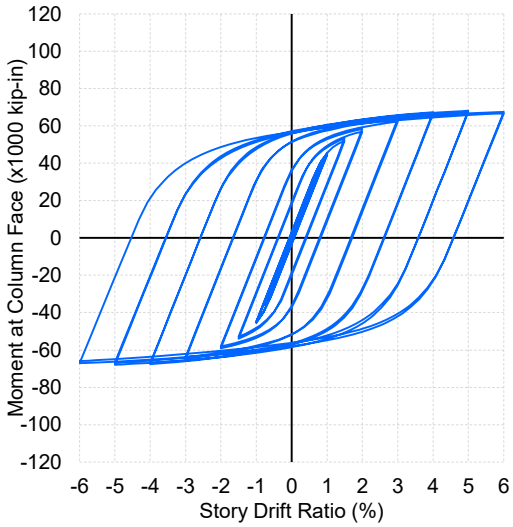

Load-displacement

Simulation 29 cont.

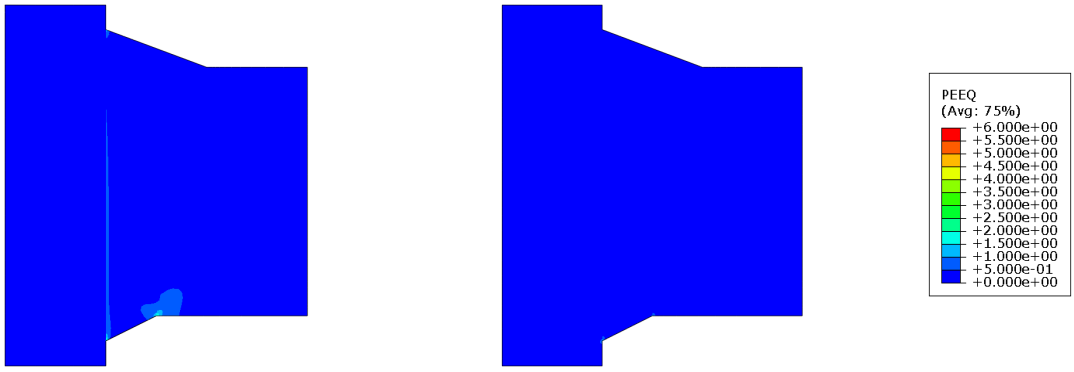

Edge Center

PEEQ at *R*=0.04 rad

Edge Center

Damage at *R*=0.04 rad

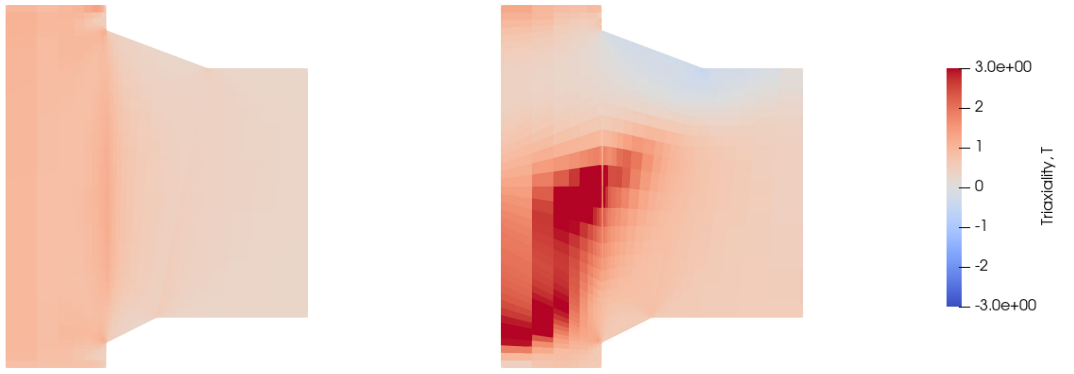

Edge Center

Triaxiality at *R*=0.04 rad (Time =133s, flange in tension)

Simulation 30

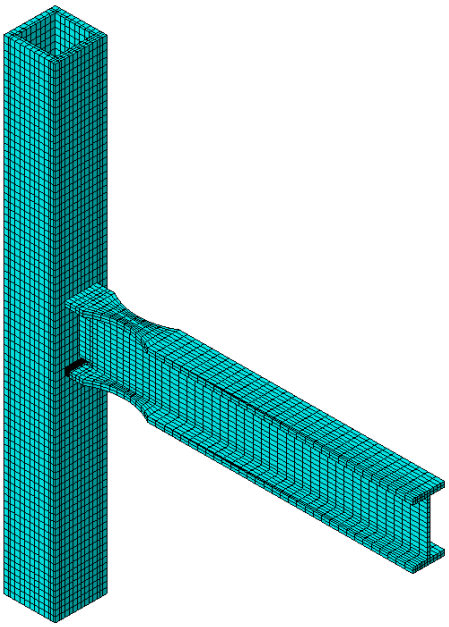

Global model

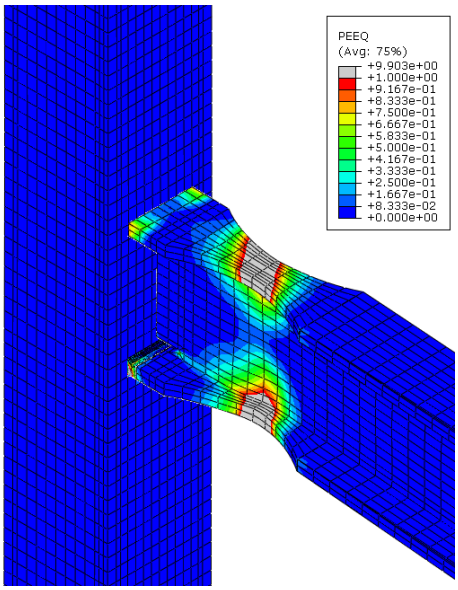

Final state of global model (PEEQ)

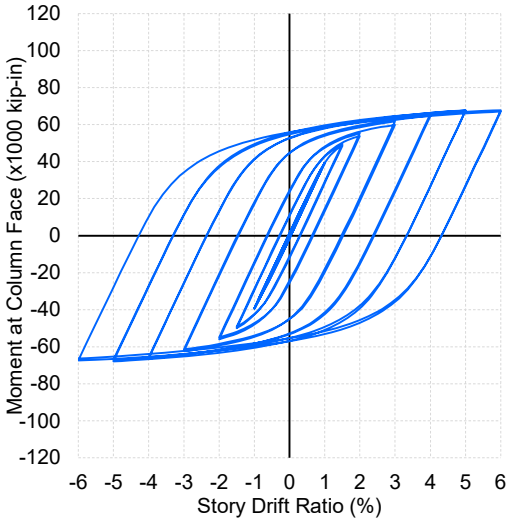

Load-displacement

Simulation 30 cont.

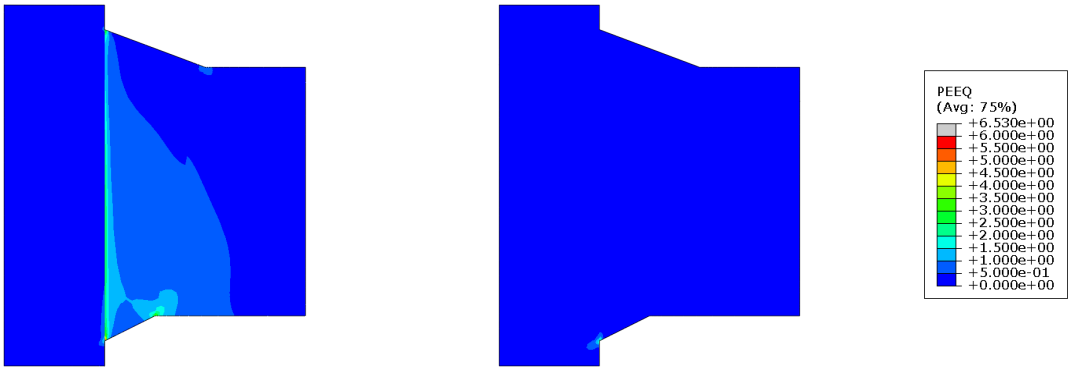

Edge Center

PEEQ at *R*=0.04 rad

Edge Center

Damage at *R*=0.04 rad

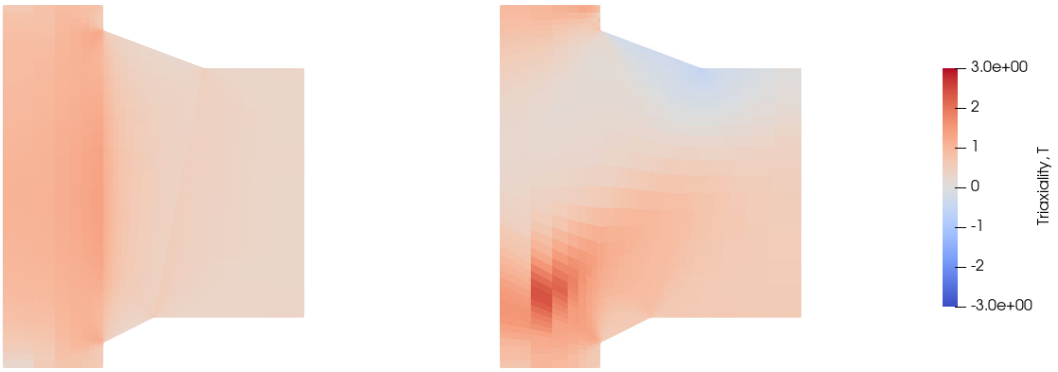

Edge Center

Triaxiality at *R*=0.04 rad (Time =133s, flange in tension)

Simulation 31

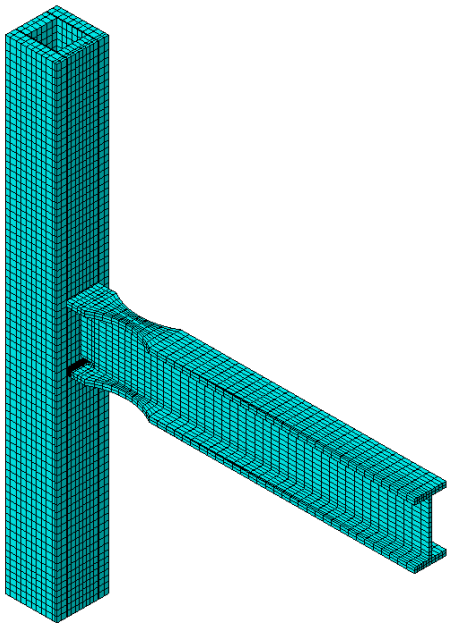

Global model

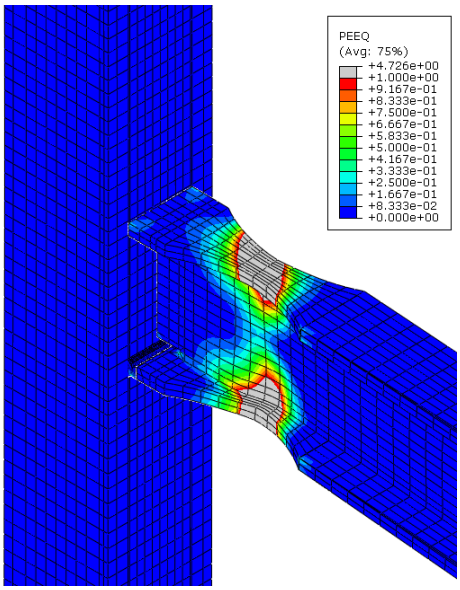

Final state of global model (PEEQ)

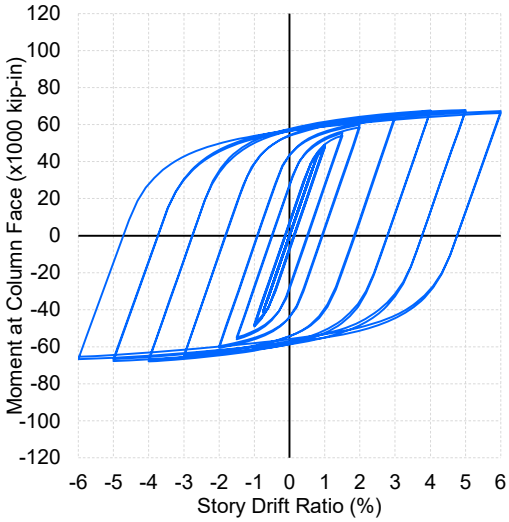

Load-displacement

Simulation 31 cont.

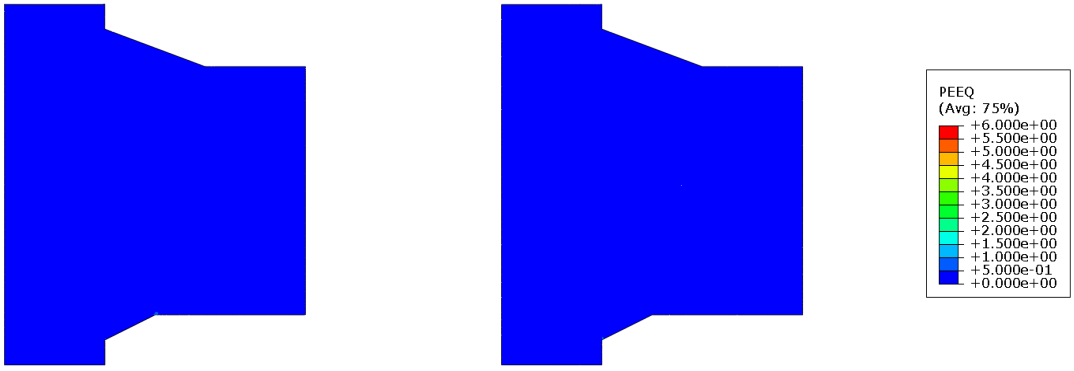

Edge Center

PEEQ at *R*=0.04 rad

Edge Center

Damage at *R*=0.04 rad

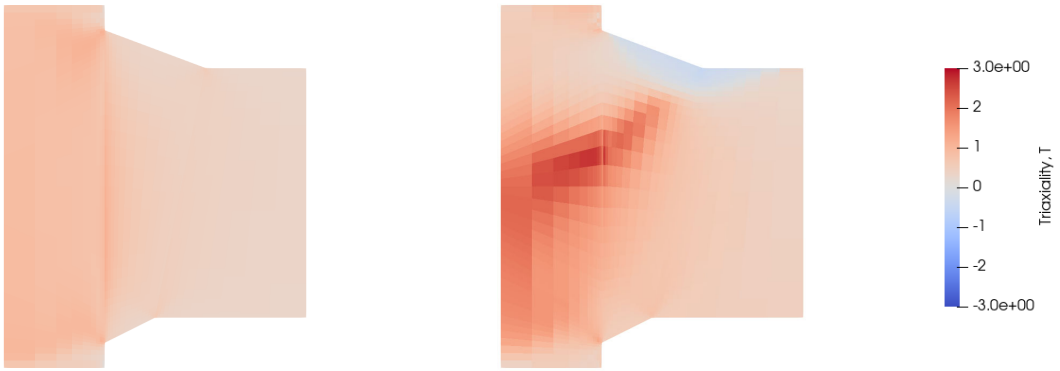

Edge Center

Triaxiality at *R*=0.04 rad (Time =133s, flange in tension)

Simulation 32

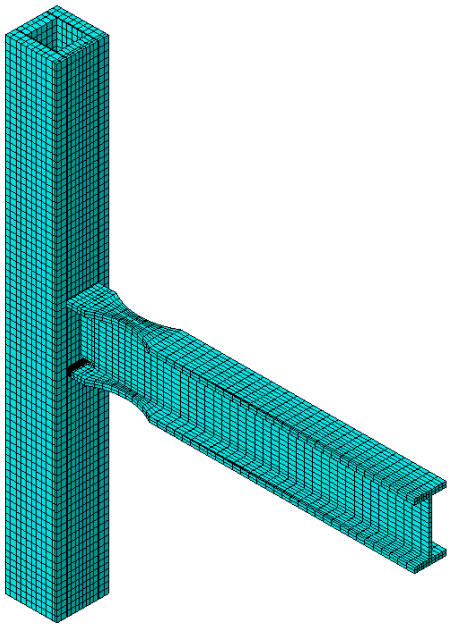

Global model

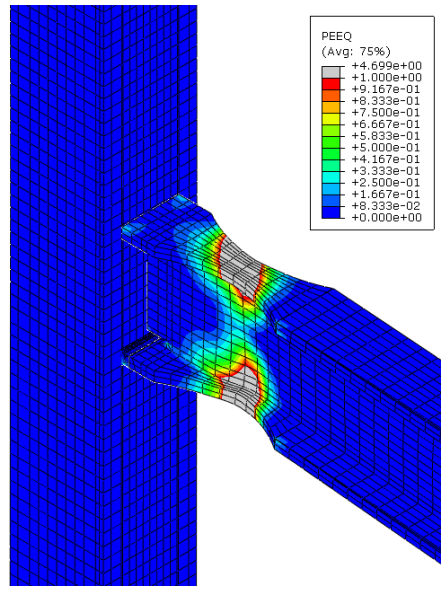

Final state of global model (PEEQ)

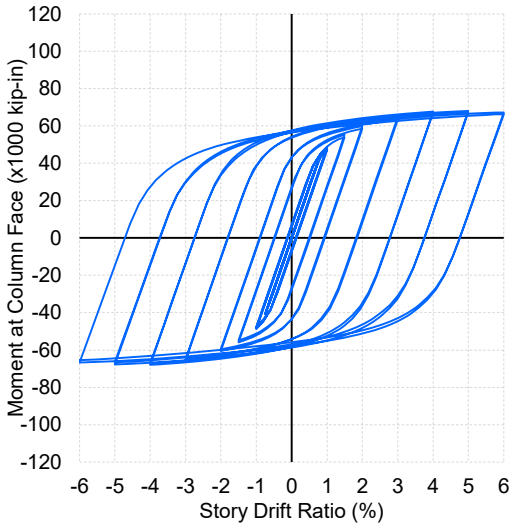

Load-displacement

Simulation 32 cont.

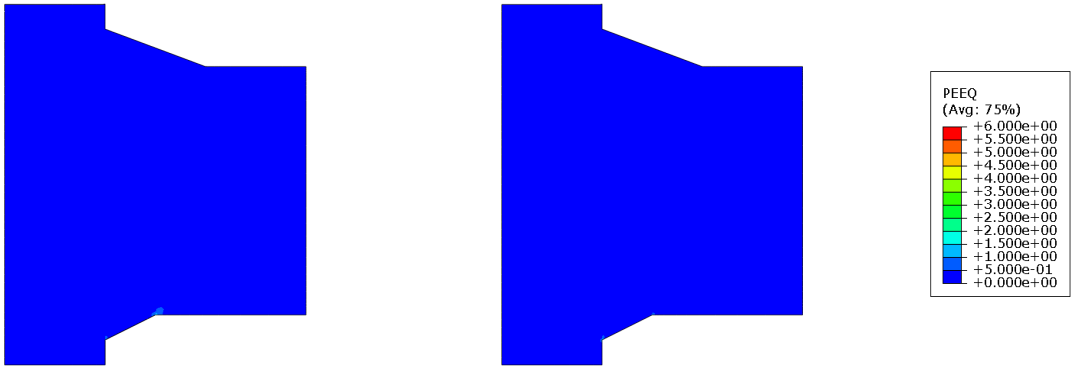

Edge Center

PEEQ at *R*=0.04 rad

Edge Center

Damage at *R*=0.04 rad

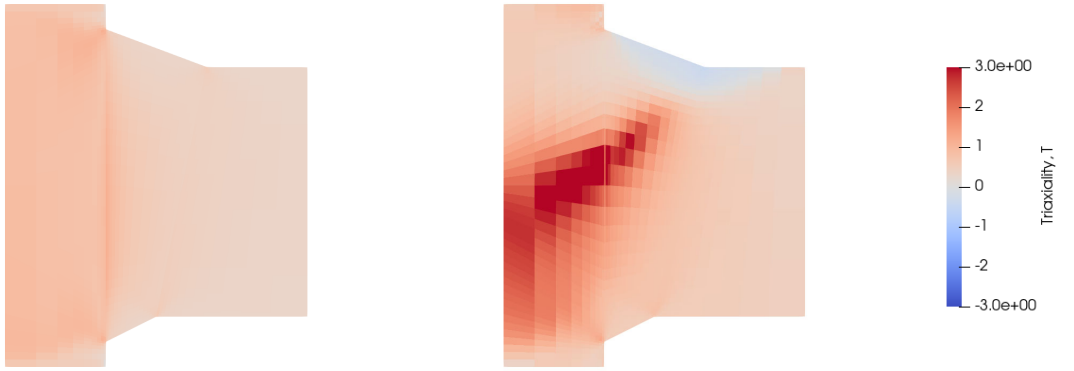

Edge Center

Triaxiality at *R*=0.04 rad (Time =133s, flange in tension)

Simulation 33

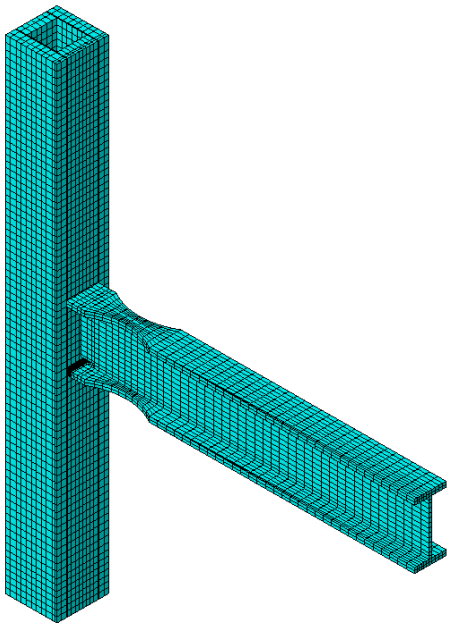

Global model

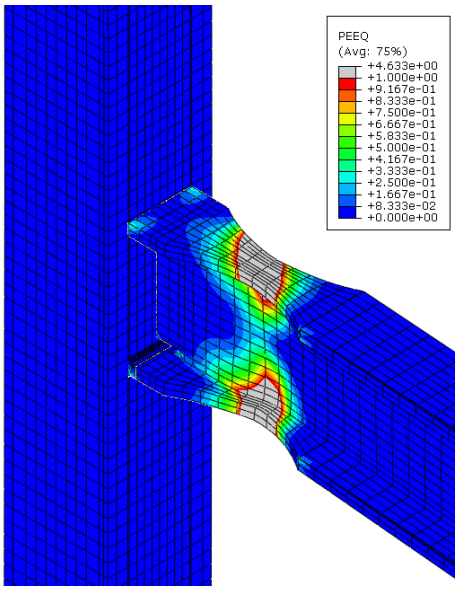

Final state of global model (PEEQ)

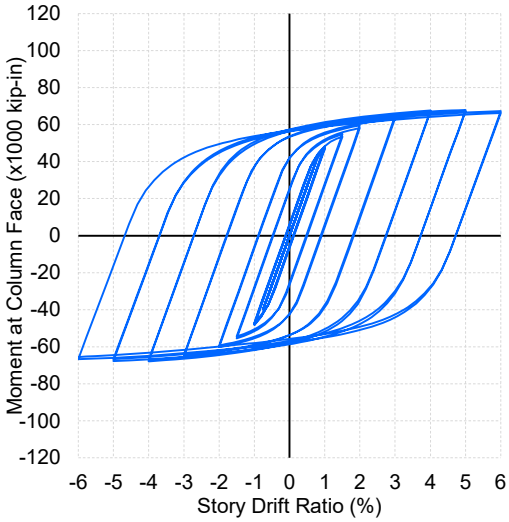

Load-displacement

Simulation 33 cont.

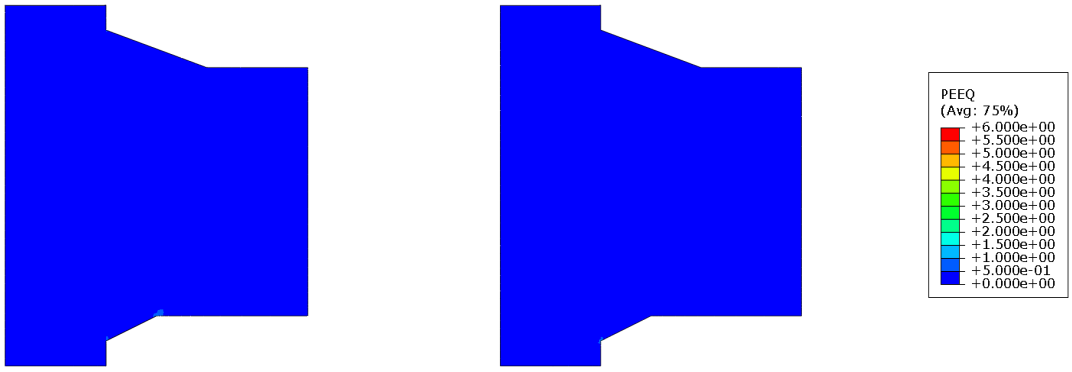

Edge Center

PEEQ at R=0.04 rad

Edge Center

Damage at R=0.04 rad

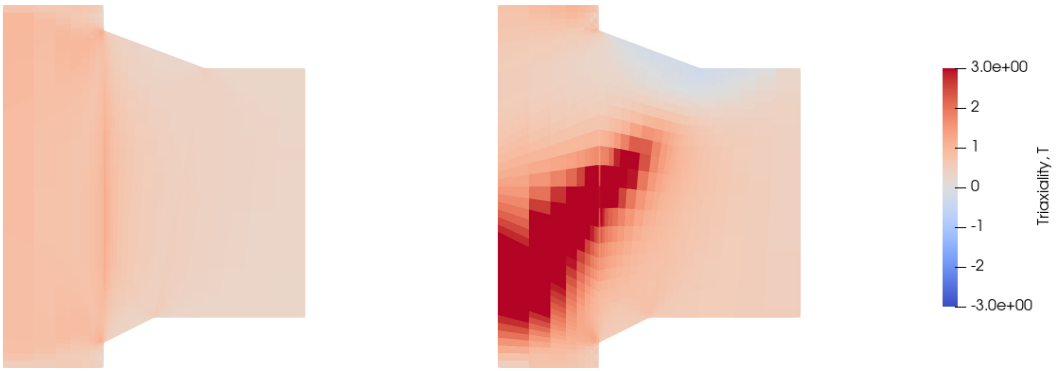

Edge Center

Triaxiality at R=0.04 rad (Time =133s, flange in tension)

Simulation 34

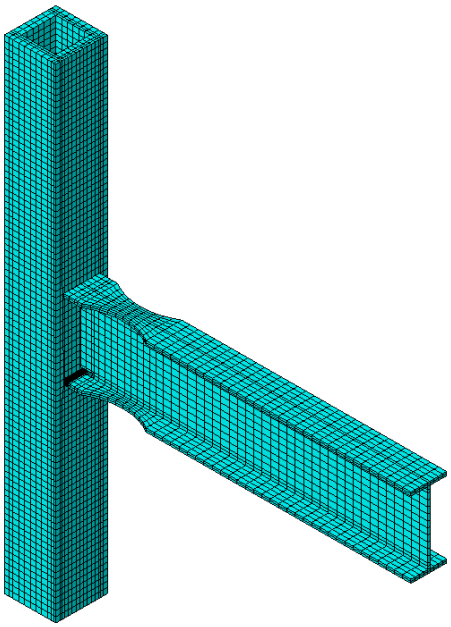

Global model

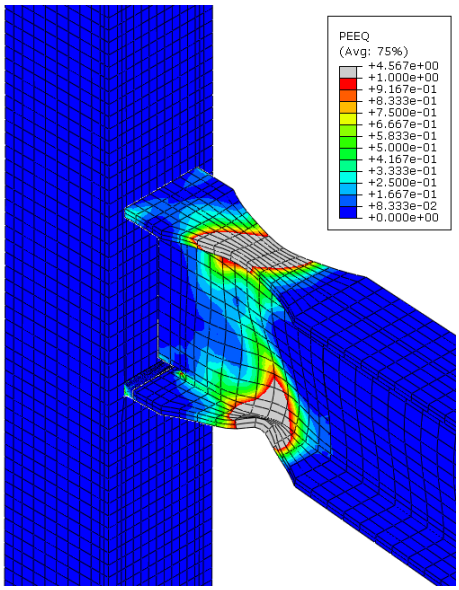

Final state of global model (PEEQ)

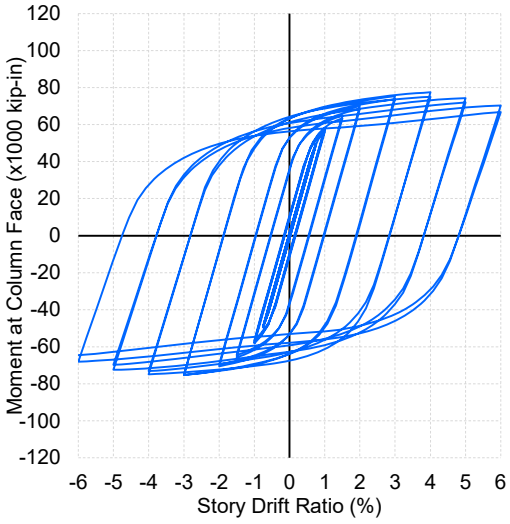

Load-displacement

Simulation 34 cont.

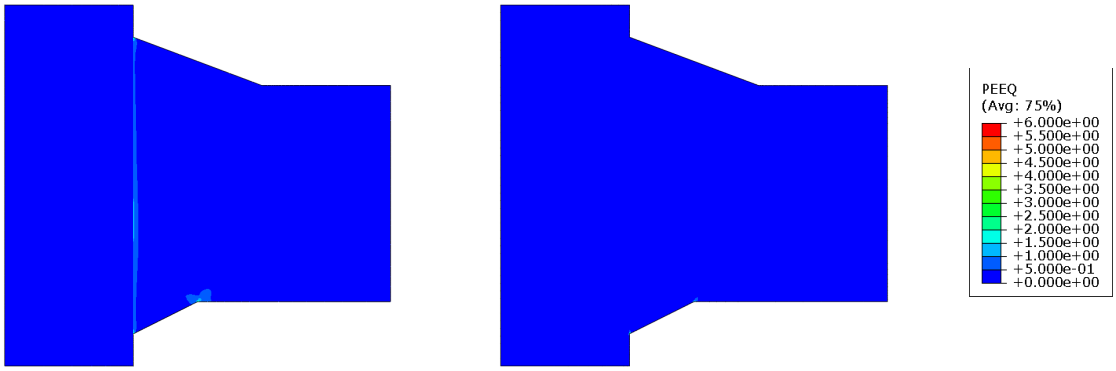

Edge Center

PEEQ at R=0.04 rad

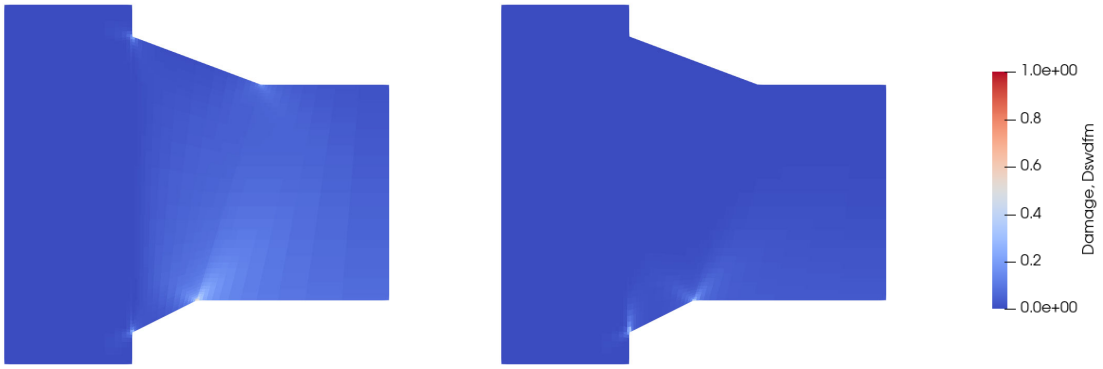

Edge Center

Damage at R=0.04 rad

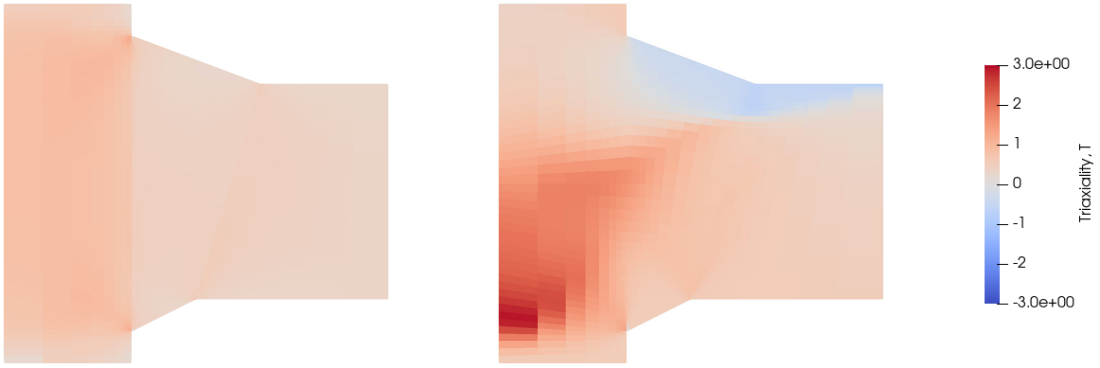

Edge Center

Triaxiality at R=0.04 rad (Time =133s, flange in tension)

Simulation 35

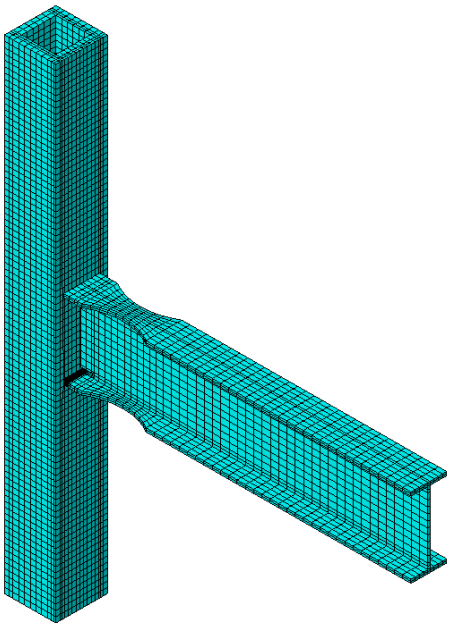

Global model

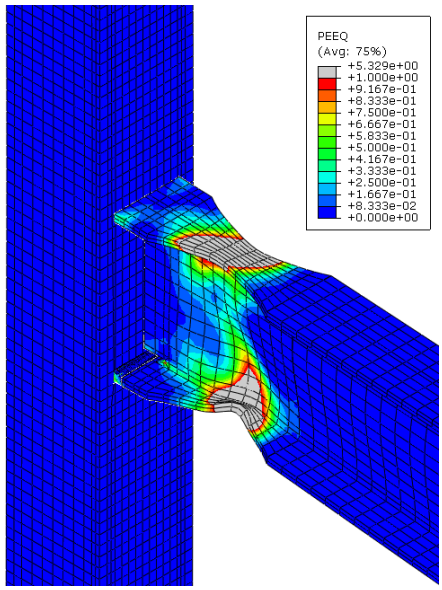

Final state of global model (PEEQ)

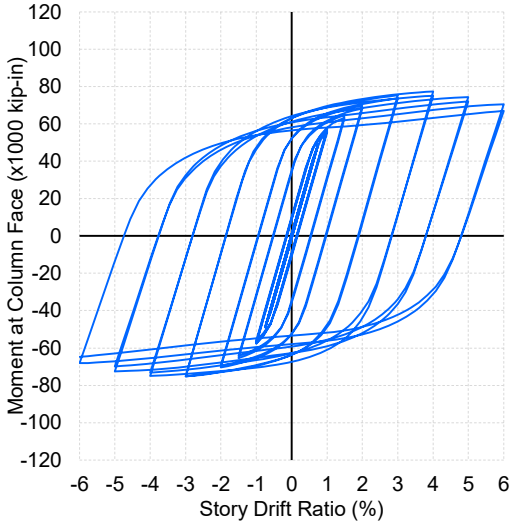

Load-displacement

Simulation 35 cont.

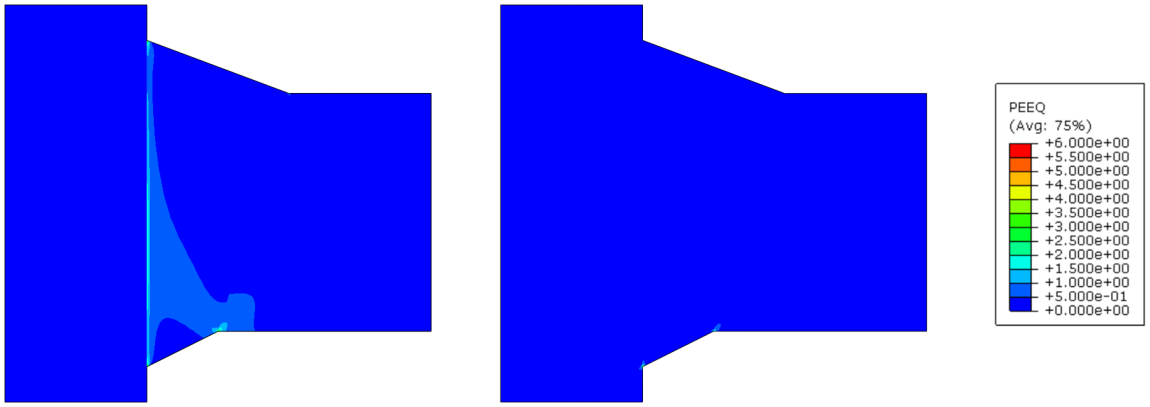

Edge Center

PEEQ at R=0.04 rad

Edge Center

Damage at R=0.04 rad

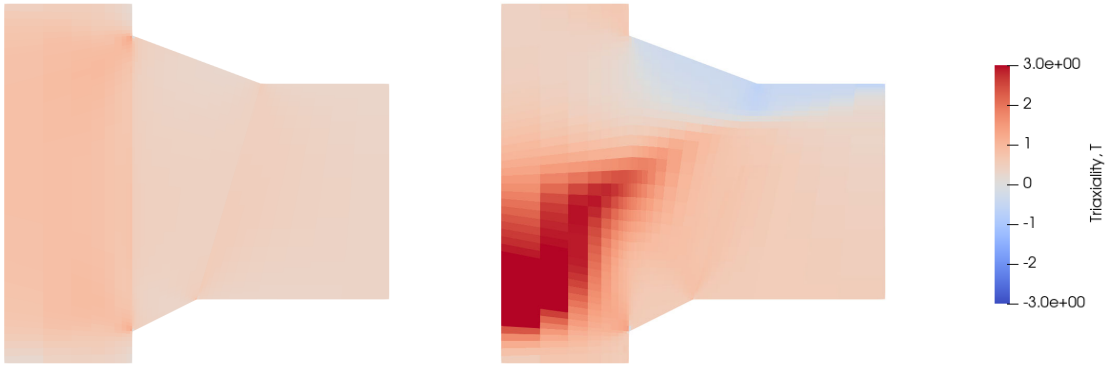

Edge Center

Triaxiality at R=0.04 rad (Time =133s, flange in tension)

Simulation 36

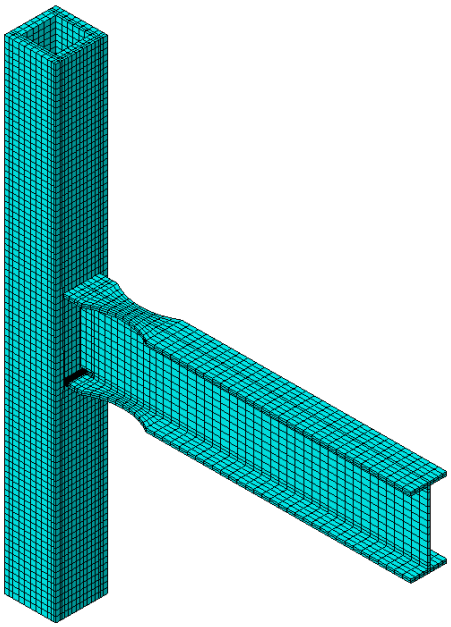

Global model

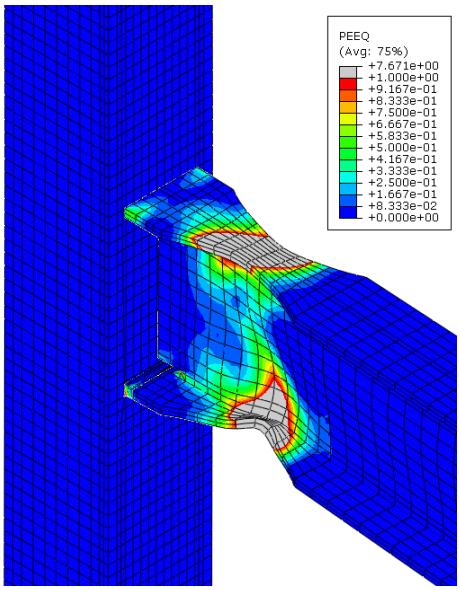

Final state of global model (PEEQ)

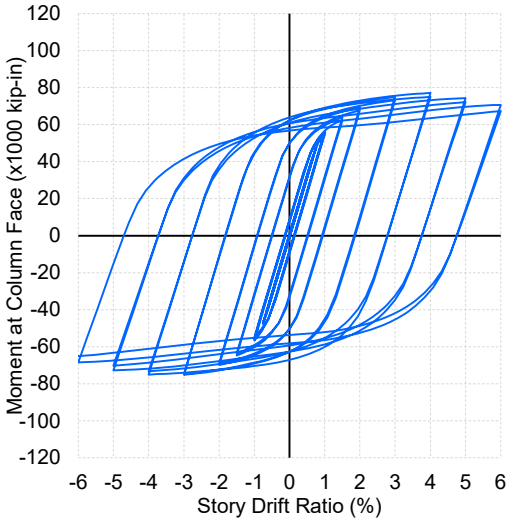

Load-displacement

Simulation 36 cont.

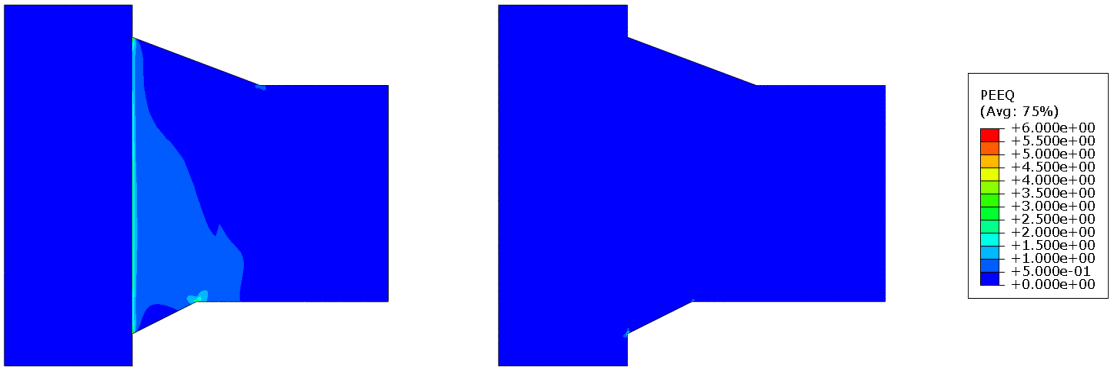

Edge Center

PEEQ at R=0.04 rad

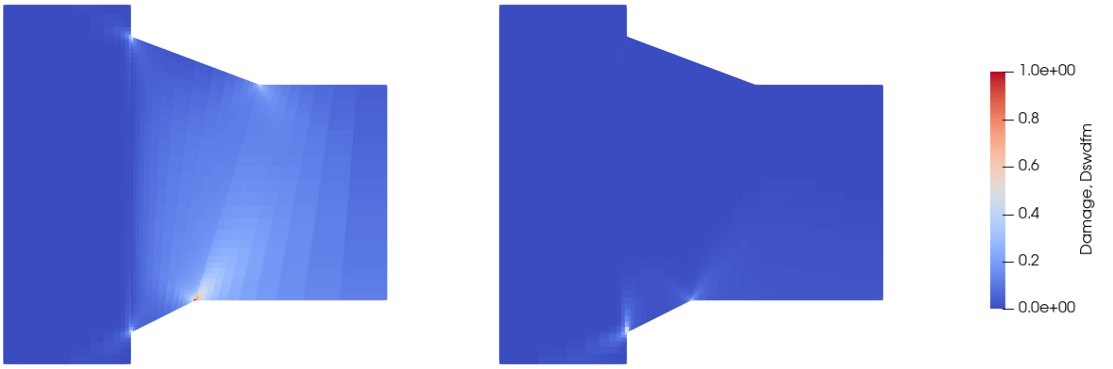

Edge Center

Damage at R=0.04 rad

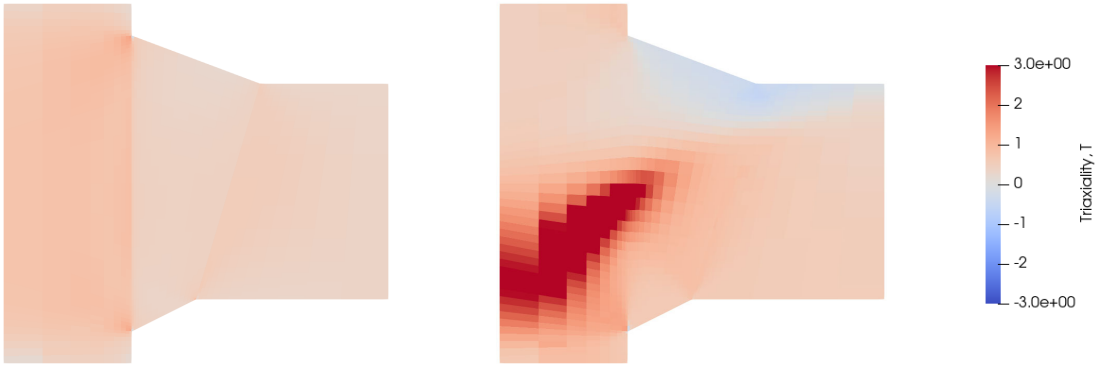

Edge Center

Triaxiality at R=0.04 rad (Time =133s, flange in tension)

Simulation 37

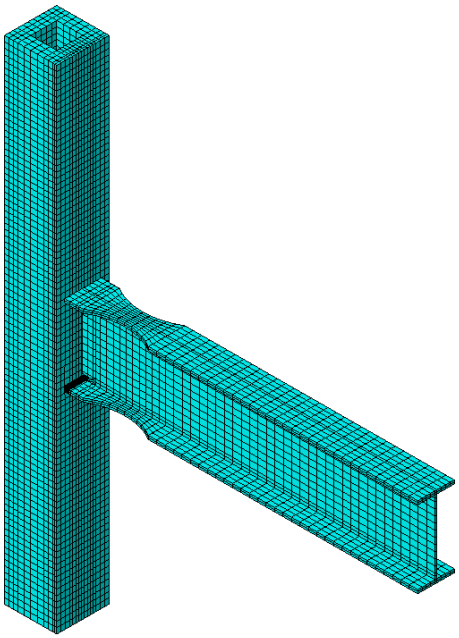

Global model

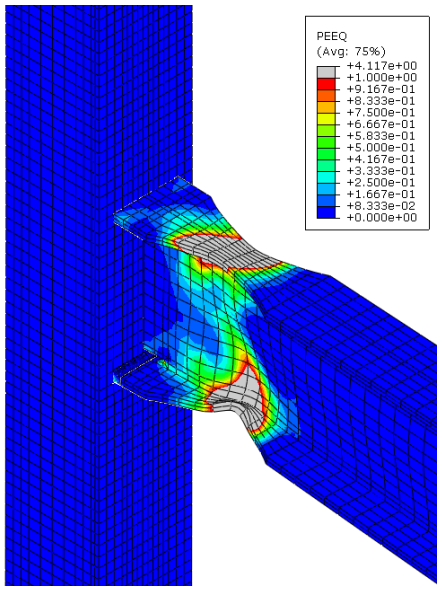

Final state of global model (PEEQ)

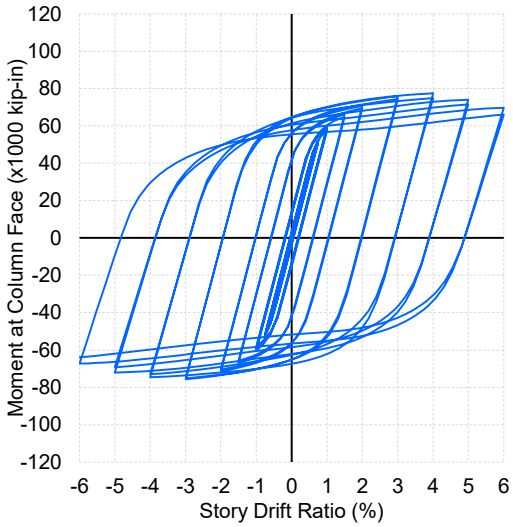

Load-displacement

Simulation 37 cont.

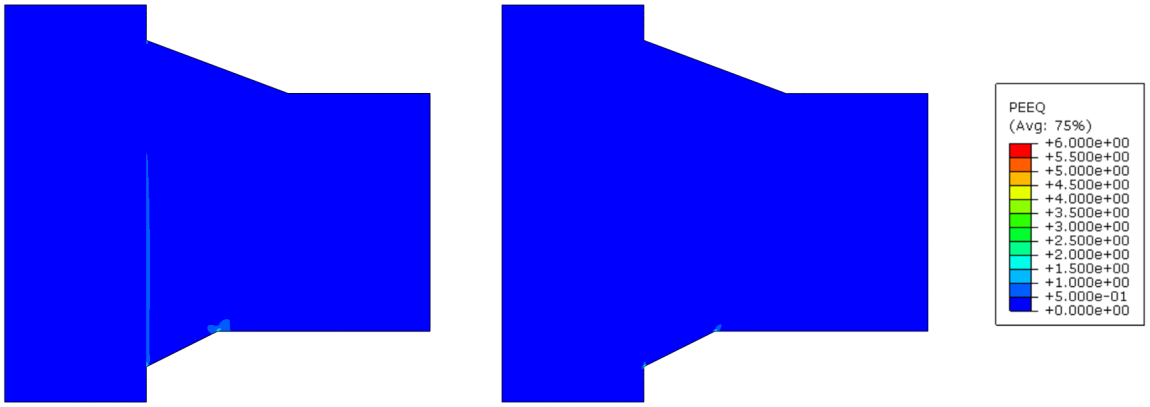

Edge Center

PEEQ at R=0.04 rad

Edge Center

Damage at R=0.04 rad

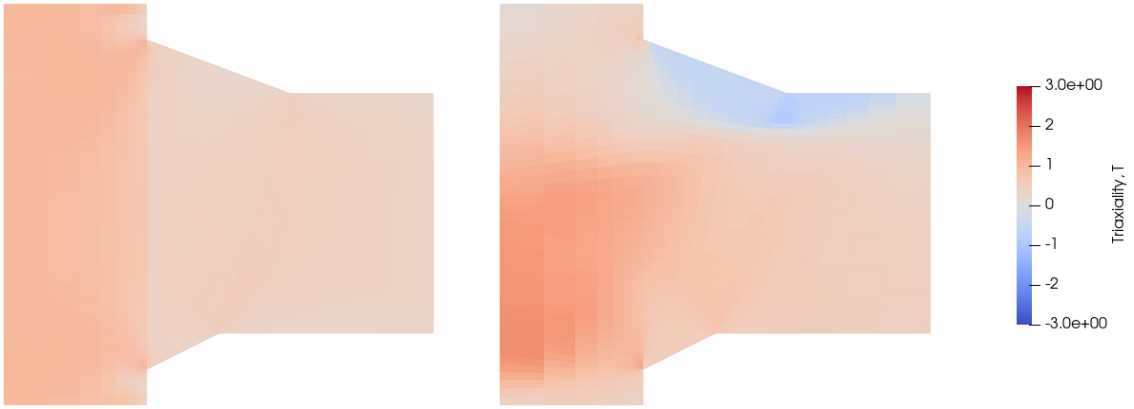

Edge Center

Triaxiality at R=0.04 rad (Time =133s, flange in tension)

Simulation 38

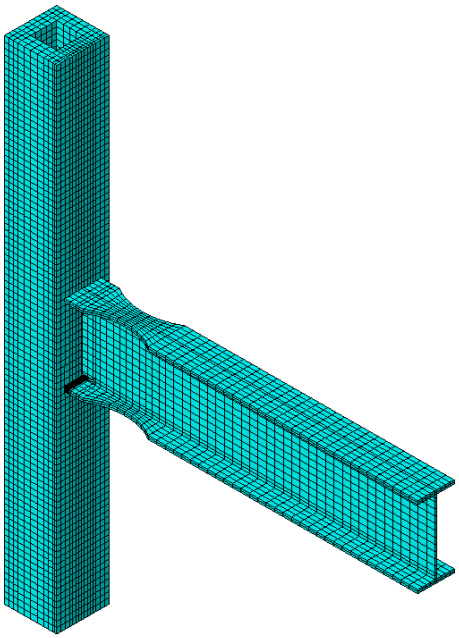

Global model

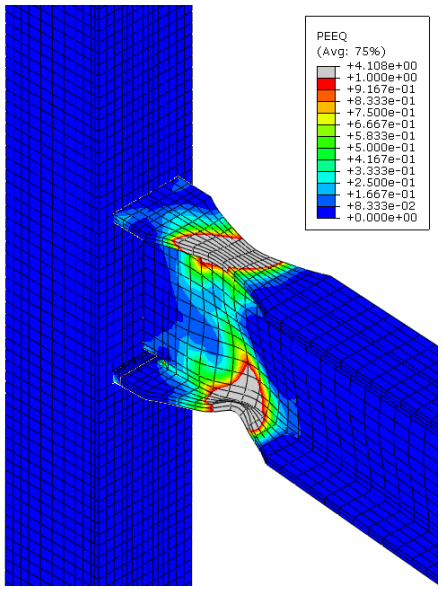

Final state of global model (PEEQ)

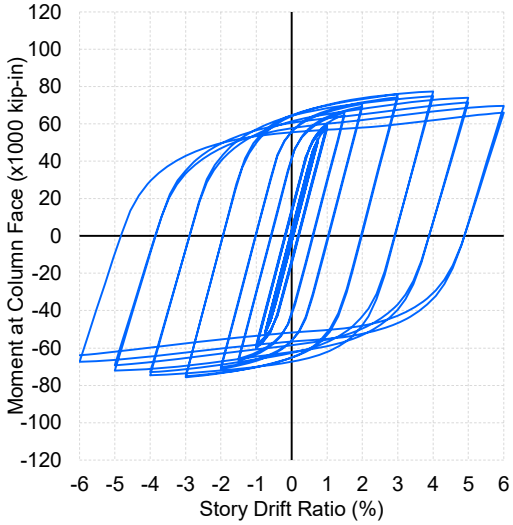

Load-displacement

Simulation 38 cont.

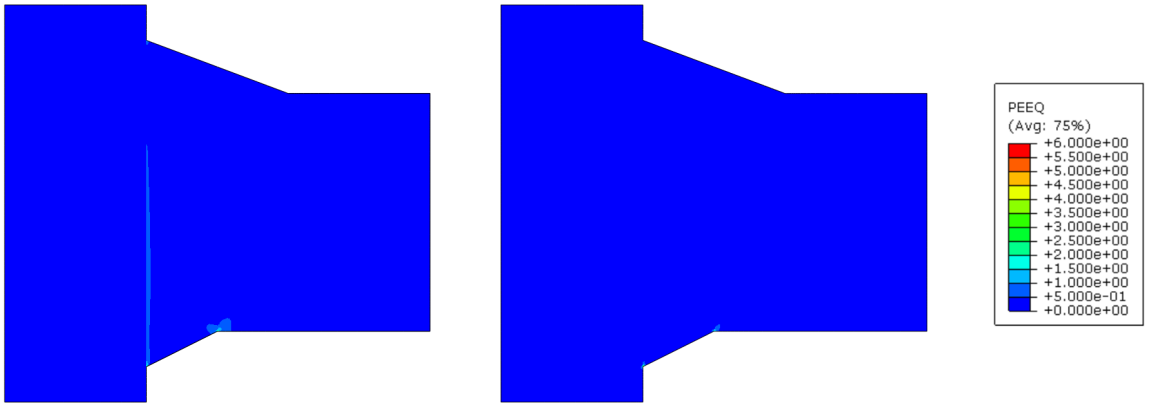

Edge Center

PEEQ at R=0.04 rad

Edge Center

Damage at R=0.04 rad

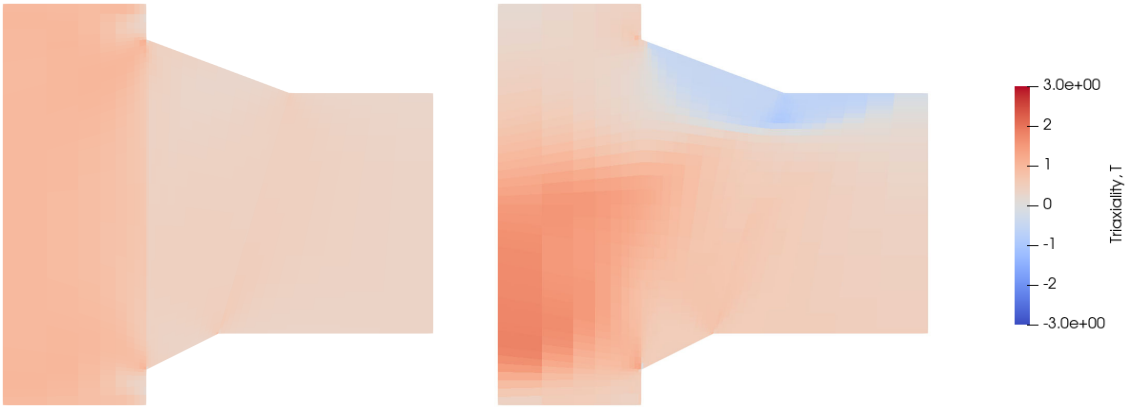

Edge Center

Triaxiality at R=0.04 rad (Time =133s, flange in tension)

Simulation 39

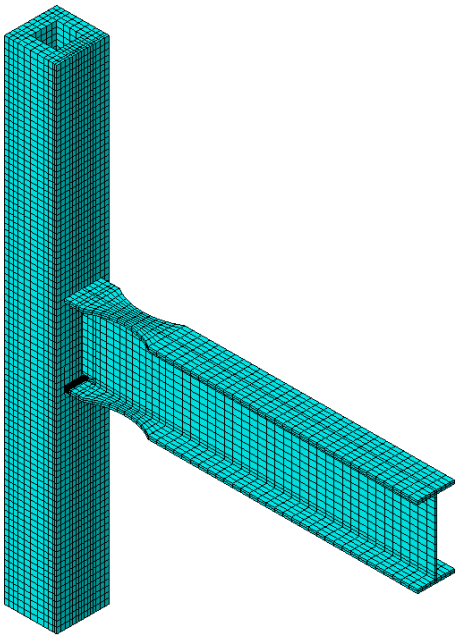

Global model

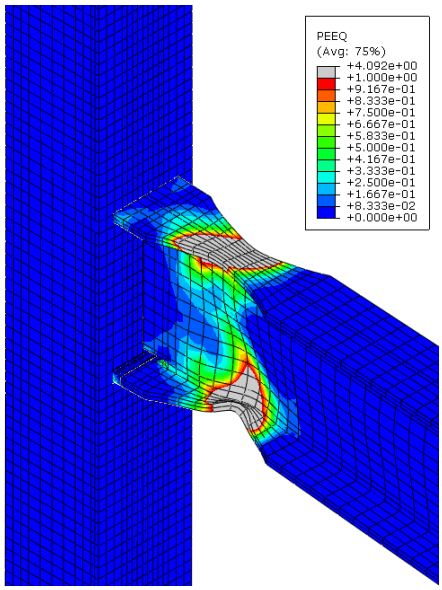

Final state of global model (PEEQ)

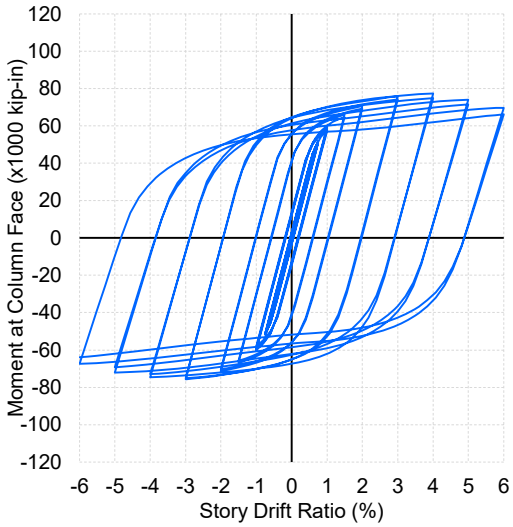

Load-displacement

Simulation 39 cont.

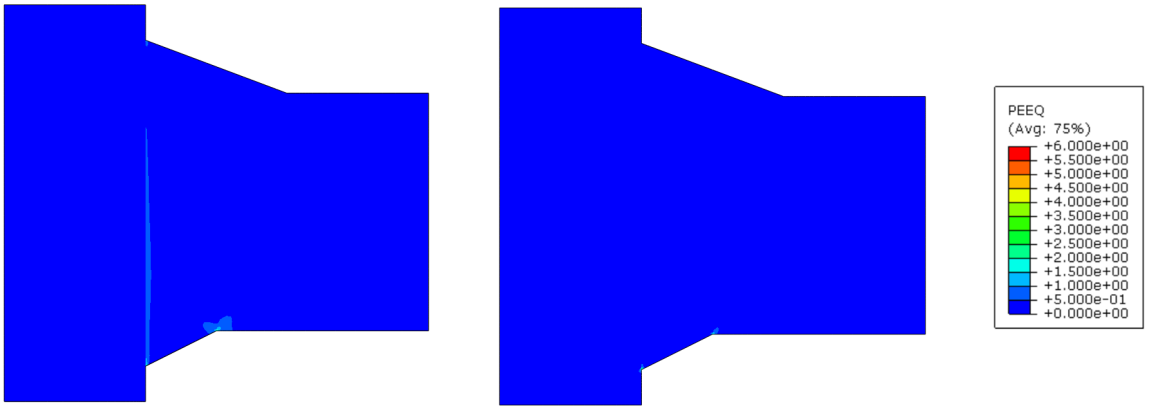

Edge Center

PEEQ at *R*=0.04 rad

Edge Center

Damage at *R*=0.04 rad

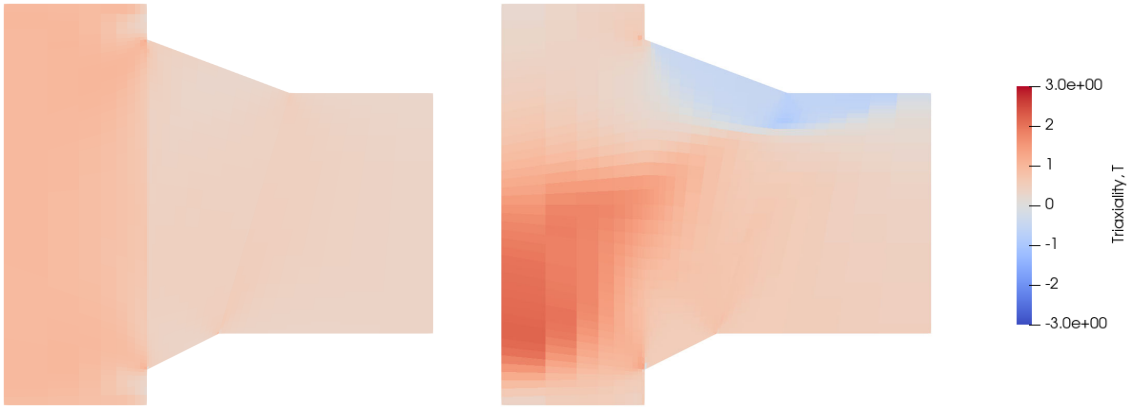

Edge Center

Triaxiality at *R*=0.04 rad (Time =133s, flange in tension)